Metal reclamation from a spent iron-based Fischer-Tropsch catalyst

A dissertation submitted in accordance with the requirements for the degree

Magister Scientiae

in the

Department of Chemistry
Faculty of Natural and Agricultural Sciences

at the

University of the Free State

by

Don Hauman

Supervisor

Prof. J.C. Swarts

Co-supervisor

Dr. J.M. Botha

Acknowledgements.

I would like to thank my supervisor, Professor J.C. Swarts, for his patience, dedication and scientific contribution to the study.

I would like to thank my co-supervisor Dr. J.M. Botha for making the study possible and for his unwavering support and guidance.

I would like to thank Sasol Technology, Research and Development for funding and support.

I would like to thank my close Sasol colleagues for their contributions with special thanks to Riaan Slabbert.

To my wife, Melene, to whom I dedicate this thesis, for her love, support and patience and to my children; Martin, Rikus and Neil who endured with me.

To GOD for the ability and health to work and to study.

To Melene

Abstract

Spent wax-coated iron-based low temperature Fischer-Tropsch catalyst were contacted with nitric acid in order to dissolve the contained metals. Dissolution experiments with wax-coated spent catalysts in concentrated nitric acid at elevated temperatures recovered 75% of the iron into a metal nitrate solution. Dissolution experiments with wax-coated catalyst caused foaming and large volumes of NOx gasses during dissolution. Severe wax separation problems were encountered after metal dissolution. This caused incomplete separation between residual solid, liquid and waxy components. Wax removal techniques, before nitric acid dissolution, in the form of thermal oxidation, anoxic thermal cracking and solvent extraction were investigated. Thermal oxidation experiments at 500 °C and 900 °C in air and anoxic thermal cracking experiments at similar temperature ranges were performed. Wax removal by solvent extraction was performed with C_9-C_{11} paraffin. Iron oxide phase transformations during wax removal techniques were studied by Mössbauer spectroscopy, X-Ray diffraction and BET surface area measurements. Spent wax-coated catalyst consisted of 71% ferrihydrite and 26% Hägg iron carbide. Hägg iron carbide were absent after all wax removal techniques. Temperature excursions during thermal oxidation were studied varying bed volume and height. Samples of bed heights of above 10 mm showed significant temperature deviations above the targeted heat treatment temperature. Samples generated from thermal oxidation at 500 °C contained 78% maghemite and 17% hematite, samples that were oxidized at 900 °C contained only 24 % maghemite but 72% hematite. Thermal cracking of the wax-covered spent catalyst 500 °C resulted in a catalyst residue containing 23% ferrihydrite and 66% maghemite which transformed to 49% and 65% hematite at 750 °C and 900 °C. A maghemite content of 39% was found in the catalyst residue after cracking at 750 °C which changed to 24% after wax cracking at 900 °C. Differences in iron oxide phases between thermal oxidation and thermal cracking were attributed to the less oxidizing environment for thermal cracking due to the absence of air. Dissolution experiments showed > 80% metal recovery for solvent extraction and thermal oxidation and cracking at temperatures up to 500 °C. Lower recoveries were obtained for treatments at higher temperatures and dissolution efficiencies were correlated to sample hematite content. Higher hematite content of low surface area correlated to less efficient dissolution. Pure commercially purchased hematite could be dissolved appreciably if the surface area of the sample obtained was high. Heat treatment of the pure hematite decreased the surface area as well as the amount of iron that could be recovered during nitric acid dissolution. Wax-coated catalyst was also de-waxed by solvent extraction with a C_9-C_{11} paraffin fraction and submitted to heat treatments varying from 350-750 °C at different residence times. The resultant samples showed marked increased hematite content and decreasing surface area for the 600 °C samples over the 350 °C samples and very rapid conversion to hematite and decrease surface area for the 750 °C samples. Thus a higher content of hematite in the de-waxed spent catalyst

indicates exposure to higher temperatures resulting in a drop of the surface area and lower metal recoveries. The overriding conclusion of this study is that the hematite phase is to be avoided. This is best achieved by low catalyst recovery temperatures. A high sample surface area also results in efficient dissolution and catalyst recovery in nitric acid. Resultant metal nitrate solutions were used to prepare a fresh catalyst that was tested for activity and selectivity and compared well to a standard commercially available Ruhrchemie type catalyst. This proved that a chemically viable metal reclamation technology was developed for spent wax-coated iron-based low temperature Fischer-Tropsch catalysts.

Key words: Metal Reclamation, Spent Iron-based Fischer-Tropsch Catalyst, Nitric acid, Wax removal techniques.

Opsomming

Uitgewerkte, was-omhulde, yster-bevattende lae temperatuur Fischer-Tropsch katalisatore is in salpetersuur opgelos om sodoende die metale te herwin. Oplossingseksperimente met was-omhulde uitgewerkte katalisatore in gekonsentreerde salpetersuur, by verhoogde oplossings temperature, het 75% yster herwinning tot gevolg gehad. Oplossingeksperimente met die was-omhulde katalisator het skuimvorming en hoë volumes NOx gasvorming veroorsaak. Was, vloeistof en onopgeloste katalisator-partikel skeiding na oplossings eksperimente was uiters problematies. Wasverwyderings tegnieke, voor oplossing in gekonsentreede salpetersuur, is derhalwe ondersoek deur gebriuk te maak van termiese oksidasie, inerte termiese kraking en was oplosmiddel ekstraksie. Termiese oksidasie eksperimente is by 500 °C en 900 °C in lug gedoen terwyl inerte termies oksidasie by soorgelyke temperature in die teenwoordigeid van 'n stikstof atmosfeer gedoen is. Ekstraksie wasverwydering is met 'n C_9-C_{11} paraffien fraksie ondersoek. Ysteroksied fase veranderinge tydens die was-verwyderings metodes is ondersoek met behulp van Mössbauer spektroskopie, X-straal diffraksie en BET oppervlak area analieses. Uitgewerkte was-omhulde yster katalisatore voor metaal herwinning het bestaan uit 71% ferrihidriet en 26% Hägg ysterkarbied. Hägg ysterkarbiedes is vernietig deur al die was- verwyderingstegnieke. Katalisatorbed temperatuur veranderinge, tydens termiese oksidasie, is ondersoek deur bedhoogte en bedvolume te varieer. Katalisator bedhoogtes van bo 10 mm het tot groot temperatuur verskille tussen beoogde en werklike bedtemperature gelei. Termiese oksidasie van was-omhulde katalisator by 500 °C het tot katalisator residu gelei wat 78% maghemiet en 17% hematiet bestaan het. Monsters wat by 900 °C geoksideer het bestaan uit 24% maghemiet en 72% hematiet. Termiese kraking by 500 °C van die was wat uitgewerkte katalisator bedek het en tot 'n katalisator residu gelei het wat uit 23% ferrihidriet en 66% maghemiet bestaan. Dit het verander na 49% en 65% hematiet indien kraking by 750 °C en 900 °C uitgevoer word. Die maghemiet inhoud verander vanaf 39% na 24% indien kraking by 750 °C of 900 °C onderskeidelik uitgevoer word. Verskille in ysteroksied fases tussen termiese oksidasie en termiese kraking word toegeskryf aan die minder oksiderende toestande wat by inerte atmosfeer termiese kraking heers. Salpetersuur oplossingseksperimente toon aan dat > 80% van die beskikbare yster in katalisator-materiaal oplossing gaan indien was verwyder word deur termiese oksidasie en termiese kraking by temperature tot en met 500 °C. Laer herwinnings persentasies vir wasverwyderingstegnieke bo 500 °C is waargeneem. Hoër hematiet konsentrasies van lae oppervlakte areas word met laer yster oplosbaarheid in salptersuur geassosieer. Suiwer kommersiele hematiet het wel hoë oplosbaarheid getoon as die oppervlak area van die hematiet monster hoog was. Hitte behandeling van die suiwer hematiet het die oppervlak area verlaag waarna die oplosbaarheid van die yster baie afgeneem het. Wasomhulde katalisator se was is verwyder deur 'n C_9-C_{11} paraffien fraksie as oplosmiddel en blootgestel aan temperature vanaf 350-750 °C vir verskillende tydsrame.

Die mosters se BET oppervlak areas en bepaling van die hematiet fase inhoudbepaling na die hitte behandelings het getoon dat monster by 600 °C vinniger begin hematiet vorm en BET oppervlak area verloor. Hierdie tendens vind by 750 °C nog vinniger plaas. Hoër hematiet en laer BET oppervlak areas is verantwoordelik vir swakker yster oplosbaarheid. Die belangrikste bevindings uit hierdie studie is dat hoër hematiet konsentrasies vermy moet word deur wasverwyderingstegnieke. Dit word die beste bewerkstellig deur van laer was verwyderings temperature gebriuk te maak . Hoë oppervlak area lei ook tot effektiewe katalisatorherwinning duer oplossing in salpetersuur. 'n Nuwe yster katalisator voorganger kon uit die resulterende yster-ryke nitraat oplossings berei word. Die katalisator voorganger is gereduseer en getoets onder standaard Fischer-Tropsch reduksie en sintese kondisies en het getoon dat die nuwe katalisator dieselfde aktiwiteit en selektiwiteit tot produkte het as 'n standaard Ruhrchemie katalisatore onder dieselfde kondisies. Dit het bewys dat 'n chemise aanvaarbare metaalherwinnings tegnologie van uitgewerkte wasomhulde ystergebaseerde lae temperatuur Fischer-Tropsch katalisatore ontwikkel is.

List of Figures

Chapter 2

Chapter 3

Chapter 4

List of Tables

Chapter 2

Chapter 3

Chapter 4

Appendix

List of Schemes

List of Photograghs

List of Terms and Abbreviations

Paraffin	Same as alkane.
Olefin	Same as alkene.
Synthesis gas	Mixture of primarily hydrogen and carbon monoxide.
Fischer-Tropsch	The Fischer-Tropsch process in essence is a chemical process that can be used to convert synthesis gas to hydrocarbon products.
FT	Fischer-Tropsch.
FTS	Fischer-Tropsch Synthesis.
MAS	Mössbauer Adsorption Spectroscopy.
XRD	X-Ray Diffraction.
TOL	Time on line or duration of experiment.
Calcination	Heat treatment under various conditions.
NOx	Term used industrially for NO, NO_2 N_2O_5 and other nitrogen oxygen gas mixtures.

Chapter 1 - Introduction

1.1 Introduction.

The world's energy demand is increasing quickly, more so, recently as economies in Brazil, Russia, India and China (BRIC) are growing rapidly.[1] In contrast the production of oil has not been significantly increased and as a resource is continually becoming more expensive. Price and supply is often threatened by political instability. It is speculated that the oil price will continue to rise significantly as the demand for oil already begins to exceed the production capacity.[2] Should oil production be increased, the effect would only be to postpone oil shortages until resources become either depleted or, more expensive as less available resourses need to be mined. The cost of natural gas has also risen sharply over the last 5 years. Natural gas and oil reserves are often found in tandem at the same site. Except in cases where natural gas volumes are low or in remote areas, more and more natural gas resources are utilized as opposed to flaring (burning) the gas as in the past. Problems associated with addressing the energy shortage and environmental challenges facing us in recovering oil or gas from increasingly difficult (remote) accessible sites are monumental. Alternative energy sources and technologies will have to be developed for the world to cope with the growing energy demand. The United States, and others, has long ago surpassed the consumption of oil from domestic sources and rely heavily on the unstable Middle East. In the United States no new grassroots oil refinery has been build since 1976.[3] However, many of the large oil consuming countries also have large, fairly under utilized, coal reserves.

Recently coal gasification as source of feed gas or synthesis gas (mixture of primarily H_2, CO, CH_4, CO_2) has received much attention as a source of synthetic oil due to the rising cost of natural gas and oil.[2] The most active countries in these investigations are the United States and China. Recoverable coal reserves have the potential to produce energy, at the current rate, more than 5 times longer than that of oil reserves. Currently 990 billion metric tons of coal is available worldwide. North America, Russia, China, Australia, India, Germany and South Africa each have more than 50 billion metric tons of coal reserves. The United States, Russia and China have the largest coal reserves in the world, but China and India together account for almost 75% of the recent increase in coal demand in developing countries and 66% of the increase in the world coal demand. The world-wide challenge is to harness the enormous coal reserves as energy source in an economically and environmentally benign way.

The process of converting coal to synthesis gas, also known as syngas, or reforming natural gas to syngas and then converting the syngas to a hydrocarbon-rich product stream via the Fischer-Tropsch (FT) process has become of increasing strategic relevance to countries who have access

to either coal or natural gas reserves. Rather than flaring the natural gas, added revenue that can be obtained from harvesting natural gas also attracts the attention of oil rich countries as natural gas and oil reserves are almost always associated with each other. The utilization of so called "stranded" reserves are also possible using FT. Stranded reserves refer to natural gas and coal reserves that are far away from the end user (markets). Converting these sources to liquid fuels allow for transportation of the high value products to the markets.

Traditionally the Fischer-Tropsch process has been extensively pursued by entities that have coal reserves but have been isolated from crude oil reserves for a number of reasons. The production of fuels via the Fisher Tropsch process rather than from crude oil refining was mostly the focus. Germany actively pursued Fischer-Tropsch processes in order to produce fuel for their war efforts towards the end of Word War 2. Germany is an oil reserve poor country and the Allied forces cut off all oil imports. Germany is, however, rich in brown coal reserves and could therefore produce fuels *via* the Fisher Tropsch process. South Africa was in a similar situation when crude oil sanctions were imposed on it due to the apartheid political ideologies of 1948-1992. Due to the vast coal reserves in South Africa, Fischer-Tropsch processes were developed and subsidised by the government when the oil price was below the production price of hydrocarbons via the Fischer-Tropsch process. This enabled Sasol to develop and improve the process to a point where subsidies were no longer necessary. The protective environment that Sasol enjoyed for this time meant that valuable commercial experience was gained. It is this experience that has made Sasol a leader in the field of oil production from coal.

The Fischer-Tropsch process in essence is a chemical process that can be used to convert synthesis gas to hydrocarbon products.[4] The hydrocarbon products vary from light gasses to heavy hydrocarbon liquids that congeal to form waxes once removed from the reactor.

The general chemical equation for Fischer-Tropsch synthesis of hydrocarbons can be written as:

$$(2n+1)H_2 + nCO \rightarrow C_nH_{2n+2} + nH_2O$$

Under the term hydrocarbons (C_nH_{2n+2}) the following are included: Gases such as methane, propane, butane, and others as well as liquid paraffins, olefins and oxygenated hydrocarbons (acids, alcohols, aldehides, etc.) and also heavy hydrocarbons such as waxes.[4]

There are two distinct types of FT processes namely high temperature (300–350 °C) and low temperature (220–270 °C) FT. Traditionally, the former produces a lighter (lower average

molecular weight) product range and is normally associated with a liquid fuels product spectrum. The latter produces a heavier hydrocarbon fraction (higher average molecular weight) product range. Especially linear waxes are obtained as high-value chemicals. In recent years low temperature Fischer-Tropsch has also been developed to produce heavier fractions that can be cracked afterwards to fuels. The primary product targeted for these applications is diesel. Diesel normally consists of a more linear hydrocarbon product range than, for instance, petrol and can therefore ideally be prepared by cracking waxes. "Clean" diesel has become, and will increasingly become, a preferred fuel as diesel engines have dramatically improved and the diesel engine is more efficient than a petrol engine.

Fischer-Tropsch (CO hydrogenation and carbon chain expansion) is typically done in the presence of an iron or cobalt catalyst. For iron, a precipitated catalyst precursor is normally used that is promoted with silica (SiO_2) as binder (strength) promoter and copper (CuO or Cu in reduced state) and potassium (K_2O) as chemical promoters. For the cobalt system, a supported catalyst is normally used with the support being either silica, titania, alumina, zirconia or carbon. Chemical promoters for the cobalt catalysts can include platinum, ruthenium, gold or silver (normally as the metal after hydrogen reduction). Both of the main catalysts have their unique advantages and disadvantages. Probably the most important difference is that the iron catalyst is less expensive, but has a shorter lifetime, whereas the cobalt catalyst is more expensive, but has a longer lifetime.[5] Several other differences exist in terms of the product spectrum produced as well as catalyst intrinsic activity and reactor operating conditions. For coal-derived syngas, there is a strong case to be made for an iron catalyst because it is more resistant to sulphur poisoning and it can be more readily replaced if it is poisoned. Sasol has two local plants that utilize an iron based catalyst (> 10000 tons/year) for both high and low temperature FT.

More stringent environmental laws as well as the price of raw materials, specifically metals and precious metals, have made the reclamation of metals from spent catalysts a necessity. The environmental legacy of FT technology is a major concern and cleaner FT technologies are a topic of much research. Recovery and re-use of spent metal catalysts in order to produce new catalyst rather than disposing of tons of spent catalyst in landfill sites is therefore of strategic and environmental importance. Iron FT catalysts cannot be easily rejuvenated as the catalyst undergoes irreversible chemical and structural changes during the FT process.[6,7] For this reason the spent catalyst has to be recovered, purified and fresh active catalyst re-prepared. Spent catalyst that was removed from a FT reactor is always covered or contaminated by the products it was used to synthesize and these products have to be removed or dealt with as part of the spent catalyst recovery procedure. In addition different FT product removal steps lead to different metal

oxidation states and phases that have different physical and chemical characteristics. This leads to different dissolution behaviour.

1.2 Aim of Study.

Against this background, the removal of organic products such as wax from spent FT catalysts, dissolution and recovery of spent metal catalysts and the synthesis of fresh catalyst from the spent catalyst are the topic of investigation of this study. The following goals were identified for this study:

1. Investigation of possible organic (wax) removal methods from spent catalysts and the effect of such methods on the chemical and physical characteristics of the remaining material.
2. Determination of the dissolution behaviour of materials remaining after the various wax removal methods have been affected.
3. Requiring of a fundamental understanding of the properties required for optimal dissolution of the residual spent catalyst after the organic material has been removed.
4. Preparation of a fresh FT catalyst from the material obtained by dissolution of the residual spent catalyst material.
5. Fischer-Tropsch activity and selectivity testing of the freshly prepared catalyst under standard operating conditions to evaluate catalyst performance.

Remark: Technically a "catalyst" does not permanently change in structure or chemical composition during a reaction; it only serves to speed up the reaction rate. However, historically Fischer-Tropsch processes have been greatly enhanced by the use of iron- or cobalt-based materials that have been labelled "catalysts" even though both chemical and structural changes are affected during the process. This study uses the term catalyst due to the FT historical use of this term although scientifically it would be more correct to substitute the word "catalyst" with "reaction promoter" or "reaction accelerator".

1.3 References.

[1] *The World in 2050, Beyond the BRIC's: a broader look at emerging market growth prospects*, PriceWaterhouseCoopers.
[2] theoildrum.com
[3] *SRI Consulting, Technology Intelligence for Coal to Liquid Strategies*, Fuels of the Future, **July 2008**.
[4] Steynberg, A.P., Dry, M.E., in *Fischer Tropsch Technology*, Elsevier, **2004**, 1.
[5] Van Steen, E., Claeys, M., in *Chem. Eng. Technology*, **2008**, 31, 655.
[6] Bukur, B.D., Norwicki, L., Manne, R. K., Lang, X., in *Journal of Catalysis*, **1995**, 155, 366.
[7] Datye, K.A., Scroff, M.D., Kohler, S.D., Jackson, N.B., in *Journal of Catalysis*, **1995**, 156, 185.

Chapter 2 – Literature Review

2.1 Introduction.

Iron oxides are commonly found in nature and are readily synthesized in the laboratory[1]. The formation of Fe(III) oxides in nature predominantly involves the aerobic weathering of magmatic rock. This occurs on land as well as in aquatic environments. Redistribution of the oxides occur *via* mechanical means such as water and wind transport or more importantly reductive dissolution followed by the migration of Fe(II) and oxidative re-precipitation. Man also contributes to the distribution as a consumer of iron metal and iron oxides for various industrial uses. Therefore the study of iron and iron oxides are of importance to many different scientific disciplines. The fields of iron and iron oxide consumption that receive significant scientific investigation are depicted in **Figure 1**.

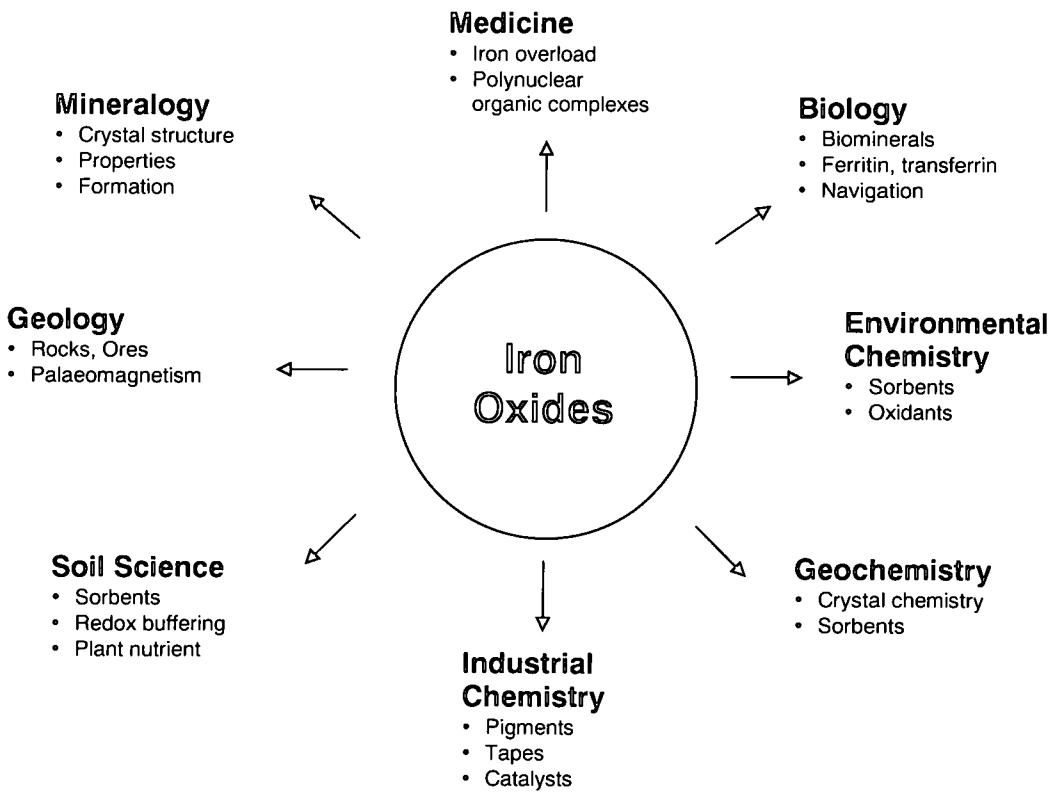

Figure 1. Multidisciplinary nature of iron oxide research (adapted from Schwertmann[1]).

During the course of this study, different iron oxide phases will be referred to. Iron oxides undergo various phase transformations depending on the chemical or mechanical environment they are exposed to. **Table 1** contains a summary of all the iron oxides, hydroxides and oxy-hydroxides.

Table 1. The Iron Oxides.

Oxide-hydroxides and hydroxides		**Oxides**	
Goethite	α - FeOOH	Hematite	α - Fe_2O_3
Lepridocrocite	γ - FeOOH	Magnetite	Fe_3O_4
Akaganéite	β - FeOOH	Maghemite	γ - Fe_2O_3
Schwertmannite	$Fe_{16}O_{16}(OH)_y(SO_4)_z \cdot n\ H_2O$		β - Fe_2O_3
Ferroxyhyte	δ' – FeOOH		ε - Fe_2O_3
Ferrihydrite	$Fe_5HO_8 \cdot 4\ H_2O$	Wüstite	FeO
Bernalite	$Fe(OH)_3$		
	$Fe(OH)_2$		
Green Rusts			

Goethite occurs in rocks and in various other compartments of the ecosystem. It has a diaspore structure which is based on hexagonal close packing of anions. Goethite is thermodynamically very stable and is therefore a primary oxide formed or it is the final phase after phase transformations. In massive crystal aggregates it has a brown of black colour and as a powder it is yellow. Industrially it is used as a yellow pigment.

Lepidocrocite is named after its platy crystal shape (lepidos = scale) and its orange colour (krokus = saffron). It is found in rocks, soils, biota and rust and is often an oxidation product of Fe(II). It has a structure which is based on cubic close packing of anions.

Ferrihydrite is found widespread in surface environments. It has a reddish–brown colour and unlike other iron oxides it exists exclusively as nano-crystals and unless stabilized in some way will transform spontaneously to more stable oxides. Structurally it consists of hexagonal close packed anions and is a mixture of defect free, and defective structural units.

Hematite is the oldest known iron oxide phase and is widespread in rocks and soils. It has a blood red colour in powder form and is black or sparkling black if coarsely crystalline. Hematite is also extremely stable and often the final oxide phase after several iron oxide phase transformations. It has a structure based on hexagonal close packing of anions.

Magnetite is a black ferromagnetic mineral containing both Fe(II) and Fe(III) species and has an inverse spinel structure. It is important in terms of the magnetic properties of rocks.

Maghemite is a red–brown ferromagnetic material and very similar to magnetite but has cation deficient sites. It occurs in soils as a weathering product of magnetite or a product of heating other iron oxides. Maghemite is also important due to its magnetic properties.

Wüstite is an iron oxide that contains only divalent iron and is usually oxygen deficient. The structure is similar to NaCl and its structure has a centre close packed anion packing. Wüstite is black and often encountered as an important intermediate during the reduction of iron oxides.

The aim of the study is to recover iron from spent Low Temperature Fischer-Tropsch (LTFT) processes. During the recovery process some of the above mentioned iron oxide phases may be found. Similar chemistry and iron phases are encountered for various other iron-based industrially used catalysts. Fundamental results for this study may therefore also be applicable to the recovery of these other commercially used iron-based catalysts. For this reason large industrial processes with iron catalysts are discussed in the next section.

2.2 General Iron Catalysis.

Iron catalysis are widely used industrially and some of the processes include ammonia synthesis, the de-hydrogenation of ethyl-benzene to styrene, methanol to formaldehyde, the water gas shift reaction and Fischer-Tropsch synthesis.[2] The purpose of this section is to highlight the importance of iron catalysis not only for Fischer-Tropsch Synthesis (FTS) but also for other significant applications. Recovering these catalysts to reduce environmental impact, or creating zero effluent plants will become increasingly important. Economic factors also drive the recovery of steel and iron. Steel prices have almost doubled over the last two years[3] and previously relatively inexpensive catalysts are increasingly affected by these prices.

2.2.1 Ammonia Synthesis.

The production of ammonia has been one of the most influential catalytic reactions of modern times[2]. Recent reviews pointed out that the development of the ammonia catalyst formulated all the general concepts used today in catalyses.[4] Towards the end of the 19th century the need to produce enough food for the growing populations became a major concern. The continuous large scale production of ammonia as a fertilizer precursor had a dramatic effect on solving this problem. Ammonia's other uses in explosives, dyes and polymers also had influential effects on history.[5]

Fritz Haber and co-workers first demonstrated that ammonia could be produced (2 $kg.day^{-1}$) in the presence of hydrogen and nitrogen utilizing an osmium catalyst at 175 bar. Carl Bosch (BASF) later scaled the process to several tons per day at 300 bar. This led to significant equipment development to operate at these extreme pressures. The quest was therefore to operate at milder conditions and to use a less exotic and a less hazardous catalyst. Mittach (BASF) was the first to experiment with a range of catalyst of which iron was one. At the time the experiments were not very successful. The discovery of a promoted iron catalyst that was reasonably successful was purely by accident. A magnetite sample that was left over from another study, and accidently tested, showed an amazingly high yield of ammonia.[6,7] The work was done by Wolf (co-worker of Mittach) on November 6, 1909. Over the next two years more that 2500 catalysts were prepared and tested in 6500 experiments. This led to the development of the Al_2O_3, CaO, K^+ promoted iron catalyst that is essentially still today the catalyst used with only minor modifications. In the 1970's, Ozaki and co-workers started with the development of a ruthenium catalyst which showed an increase of 20-50 times of the activity over the iron catalyst. Ruthenium also has a superior resistance to poisons. This has led to recent plants built with ruthenium catalysts which are operating at significantly lower pressures and temperatures.

Ammonia synthesis occurs by a relatively simple exothermic, stoichiometric reaction conducted at 450–500 °C and 300 bar (**reaction 1**).

$$\mathbf{3H_2 + N_2 \rightleftarrows 2NH_3} \qquad \mathbf{\Delta H\ (500^{\circ}C) = -109\ kJ/mol} \quad \mathbf{----- (1)}$$

$$\mathbf{\Delta H^{o} = -92.44\ kJ/mol}$$

A typical fresh commercial iron catalyst is composed of 89-95% Fe_3O_4, 2-4 % Al_2O_3, 0.5–1 % CaO and possibly other additives such as MgO, CrO_3 and SiO_2. Each play a key role in the performance of the catalyst. Al_2O_3, CaO, MgO, CrO_3 and SiO_2 are textural promoters that aid in the dispersion of the iron and counters sintering. Ca renders the catalyst more resistant to sulphur poisoning whereas SiO_2 is though to increase the catalysts resistance to water. Alumina aids as a structural promoter inhibiting sintering of the catalyst.

A typical ammonia synthesis catalyst is prepared by fusing a high grade magnetite ore and promoters at 1700 °C. The molten metal mixture is then poured into water to produce fine particle "shot". After grinding, the mixture is sometime directly loaded into the reactor where it is reduced slowly with H_2 to metallic iron at temperatures of up to 500 °C and 70-100 bar for a period of 100 h (**reaction 2**). The catalyst precursor is slowly reduced to ensure that water formation is slow and can be sufficiently removed before damaging the catalyst *via* a sintering mechanism.

$$\underset{(1\ m^2/g)}{FeO} + Fe_2O_3 + \text{promoters} \rightarrow \underset{(20\ m^2/g)}{Fe} + H_2O \qquad \text{-----(2)}$$

Sintering is generally accepted as the formation of larger metal crystallites by the coalescence of smaller metal crystallites and leads to a loss in surface area and hence catalyst activity. A two step reduction process is also sometimes used with an isothermal break of several hours at the point of maximum water production. This has led to reduced times of 40 hours[8] for some applications in comparison to 100 hours. Rapid activation, within several hours, leads to irreversible structural damage of the catalyst system[9] and poor catalytic performance. The removal of oxygen during reduction results in a 20 times increase in the surface area (**reaction 2**).

The oxide precursor that is typically used mainly consists of magnetite (Fe_2O_3) and wüstite (FeO). Further phases that can be identified are calcium ferrite ($CaFe_3O_4$), potassium hydrogen carbonate ($KHCO_3$), and *alpha* iron. This combination is unique for a catalyst precursor as, within one solid, metastable phases coexist of varying oxidation states.

The most frequently encountered non-permanent poisons are CO, CO_2 and H_2O. These gasses adsorb and desorb without significantly affecting the catalyst activity. However, oxygen is less reversibly adsorbed especially if allowed to accumulate over long periods because of metallic iron oidation and should be avoided. Irreversible poisons are copper, chlorides, sulphur, phosphorous and arsenic. With proper maintenance the ammonia catalyst can have a lifetime of up to 10 yrs.[4]

2.2.2 Dehydrogenation of Ethyl-benzene to Styrene.

Styrene, the monomeric building block of polystyrene, is produced by dehydrogenation of ethyl-benzene by a reaction favoured at high temperature and low pressure (**reaction 3**).

$$C_6H_5CH_2CH_3 \rightleftarrows C_6H_5CH{=}CH_2 + H_2 \qquad \text{----- (3)}$$

On a tonnage basis styrene manufacture as per **reaction 3,** is the largest catalytic dehydrogenation process in the world. In 1993 about 15 million tons of styrene was produced worldwide.[2] The US production in 2003 was 11.4 million tons while the estimated global production was 21 million tons.[10]

It is a highly endothermic reaction (124 kJ/mol) and is typically operated at pressures less than 1 bar and a temperature of between 550–650 °C in the presence of a potassium promoted iron oxide

catalyst with the addition of steam. Near equilibrium conversions of 50-70 % are achieved with a styrene selectivity of 90–95%. By-products are typically 1% benzene and 2 % toluene.

The catalyst of choice is an iron oxide promoted with K_2O_3, Cr_2O_3 and other oxide additives such as TiO_2, V_2O_5 MoO_3 and CeO_2. A typical catalyst is prepared by co-precipitation and an initial composition of around 88% Fe_2O_3, 2.5% Cr_2O_3 and 10% K_2O is obtained. The catalyst is usually supplied in the form of 4–6 mm (diameter) cylinders. For an increase in pore diameter and strength the catalyst is calcined (heat treated) at 900 – 950°C. The calcination reduces the surface area to approximately 1.5–3 m^2. Potassium oxide is a key promoter that enhances the activity of the catalyst ten fold.

Catalyst deactivation has four main causes namely:

1. Short term reversible deactivation due to CO_2 oxidation and surface adsorption.
2. Reversible coke formation (e.g. tars) caused by product condensation.
3. Irreversible damage due to promoter (K_2O) migration.
4. Slow volatilisation of potassium.

Six volumes of superheated steam are added for every volume of ethyl-benzene in order to:

1. Provide heat for the dehydrogenation.
2. Maintain the iron oxide phase.
3. Retard coke formation.
4. Reduce the partial pressure of hydrocarbons to shift the equilibrium to higher conversions.

2.2.3 Methanol to Formaldehyde.

Formaldehyde (HCHO) is a versatile, reactive, organic building block with a multitude of applications. It is an important intermediate for the production of urea, phenolic resins and melamine resins for the wood industry. It is also a disinfectant and preservative and an intermediate for the synthesis of several other organic components. United States production was around 4.33 million tons in 2003.[11] It is generally produced on site due to high transport costs.

Commercial production began in Germany in 1890 with a copper catalyst. The copper catalyst was replaced with silver by 1910. In 1950 an iron molybdenum catalyst was introduced. Today formaldehyde is almost exclusively produced by the oxidation of methanol by either of two routes.

The Fe–Mo oxide catalyst is used in the dilute methanol process which proceeds *via* direct oxidative dehydrogenation of methanol in a large excess of oxygen. Complete methanol conversion is achieved at temperatures ranging from 350–450°C. The reaction is highly exothermic.

The Fe–Mo oxide catalysts are composed of 17–19% Fe_2O_3, 81–82% MoO_3 and 1–3% Co-or–Cr–oxide as stabilizer. The catalyst is normally supplied as an extrudate or rings and silica may be added to increase the strength. Primary modes of deactivation are mechanical break-up due to loss of molybdenum. This causes an undesirable pressure drop over the catalyst bed. Catalyst lifetime is in the order of 2 years.

2.2.4 Water Gas Shift reaction.

The Watergas Shift Reaction (WGS) represents a very important step in the industrial production of hydrogen, ammonia and other commodity chemicals with syngas H_2:CO ratio's higher than that produced by coal gasification or steam reforming (**reaction 4**).

$$\mathbf{CO + H_2O \rightleftarrows H_2 + CO_2} \qquad \text{----- (4)}$$

The WGS reaction has therefore been studied extensively.[12-17] During the production of hydrogen or to influence the H_2:CO ratio in the production of syngas the Water Gas Shift reaction (WGS) is of importance. Syngas can be produced by steam reforming of natural gas (CH_4). Steam reforming is the most widely used technology. CO_2 reforming, auto-thermal reforming and catalytic partial oxidation are also technologies used. The gas that exits the reformers is not always ideal for a particular application and some modification in exit gas ratio of mixtures may be required. The water gas shift or reverse water gas shift reaction can be used to tailor the exit streams for processes requiring a specific H_2:CO ratio.

The water gas shift reaction is also important for Fischer-Tropsch synthesis because it also occurs under typical operational conditions in the presence of an iron-based catalyst and the relative ratio's of these two reactions are of primary importance. In some cases the WGS reaction forms part of other complex reactions such as the steam reforming of aliphatic hydrocarbons[11,18] or steam de-alkylation of alkylaromatics.[19] The recovery of iron catalysts from WGS catalysts shares close similarities with the Fischer-Tropsch process and this study will aid in the understanding of the recovery process. During the past 50 years three technical processes, based on WGS, have been developed.

These are:

1. High temperature shift (360-530 °C).
2. Low temperature shift (210-270 °C).
3. "Sour gas" shift which converts raw gasses from coal or crude oil gasification containing sulphur and traces of hydrocarbons.[20]

2.2.4.1 High Temperature Shift (HTS).

In industrial HTS converters, iron oxide catalysts are applied exclusively. These catalysts are commercially available[21] and are generally supplied as pellets. These catalysts normally contain 8–12% Cr_2O_3. The function of the chrome has been studied in the past[22,23] and it has been found that the Cr_2O_3 prevents the iron oxide from sintering (loss of surface area due to crystallite coalescence) at elevated temperatures. Other additives besides Cr_2O_3 are MgO and ZnO in Fe-HTS and aim to improve their selectivity towards methane formation, sulphur resistance and mechanical strength.[24-27] Copper promoted Fe-Cr catalysts exhibit higher activity and selectivity especially in the case of low steam/CO ratios, when methane is favoured.[24,28]

Gas from a reformer may for instance contain 10-13% CO and the CO can be reduced to 2-3% while increasing the hydrogen content. The reactor operates at temperatures ranging from 350-500 °C, 20-80 bar and gas hourly space velocities of 400-1200 h^{-1} (gas hourly space velocity = m^3 reagent gas / ton catalyst / hr). The equilibrium conversion of CO and H_2O to CO_2 and H_2 increases sharply with a decrease in temperature. Because equilibrium strongly favours WGS (**reaction 4**) at lower temperature, the feed gas is cooled to about 350-400 °C (reforming is normally at temperatures > 900 °C) before it is passed through the high–temperature– shift catalyst composed of Fe_3O_4 and Cr_2O_3. Thermodynamically, 200 °C would be preferred but iron catalyst activity is too low under these conditions. The catalyst also acts as a clean–up system for further processes as it adsorbs residual sulphur and chlorine containing components.

Fe-Cr catalysts are produced mainly by the precipitation of aqueous $FeSO_4$ with sodium hydroxide in the presence of air.[10,21,29] The simple and inexpensive production is, however, followed by an extensive washing process to reduce the sulphur content to below 0.2 wt%. The material is calcined at 500°C and consists of hematite (α-Fe_2O_3) and in some cases small amounts of γ-Fe_2O_3 if lower calcination temperatures are employed. X-Ray Diffraction (XRD) analysis identifies α-Fe_2O_3 with chrome incorporated by substituting iron in the lattice.[21] At Cr concentrations above 14 wt% separate phases between the iron and chrome are formed.

Commercially catalysts are supplied in the oxidized form and require activation prior to use. This is normally achieved in the presence of hydrogen or synthesis gas (**reaction 5**).

$$Fe_2O_3 + H_2 + CO \rightleftarrows Fe_3O_4 + H_2O + CO_2 \quad \text{----- (5)}$$

The activation is performed at temperatures between 315-460°C.[10,11,18,21] The reduction of Fe_2O_3 is exothermic and reaction heat has to be removed to avoid over reduction (**reactions 6 – 8**).

$$3Fe_2O_3 + H_2 \rightleftarrows 2Fe_3O_4 + H_2O \qquad \Delta H = -9.6\ kJ/mol \quad \text{----- (6)}$$

$$3Fe_2O_3 + CO \rightleftarrows 2Fe_3O_4 + CO_2 \qquad \Delta H = -50.7\ kJ/mol \quad \text{----- (7)}$$

$$3Fe_2O_3 + 4CO \rightleftarrows 3Fe + 4CO_2 \qquad \Delta H = -14.7\ kJ/mol \quad \text{----- (8)}$$

In reactions 6,7 and 8 steam (10 vol%) is also added to the reduction process to control the temperature and to avoid the formation of wüstite and metallic iron.[10,20] Metallic iron would lead to methanation and iron carbide formation. An average expected lifetime of the industrial catalyst is around 3 years.[11] The activity of the catalyst, however, declines with time on stream,[19,30,31] most probably due to the sintering of the magnetite and subsequent loss in surface area.

This catalyst is not so susceptible to sulphur and chlorine poisoning but deactivates due to carbon formation and heavy metals poisoning. H_2S and carbonyl sulphide (COS) have no particular effect on the process as long as the concentrations in the feed gas are below 100 ppm. Values above 100 ppm leads to the formation of FeS (**reaction 9**).

$$Fe_3O_4 + 3\ H_2S + H_2 \leftrightarrow 3\ FeS + 4\ H_2O \quad \text{----- (9)}$$

FeS also has WGS activity but is only about half of Fe_2O_3.[11] Catalyst fouling is observed due to "gumlike" deposits when the feedgas contains acetylene, butadiene, oxygen and nitric oxide.[10,21]

The presence of Cr in the final catalyst creates various disposal problems and hence the replacement of Cr by other elements have been studied.[32,33]

2.2.4.2 Low Temperature Water–Gas–Shift.

The exit gas from the HT WGS shift reactor needs to be reduced from the 2–3% CO to below 0.2%. The process gas is therefore further cooled to reach a favourable equilibrium. Below this temperature the steam would condense. The catalyst for this process is, however, a $CuO/ZnO/Al_2O_3$ catalyst and not an iron-based catalyst and will therefore not be further discussed.

2.2.4.3 "Sour Gas" Shift.

The conversion of sulphur containing gases from the production of syngas from coal requires the application of sulphur tolerant catalysts. These catalysts are normally molybdenum-based and will also therefore not be further discussed.

2.3 Fischer-Tropsch Synthesis.

2.3.1 Introduction.

One of the aims of the study is to produce a FT catalyst with the same physical properties as a typical "Ruhrchemie" iron-based FT catalyst and also to ensure that the newly synthesized catalyst has the same operational performance (Goal 5, Chapter 1) as typical Ruhrchemie industrial catalysts. In order to evaluate the performance of the new FT catalyst, a reasonable background understanding of the technology is required. A brief history of the Fischer-Tropsch process, important parameters and evaluation criteria are therefore discussed.

2.3.2 A brief history.

The process of CO hydrogenation has a history of almost 100 yrs and has been of chemical, economical and political interest through the years.[34]

The development of the coal-to-petroleum industry evolved in three stages:

1. Invention and early development of the Bergius coal liquefaction (hydrogenation) and Fischer – Tropsch synthesis (FT) from 1910 -1926.
2. Germany's industrialisation of the Bergius and FT processes from 1927 – 1945.
3. The transfer of the knowledge to the world from 1930 – 1990.

Petroleum had become an essential part of the world economics and growth by the 1920's. The mass production of transport means such as automobiles, planes and ships required extended reserves of petroleum.[35] The high energy associated with petroleum as opposed to solid fuels such as coal and wood inspired the shift from solid to liquid fuels. Some countries increased the import of petroleum (Germany, Britain, Canada, France, Japan and Italy). Germany, Japan and Italy also acquired, by force, petroleum from other sources during their World War 2 occupations of Europe and the Far East. Germany, France, Britain and Canada also produced petroleum from coal and bitumen sources during the 1920's - 40's.

The starting point for the process is generally credited to the discovery by Sabatier and Senderens that carbon monoxide and hydrogen form methane over Nickel and Cobalt catalysts.[36] Thereafter Orlov was probably the first to observe the formation of longer chain hydrocarbons.[37] In 1913 a BASF patent was filed reporting that under higher pressures and with a cobalt catalyst liquid products could be produced.[38] In 1923 Fischer and Tropsch disclosed their invention[39] and several patents of an iron catalyst, promoted with group 1 alkali metal compounds, for the production of liquid fuels from syngas (mixture of CO and H_2) at elevated pressures. The catalyst was very similar to the ammonia synthesis catalyst. Strategically, at the time, the importance of the find for Germany, with large coal reserves, was very important. Later strategic importance and commercialization of the Fischer-Tropsch process by SASOL, in South Africa, with large coal reserves was similarly important. Therefore during the second World War the process received intensive investigation in Germany and later in South Africa. During 1945-1955 the process also received attention in the USA due to fears of crude oil shortages as an impact of the growing motor transport sector. Although the fear was unjustified, valuable information was gathered during this period. Following 1955 the FT process received little attention internationally with the notable exception of South Africa (SASOL) where the process was commercialized between 1955 and 1970. Fears of crude oil supply in 1973 again led to renewed interest in the FT process.

The FT process gains in popularity whenever the oil supply is threatened or the price becomes excessive and as the oil reserves are placed under more pressure in future the process is likely to receive increased attention. The development of other processes that can convert several of the lower value products from Fischer-Tropsch to higher value products as well in the advances in

product and chemicals work-up has also increased the marketability of the process in recent years. Natural gas in remote areas can be utilized by the Fischer-Tropsch process and this will become important in the future. The production of syngas from coal remains an area of high capital and process cost and can account for 70% of the cost of such a facility.

Today Fischer-Tropsch is practised by SASOL and Petro SA in South Africa (Sasolburg, Secunda) and in Qatar (Ras Laffan). Proposed plants are under investigation by SASOL for Nigeria (under construction) and China. Shell has a Fischer-Tropsch plant in Malaysia (Bintulu) and is currently constructing a plant in Qatar (Ras Laffan - Pearl Project). Other commercial players are Rentech and STATOIL.

2.4 Fischer-Tropsch Catalysts.

For the purpose of this study only FT catalysts of commercial significance will be discussed. The catalysts will be discussed in terms of catalyst production, reduction/activation and general synthesis comments.

There are mainly three classes of catalysts used for Fischer-Tropsch Synthesis (FTS) namely:

1. Fused iron-based catalysts.
2. Precipitated iron-based catalysts.
3. Supported cobalt-based catalysts.

The iron-based catalyst precursor is normally in the oxide phase (hematite, ferrihydrite or magnetite) and later activated (reduced) in the presence of hydrogen, CO or mixtures thereof before used for the production of FT products. The active catalyst phases for FT are believed to comprise of iron carbides. Similarly the cobalt-based catalyst precursor is in the oxide phase and reduced in the presence of hydrogen to cobalt metal that is believed to be the active catalytic phase for the FT process. Each of these catalysts fit a unique environment and process conditions and has disadvantages and advantages depending on the application. A further complication is that these catalysts differ from the classical catalyst definition in that catalyst structural and phase changes, some reversible and some not, take place under synthesis conditions. The main areas of catalyst research involve increasing catalyst activity, changing selectivity from undesirable products, such as methane, to desirable products, such as long chain paraffin's, and increasing catalyst lifetime (chemically and physically).

Only the four group VIII metals Fe, Co, Ni and Ru, or metal complexes thereof, have sufficiently high activities for the hydrogenation of carbon monoxide. Ruthenium-based catalysts are the most active but the cost and availability of ruthenium makes it unsuitable for commercial application. Nickel complexes unfortunately have very high methane selectivity and the production of volatile nickel carbonyls results in a continuous loss in metal. Therefore iron and cobalt-based catalysts are the only commercializable options for FTS.

2.4.1 Fused Iron Catalysts for high temperature Fischer-Tropsch Synthesis.

Precursors to suitable catalysts for the high temperature FTS process are comparatively inexpensive. However, the volumes of spent catalyst discarded are significant. In South Africa a fairly inexpensive starting material is available but this situation may change in future or for other plants situated elsewhere in the world. Although the spent iron-based catalyst from this process was not extensively used during this study the importance of being able to recover the metals from this catalyst or to use it as a precursor material for the production of a low temperature FTS catalyst is important. Part of one of the aims of this study is to determine and understand the solubility of different iron phases (goal 3, Chapter 1) and therefore the high temperature iron-based catalyst is important.

2.4.1.1 Preparation of high temperature FT catalyst precursor.

The preparation of the catalyst currently used by Sasol is very similar to that of the ammonia synthesis catalyst, namely, fusion of iron oxide together with the chemical promoter K_2O and structural promoters such as MgO or Al_2O_3.

In the presence of air, molten iron oxide at about 1500°C should consist only of molten magnetite (Fe_3O_4). Theoretically wüstite (FeO) should oxidize to Fe_3O_4 and hematite (Fe_2O_3) would lose oxygen.[40] Under these high temperature conditions, however, in practice, due to the use of carbon electrodes in the arc furnace the chemical environment within the molten oxide pool becomes somewhat reducing and so some wüstite can be formed. The molten mixture of oxides is poured into ingots and rapidly cooled. The ingots are then crushed in a ball mill to the particle size distribution required for effective fluidization in the high temperature Fischer-Tropsch (HTFT) reactors. For effective mechanical strength properties, magnetite is the preferred iron oxide phase. If a hematite-rich ore is fed to the fusion furnace it has been observed that the cooled solid ingots

contained small voids (bubbles) presumably as a result of the release of oxygen during the fusion process. This decreases the mechanical integrity of the ingots.

In the 1950's Sasol imported a magnetite ore (Allenwood ore) from the United States for the production of the fused catalyst since this was the ore on which the design of the reactors had been based. Due to the relatively short useful life of the catalyst (< one year) in the HTFT operation, importation of the ore from the U.S.A. obviously increased the cost of catalyst manufacture. Research in the Sasol pilot plants was undertaken to evaluate the suitability of various locally available ores and oxides. It was found that mill scale from a nearby steelworks was in fact a suitable substitute for the imported Allenwood ore. The mill scale, however, was rich in wüstite and also was contaminated with sulphur-containing oils. It was therefore necessary to roast the mill scale at a high temperature in air to increase its ferric ion content and to burn off the contaminating oil and associated sulphur. Currently Sasol still uses this mill scale for the preparation of their HTFT catalysts.

During the solidification process structural promoter cations can enter into solid solution. Mg(II) and Al(III) have similar sizes to Fe(II) and Fe(III) ions and can therefore replace the iron ions in the crystal lattice. These promoter cations are therefore well dispersed inside the catalyst and form aggregates of Al_2O_3 or MgO during hydrogen reduction. These aggregates act as spacers and inhibit sintering of the ions crystallites in the iron catalyst.[41]

The regeneration of spent catalyst was investigated and it was found that a satisfactory catalyst could indeed be produced but this involved extensive air oxidation to burn off all the heavy oils and carbon deposits and to fully re-oxidize the iron.[40] The remaining oxide particles were not on specification regarding particle size distribution and alkali content and so had to be re-fused with promoter top-up. In principle the direct feeding of spent catalysts to fusion furnaces or smelters that are used in metallurgical industries is possible but this has not yet been commercially demonstrated. Because of the low cost of the locally available mill scale, the regeneration of spent catalyst has not yet been considered to be a priority development. The spent catalyst is also suitable as a feed material for the iron and steel industry.[40]

2.4.1.2 Reduction and Conditioning of the fused iron-based catalyst precursor.

Unreduced precipitated iron-based catalyst precursors normally have high BET (Surface areas determined by nitrogen adsorption theory) surface areas. Fused iron oxides catalysts are non-porous and hence their surface areas are virtually zero. Pre-reduction is therefore essential, both

to produce an iron phase active for FT and for the fused iron-based catalysts to develop the surface area required (high surface area = high activity) for acceptable FT activity. Reduction of iron(II) and iron(III) oxides is normally carried out with H_2 in the temperature range of 350-450 °C. The high temperatures are used to ensure a reasonable rate of iron reduction and also depend on the type and quantity of mechanical (strength) promoter added during the fusion process. The presence of structural promoters generally retards the reduction rate. The promoters have a lower affinity for hydrogen as opposed to the iron and the "spillover" effect of hydrogen that enhances the reduction rate of adjacent metal crystallites are inhibited. Precipitated iron catalyst precursors are readily activated for FT synthesis by mixtures of H_2 and CO. Thermodynamically, reduction of iron oxides with CO, should be more favorable than reduction with hydrogen by virtue of the larger negative ΔG value. Reduction with CO may therefore be expected to have a beneficial effect on the rate of reduction of iron oxides over hydrogen reduction. However, the reduction of fused iron oxide is markedly retarded when CO is present in the H_2.[38] This is illustrated by the results shown in **Table 2**. The presence of only 2% CO in the H_2 lowered the degree of reduction attained under set conditions by a factor of four. The negative effect of CO is probably linked to carbide formation. Any metallic iron formed would immediately, with any CO present in the gas react to form carbides. In this case, Hägg carbide is formed during the reduction process as shown in **Table 2**. The diffusion of the oxygen to the surface of the crystals during reduction may be retarded by the presence of an outer surface layer of carbide. In any event at 400 °C the formation of elemental carbon proceeds rapidly *via* the Boudouard reaction (**reaction 10**) and so the use of CO containing gas for reducing fused catalysts is not recommended.

Table 2. Percentage of reduction of promoted fused iron-based catalyst at 400 °C and 8 hours at fixed space velocity. [38]

Gas	Reduction (%)[a]	Phases present
100% H_2	80	α-Fe, Fe_3O_4
98% H_2 + 2% CO	20	Fe_5C_2[b], Fe_3O_4
100% CO	4	Fe_5C_2[b], Fe_3O_4

a Amount of iron in the oxide form converted to either metallic or carbidic iron.

b Hägg carbide.

2.4.1.3 Fischer-Tropsch synthesis with the fused iron-based catalyst.

The fine iron-based catalyst precursor particles are reduced to the metallic form before being introduced into the reactor. When the reduced particles are exposed to FT synthesis conditions the iron metal is rapidly converted to iron carbide (Hägg carbide) due to the presence of CO. This is a highly exothermic reaction and localized hot spots may damage the catalyst by means of sintering,

fouling and excessive carbon deposition. Therefore the reactor is normally commissioned such that low CO partial pressures exist initially to counter excessive heat formation. Inside the reactor the core of the activated catalyst particle is later found to be magnetite while the area closer to the surface is iron carbides. The carbides are generally accepted to be the catalytically active phase for Fischer-Tropsch Synthesis. During HTFT carbon formation also takes place according to the Boudouard reaction (**reaction 10**).

$$2CO \rightarrow C + CO_2 \text{ ----- (10)}$$

This means that elemental carbon is formed continuously during the FT process under these conditions. The formation of the elemental carbon on the catalyst particles results in a change of the particle density as well as break-up of the catalyst particles and catalyst fines (fragments) are produced. The fine material and lower density material is entrained in the gas product stream leaving the reactor and is therefore undesirable. To counter the formation of carbon, various additives to the catalyst formulation have been investigated.[38, 42-44] The conditions under which FT is operated have also been extensively studied in order to reduce carbon formation.[45-47] Currently the formation of carbon is still the primary reason that the working catalyst has to be frequently replaced.

Fused iron catalysts are generally alkali metal oxide promoted. This enhances both activity and selectivity depending on the alkali metal oxide loading. Higher loadings of alkali metal oxide generally increase the activity of the catalyst up to a maximum. Alkali metal oxide promotion also suppresses methane formation. Currently a methane selectivity of around 8% is attainable.[4] Alkali metal oxide addition also increases the rate of free carbon deposition which has several negative effects. Carbon deposition causes the particles to swell and break and also changes the density of the catalyst so that it is carried out of the reactor as previously described. Alkali metal oxide promotion further leads to increased organic hydrocarbon acid formation which can cause equipment damage in the reactor or down stream applications. The catalyst is therefore added and removed online to maintain a certain age distribution inside the reactor. Liquid product generated from HT FTS has a high olefinic content. Olefins are high value chemicals and the building blocks for many processes. Promoter addition is also aimed at reducing secondary olefin reactions such as hydrogenation. A decrease in the rate of carbon deposition is also targeted with promoter modifications. Alkali metal oxide surface distribution is also important and a better dispersion is aimed for.

2.4.2 Precipitated Iron Catalysts for low temperature Fischer-Tropsch synthesis.

This study mainly consists of work performed on the spent low temperature precipitated iron-based catalyst, used for both slurry bed and fixed bed applications. Once the metals (Fe, Cu, K^+, Na^+) have been recovered, as metal nitrates, by nitric acid dissolution of the spent catalyst the standard preparation procedure needs to be followed to produce a fresh catalyst precursor.

2.4.2.1 Preparation of the low temperature Fischer-Tropsch catalyst precursor.

A typical iron-based low temperature FTS catalyst precursor[48] can be prepared by using the "Ruhrchemie" process. The "Ruhrchemie" catalyst is prepared in the following fashion: Scrap iron, of a suitable purity, together with metallic copper is dissolved in nitric acid. The near boiling solution of iron and copper nitrate (40g Fe, 2g Cu per litre) is then poured into a hot solution of Na_2CO_3 under vigorous agitation until a pH of around 7 is reached. Precipitated, hydrated ferric oxide is then filtered and thoroughly washed with distilled water to remove the sodium ions present as sodium nitrate. The precipitated mixed metal oxide cake is then re-slurried with deionised water and silica added as potassium waterglass (potassium silicate). Sufficient nitric acid is added so that after filtration 5g K_2O / 100g of Fe was retained in a gel like cake. In order to compare different catalyst formulations, compounds are normally expressed as mass of compound per iron content. This makes it easier to evaluate the effect of an additive when compared to the amount of iron in the final catalyst. The iron is present as ferrihydrite of hematite and not metallic iron but when presented in this fashion different catalyst systems are more easily evaluated with regards to the interaction between the promoters and iron content. This process is a batch process but can also be done continuously by mixing the metal nitrate solution with the sodium carbonate and controlling the resultant slurry pH at around 7.[49]

For the fixed bed application the above prepared filtercake is extruded and dried.[38] For slurry bed applications the resultant filtercake is spray dried[50] into spherical particles. The final active slurry bed catalyst precursor is eventually submitted to a more challenging environment inside the reactor and is therefore heat treated to improve the strength. The heat treatment is normally between 400–500 °C.[41] The heat treatment causes a BET surface area loss of about 15% but no appreciable loss in activity. For fixed bed applications extrudite break–up is less of a problem and therefore the catalyst precursor is not heat treated.

A typical catalyst precursor contains 25 g SiO_2, 5 g Cu and 5 g K_2O per 100 g of Fe.[41] The silica does not act as a classical support but rather as a binder and sintering inhibitor. Of primary

importance is the surface area and pore volume of the final catalyst as this is the surface available for reaction. Factors that influence the pore volume and area of the precipitate are the iron and carbonate solution concentrations, order of precipitation reagent addition, time for precipitation as well as the final pH. The drying or calcination of the catalyst is also important due to the amount of shrinkage that takes place. The shrinkage is important for fixed bed application where more catalyst can be loaded if pre-shrunk.

2.4.2.2 Reduction and Conditioning of the low temperature Fischer-Tropsch catalyst precursor.

During conditioning (reduction) as well as FT synthesis various phase changes of the iron species occur. These phase changes are of primary importance when the dissolution behaviour of the spent catalysts is evaluated. Reduction studies also gives insight into which condition relates to different phases formed as well as their surface area characteristics. The available surface area for dissolution could also influence the rate of dissolution. Reduction and conditioning methods will here only be briefly discussed but later discussed in more detail.

Reduction is a necessity for iron-based catalyst activation and is normally done at relatively mild conditions in comparison to FT synthesis conditions. The objective is to generate large metallic or iron carbide surface areas. Pichler reported that an unreduced iron-based catalyst was not very active but that reduction at 360°C did not improve matters much.[39] Scheuermann reduced at 200 °C and obtained an active catalyst, whereas reduction at 300 °C resulted in a lower activity.[41] In these studies, H_2 was used as the reduction medium or mixtures of H_2 and CO or CO only.[41] The FT selectivity was also influenced by the reduction temperature. It was found that pre-reduction with hydrogen at 300 °C produced a more active catalyst than one reduced with syngas at 230 °C but with lower wax selectivity. More recently Bukur[51-53] and Davis[54] re-investigated reduction procedures. Davis reported that, compared to activation with hydrogen-rich syngas, activation with CO or CO rich syngas resulted in more active catalysts. Bukur reported that a catalyst precursor reduced with H_2 at 250 °C had a higher activity but lower wax selectivity than the same catalyst precursor reduced with CO at 280 °C. When the H_2 reduction temperature was lowered to 220 °C, however, there was a smaller difference in the wax selectivity. A catalyst precursor reduced with H_2 at 250 °C for four hours was found to be significantly more active than when it was reduced for eight hours at the same temperature. The activities of all the catalysts declined with time on steam. At steady state the activity of the catalyst reduced with CO at 280 °C was the highest. The reason for adding copper compounds to the precipitated $Fe_2O_3/CuO/K_2O/SiO_2$ catalyst precursor is to facilitate the reduction of the iron oxide at lower temperatures, typically 220 °C.[40] Increasing the

temperature of reduction of a Cu-free catalyst does increase the rate of reduction but generates a catalyst with inferior FT activity performance.

The activation procedure of the catalyst used in the Sasol multi-tubular fixed bed reactors is carried out in several steps.[40] The extrudates are first pre-shrunk by H_2 reduction at atmospheric pressure. This initial reduction rate is high and about 20% of the theoretical amount of water expected from the reduction of Fe_2O_3/CuO is produced in this period. This initial rapid reduction phase is characterized by a marked exotherm, which is probably due to the exothermic reductions of the nitrates and copper oxide as well as the exothermic reduction of hematite to magnetite. In practice the reduction is not taken beyond this stage as further reduction only occurs very slowly. After the partial reduction procedure described above the catalyst precursor is coated with wax to protect it from re-oxidation and then loaded into the fixed bed FT reactors. The temperature of the reactor is raised to about 200°C under a H_2 atmosphere in order to avoid the formation of volatile iron carbonyls which would otherwise contaminate the FT wax product. Synthesis gas is then slowly introduced and the system is taken to full FT operating conditions. During this 'conditioning' period the mixed iron oxide catalyst precursor is converted to Hägg carbide (Fe_5C_2), the active Fischer-Tropsch catalytic phase. This process takes place over several days.

In comparison to the activation procedure for the fixed bed catalyst just described the reduction of the slurry bed catalyst precursor is done in a separate vessel from the synthesis reactor. The catalyst precursor is loaded, into the reduction reactor, in molten wax and activated with H_2 , CO or mixtures thereof depending on the required catalyst Fischer-Tropsch synthesis requirements. No evidence of metallic iron has been detected as the metal would rapidly form a carbide in the presence of carbon monoxide.

2.4.2.3 Low temperature Fischer-Tropsch synthesis with the precipitated iron-based catalyst.

Fixed bed LTFT operations behave as a trickle bed because under normal operational conditions the wax product is liquid and flows down the reactor. Washing the catalyst with a solvent results in a big increase in conversion but the effect is short lived as the catalyst pores are again filled with wax product produced. This is, however, an indication that diffusion restrictions have a large effect on the reaction rate. This was also confirmed by experimentation showing that conversion is inversely proportional to the catalyst particle size. For slurry bed applications the catalyst particles are sufficiently small so as to negate mass transfer limitations. During operation, the activity of the catalyst declines with time on line. BET area determinations show a decrease in surface area and

XRD patterns become sharper and hence crystal growth takes place under synthesis conditions. Crystal growth or sintering is enhanced by the addition of water to the reactor and a further loss in activity may also be attributed to oxidation of the iron under elevated water partial pressures.

For fixed bed applications the reactor was carefully shutdown under inert conditions and samples of active catalyst were carefully unloaded at different parts of the reactor and analyzed as well as placed under FT synthesis conditions in a laboratory scale reactor to determine activity. From these tests it was found that catalyst at the top of the reactor, where the gas is introduced, showed a marked loss in activity with time on line. Tests revealed that the main cause of this loss in activity was due to sulphur poisoning and not sintering of the catalyst. As the gas proceeds down the reactor the partial pressures of reagents become less and product partial pressures increase. Therefore, the catalyst lower in the reactor sees higher partial pressures of water which enhances sintering and oxidation of the catalyst to Fe_3O_4. This can be seen when BET surface area analyses show a marked decrease towards the bottom of the reactor. XRD patterns also show an increase in the crystallinity from catalyst towards the bottom of the reactor. The lower activity of the catalyst at the bottom of the reactor is therefore mostly attributed to sintering and oxidation while the top part of the bed is damaged by sulphur poisoning.[55]

For the LTFT slurry bed applications the catalyst is continually well mixed and sees more uniform conditions. All the catalyst is therefore exposed to sintering, sulphur poisoning etc. to the same extent.

2.4.3 Supported Cobalt Catalysts.

Although cobalt-based Fischer-Tropsch catalysts are considered outside the boundaries of the present study, for the sake of completeness it is important to present a short summary of the principles surrounding this important FT catalyst.

2.4.3.1 Preparation of low temperature, supported, cobalt-based catalyst precursor.

Cobalt-based catalyst precursors are generally prepared by deposition of the cobalt containing compounds onto a pre-shaped support.[56] Cobalt-containing solutions are used to impregnate the pores and surface of the support and dried in order to precipitate the cobalt compounds. Typical supports can include silica, alumina, titania, zirconia carbon or mixtures thereof.[40] The support is generally made *via* spray drying in order to obtain particles of similar size and sphericity for optimal

strength and "fluidization" properties inside the slurry bed reactor. For fixed bed applications extruded supports are used.

2.4.3.2 Reduction of the low temperature, supported cobalt-based catalyst precursor.

Cobalt compounds are impregnated onto the support along with other metal compounds such as lanthanum, platinum, palladium, rhenium and ruthenium. These metals compounds mainly aid in the reduction process, being more easily reduced than cobalt, to provide an active surface. Reduction takes place in the presence of hydrogen.[57]

The distribution of the eventual active catalytic metallic cobalt crystallites of the correct size on the support is important and therefore various methods have been described to control the crystallite size.[58] Various techniques to modify the supports in order to maintain the reduced cobalt metal crystallite size can be done. Originally supported cobalt catalyst precursors (with thoria on kieselguhr) were used when FT originated. Modern day catalysts look different due to the understanding and analysis of the geometry of the cobalt crystals on the surface. Cobalt catalysts, unlike precipitated iron catalysts, can be rejuvenated, in some cases to activities higher than the original catalyst.

2.4.3.3 FT Synthesis of the precipitated and supported low temperature cobalt-based catalyst.

The hydrocarbon products formed by supported cobalt catalysts consist predominantly of paraffins with a high degree of linearity.[59] This is in contrast to the iron catalyst that usually produces olefins as a primary product. If high CO concentrations are employed the olefin yield from the cobalt catalyst can become economical. The methane selectivity of cobalt catalysts is normally higher than that of iron and the amount of oxygenated components lower.

One advantage of cobalt is the very limited Water Gas Shift (WGS) (**reaction 4**) activity of the system which means that CO_2 is not formed in significant quantities under synthesis conditions.

$$CO + H_2O \rightleftharpoons H_2 + CO_2 \text{ ----- (4)}$$

This enables the exclusion of CO_2 removal in the down stream process and also reduces the amount of gasses that have to be handled. For precipitated low temperature iron applications, large volumes of CO_2 are formed. Cobalt-based catalysts are significantly more expensive the iron

catalysts but are more active and have a longer lifetime. Cobalt is very susceptible to poisons, specifically sulphur. Extensive gas clean-up will be required if coal-derived syngas is to be used for cobalt catalysis in a FTS environment in order to render the feed gas sulphur free.

2.5 Chemical concepts for engineering design.

2.5.1 Introduction.

Several concepts were developed that are used to describe the catalyst rate of reaction and product distributions in order to allow scientists and engineers to evaluated catalyst systems. The purpose of this section is to describe these basic concepts in order to understand what is expected of a potential catalyst. It ties in with goal 5 (chapter 1) of this study in order to evaluate the newly prepared catalyst from the recovered spent catalyst material. Various different concepts are encountered in the Fischer-Tropsch literature and concepts used in this study will be explained in order to evaluate the performance of a particular catalyst in a micro reactor. Emphasis will be on the LTFT iron-based catalytic process as this process was the topic of the study.

2.5.2 Stoichiometry (H_2:CO ratio).

Stoichiometry is commonly used to describe the ratio in which components react to form products. For Fischer-Tropsch synthesis the most important stoichiometry revolves around the relative consumption of H_2 and CO, that is the H_2:CO ratio.

The feed H_2:CO ratio into a FT reactor determines to some extent the product spectrum obtained. Ideally, if linear long-chain hydrocarbons are targeted, the process should consume 2 hydrogen molecules for every CO molecule. This would relate to a usage ratio of 2, meaning the ratio of consumption of hydrogen relative to CO. In reality, however, various reactions take place and the usage ratio is much lower. **Table 3** shows the usage ratio's for some FT products. For a typical LTFT operation the usage ratios can be between 0.7 and 1.9. The importance of the ratio's can be explained with a few examples. In the examples below the feed ratio is the ratio of H_2:CO that enters the reactor. Usage ratio refers to the H_2:CO ratio that is consumed during the bulk of the run in an FT reactor and tail ratio refers to the H_2:CO ratio of gasses that exit the reactor.

If the feed gas ratio is higher than the usage ratio the tail gas ratio will be higher. For example if the feed gas ratio is 1.6 and the usage ratio is 1.5 it will lead to a tail ratio of 1.7. Alternatively the feed

ratio may be lower than the usage ratio. This will lead to a tail gas ratio that is even smaller. This will mean that the reaction becomes starved of CO. For example if the feed gas ratio is 1.5 and the usage ratio is 1.6 then the tail gas ratio may be 1.4.

Table 3. Usage ratios for selected Fischer-Tropsch reactions in the absence of other reactions.

FT product	Reactions	H_2:CO ratio
CH_4	$CO + 3H_2 \rightarrow CH_4 + H_2O$	3
C_2H_6	$2CO + 5H_2 \rightarrow C_2H_6 + 2H_2O$ $(H_3C\text{-}CH_3)$	2.5
Alkanes	$nCO + (2n+1)H_2 \rightarrow C_nH_{(2n+2)} + nH_2O$ (e.g. $H_3C\text{-}(CH_2)_6\text{-}CH_3$)	(2n+1)/n
Alkenes	$nCO + 2nH_2 \rightarrow C_nH_{2n} + nH_2O$ (e.g. $H_2C{=}CH\text{-}CH_3$)	2
Alcohols	$nCO + 2nH_2 \rightarrow C_nH_{(2n+1)}OH + (n\text{-}1)H_2O$ $(H_3C\text{-}OH)$	2

A simplified interpretation of the implications of these ratios lies therein that in a hydrogen-rich environment (high H_2:CO ratio) the chances of chain growth termination may occur more readily because the hydrogen will saturate the carbon and no further reaction will take place. In a CO enriched environment C incorporation in the structure i.e. growth of a C_nH_{2n} fragment or $C_{n+1}H_{2n+2}$ fragment is higher. Hence longer-chain aliphatic or olefinic products can be expected.

The importance of CO_2 and water vapour varies depending on the process conditions. At elevated temperatures the Water Gas Shift reaction becomes more pronounced and the CO_2 contributions become more important. When CO_2 becomes a reagent, H_2 now becomes a product. This can skew results as the process now consumes and produces H_2.

2.5.3 Conversion.

The conversion performance is a measure of the amount of reactants, H_2 + CO, consumed during the Fischer-Tropsch reaction. A measure often used for Fischer-Tropsch Synthesis is H_2 + CO conversion. This implies that the difference in H_2 and CO concentrations present in the feed and tail gasses are expressed as a percentage of the feed concentrations. A H_2 + CO conversion of 50% would imply that half of the reagents were present in the tail gas. Care must be taken when these results are interpreted because FT consumes CO and Hydrogen and the WGS reaction also consumes CO but produces H_2. When reactor conditions are changed and the relative reaction rate of these two reactions are affected differently, the H_2 + CO conversion have to be interpreted with care. Due to this limitation the CO conversion to FT products was developed. This method subtracts the WGS reaction by using the CO_2 generated. By measuring the CO_2 evolution, the

amount of hydrogen produced by the WGS reaction is known and the amount of CO consumed by the WGS reaction is known. From these results the amount of CO and H_2 consumed for the FT reaction can be calculated.

Other conversion calculations used are CO conversion (to both WGS and FT) and hydrogen conversion or combinations of both.

For HT FTS the WGS reactions are sometimes close to equilibrium and the reaction can go both ways. Cobalt catalysts exhibit virtually no WGS activity and this simplifies the interpretation of results somewhat.

2.5.4 Selectivity.

By knowing the conversion, it is possible to describe how much of the reagents were converted to products. To describe the way in which the products are distributed is equally important. The product distribution can broadly speaking be regarded as a measure of catalyst selectivity. A convenient way to express product selectivities is % carbon selectivity. It may be desirable to express selectivity as a mass % of total products. Moles are easily transferred to mass using the component molecular mass. Carbon selectivities and mass selectivities produce similar numbers because the hydrocarbons are made up of $-CH_2-$ building blocks. The exceptions are methane and low molecular mass alkanes as well as oxygenated products.

Typical selectivities for different components are shown **Table 4**. Typical selectivities that are often used when catalyst performance is evaluated are methane selectivity and CO_2 selectivity. Methane is an unwanted product, but gives an indication of the product range expected. The FT product range can be described by using a chain polymerization kinetic model developed by Anderson, Schultz and Flory. The model indicates that high methane weight fractions will lead to low chain growth probability, α, (**Figure 2**) and **equation 11**. The product range can therefore be predicted to some extent if certain compounds are identified. From **Figure 2** it can be seen that high methane product mass fractions indicate that longer chain lengths, high α-values, are not expected. Similarly high mass fractions of C_2-C_4 also indicate that little wax is to be expected from the product slate.

Table 4. Fischer-Tropsch product range at 2 MPa expressed as % selectivity's on a C atom basis.

Catalyst Reactor Type Temperature	Cobalt Slurry 220 °C	Iron Slurry 240 °C	Iron Fluidized 340 °C
CH_4	5	4	8
C_2H_4, $H_2C=CH_2$	0.05	0.5	4
C_2H_6, H_3C-CH_3	1	1	3
C_3H_6, $H_3C-CH=CH_2$	2	2.5	11
C_3H_8, $H_3C-CH_2-CH_2$	1	0.5	2
C_4H_8, $H_3C-CH_2-CH=CH_2$	2	3	9
C_4H_{10}, $H_3C-(CH_2)_2-CH_3$	1	1	1
C_5 - C_6	8	7	16
C_7 – Wax fraction boiling point < 160 °C	11	9	20
Wax fraction boiling point between 160-350 °C	22	17.5	16
Wax fraction boiling point > 350 °C	46	50	5
Water soluble oxygenates	1	4	5

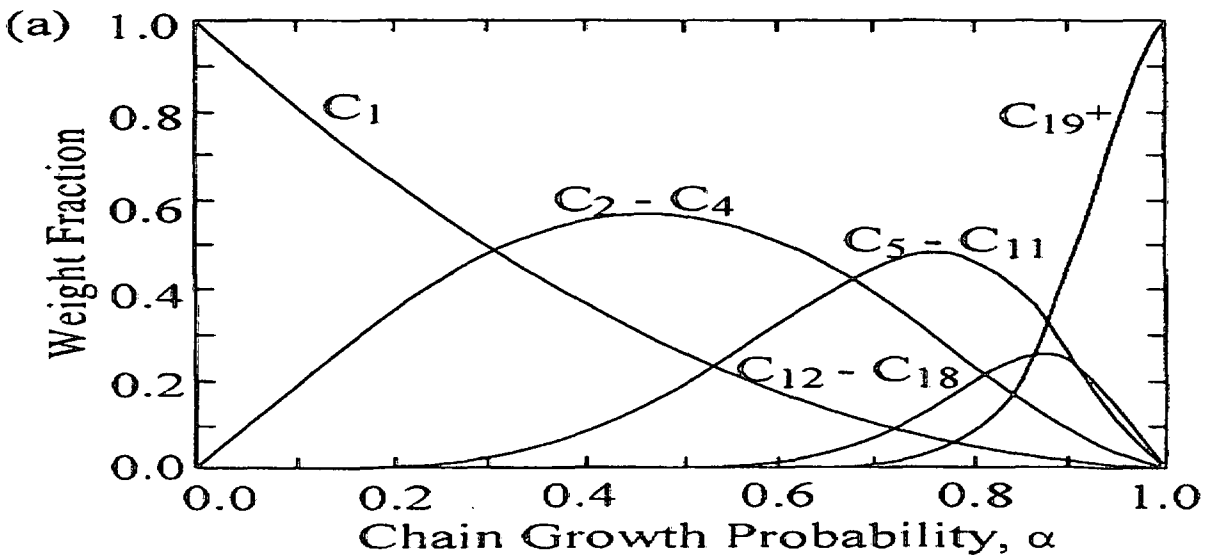

Figure 2. Anderson Shultz Flory distribution of weight fraction of products as a function chain growth probability during FTS.

A catalyst system with high methane selectivity is therefore likely to produce a lighter product spectrum and *vice versa*. CO_2 selectivity is an indicator of the WGS reaction and high CO_2 selectivity would indicate that the catalyst is active towards WGS. When the CO_2 selectivity increase with time on stream it indicates that the catalyst is being oxidized to magnetite which is a known WGS catalyst.

2.5.5 Rate of reaction (kinetics).

The rate at which the reagents are converted to products are described by various methods. For the purposes of this study the concepts will only briefly described as the purpose of this study is only to produce a catalyst that is on par with a typical "Ruhrchemie" iron-based FTS catalyst. Kinetic studies were considered outside the boundaries of this study. As long as similar operating conditions are used in a comparative study an understanding of the kinetic process is not essential. A proposed mechanism for Fischer-Tropsch synthesis will also be omitted since it falls beyond the scope of this study.

Chemical reactor design and control requires knowledge of the macrokinetics. For gas applications the effect of partial pressures and temperatures on the rate of the reaction is used to develop kinetic models. Many kinetic models for Fischer-Tropsch have been proposed[60,61,62] (**equations 15–17**).

$$r = K\frac{(\rho_{H_2}^{m} / \rho_{CO})}{1 + K'\left(\frac{\rho_{CO_2} + \rho_{H_2O}}{\rho_{CO} + \rho_{H_2}}\right)^{n}} \qquad \text{-----(15)}$$

$$r = K\frac{\rho_{H_2}^{2}\rho_{CO}}{1 + K'\rho_{H_2}^{2}\rho_{CO}} \qquad \text{-----(16)}$$

$$r = K \frac{\rho_{H_2}}{1 + K' \left(\frac{\rho_{H_2O}}{\rho_{CO}} \right)} \qquad \text{-----(17)}$$

These similar equations all have limited use and the quest for an accurate Fischer-Tropsch rate law continues. For the purposes of this study, only the catalyst intrinsic activity will be reported. The intrinsic activity of the catalyst will be expressed as moles of CO converted per unit time per gram of catalyst at specific reactor conditions.

2.6 Iron Dissolution Literature.

2.6.1 Introduction.

In order to reclaim iron from spent iron-based FT catalyst, the solubility properties of iron oxides especially play a role. Iron oxides are compounds with low to very low solubility.[1] In nature, Fe(III) oxides should therefore be in an immobile from. However, large amounts of iron circulate in all parts of the ecosystem. Dissolution of the iron oxides therefore has to take place. Processes in nature include complexation of iron by compounds in plant roots, fungi and bacteria, siderophores and the storage of iron ferritin in biological media. Transferrin serves as a iron shuttle in mammals. These processes are, however, slow and although of extreme importance have little relevance to industrial processes where the rate of dissolution required is much higher.

In industry, processes of importance are the rate of dissolution of iron oxides, acid leaching of iron ores and the removal of corrosion products form equipment surfaces. The cleaning of heat transfer equipment plays a prominent role as this improves the heat transfer rate inhibited by the iron oxide. Important characteristics investigated are the effect of passive layers on iron and pickling of steel. Corrosion products and also millscale from steel are usually removed using strong acids or acid / complexant mixtures.

The dissolution behaviour of iron oxides is normally approached in two ways namely:

1. The use of the electrochemical aspects and in particular the effect of applied potential.
2. The solution parameters and solid properties such as surface area and crystal morphology.

2.6.2 Dissolution Reactions and Mechanisms.

Iron oxide dissolution has been the topic of several reviews.[63-65] The driving force for the dissolution is the extent of under-saturation with respect to the oxide. Under-saturation is required for dissolution just as super-saturation is required for precipitation. Therefore the rate of dissolution should increase as the amount of under-saturation increases, meaning that low concentrations of dissolved iron species will have a greater driving force for dissolution as compared to high concentrations of dissolved iron species at similar conditions. Dissolution of anodic Fe oxide films is often performed in nearly saturated acid solution while metal ore leaching is often done with high under-saturation (metal content) to increase dissolution rates. The dissolution process can be accelerated at low pH and the use of chelating ligands.

The properties that influence the rate of dissolution are the properties of the overall system, properties of the oxide and properties of the solution phase. In general the surface area of the iron oxide and the composition of the solution are important parameters. When studying the dissolution of iron oxides it has been noted that no unique dissolution rate can be attributed to a given oxide.[66] This means that if the surface areas of different fractions of the same sample are normalized, dissolution rates are determined by the structural factors of a given sample. Therefore two samples taken from the same batch of iron oxide may dissolve at different rates. Only if a sample was 100% crystalline would the dissolution rate for that sample be constant and predictable. However, very few iron oxide materials are extremely crystalline and hence the dissolution behaviour depends on actual surface defects. Defects or surface irregularities may be point defects, dislocations, micro fractures, kinks, domain boundaries, corners edges and ledges. The degree of irregularities from one sample to the next may differ and hence a difference in dissolution rate is observed.

Chemical "additives" to the acidic solution may retard or enhance the rate of dissolution and have therefore been extensively studied. Additives may aid dissolution *via* complexation reactions, but most often the additive more easily adsorbs on the metal oxide surface and raises or lowers the energy between the surface atoms and the bulk solvent. pH also has a strong influence on the dissolution of iron oxides. For instance at atmospheric pressure the dissolution of crystalline Fe_2O_3 requires a pH of less than one. pH also influences the electrochemical surface and hence redox processes at a specific potential are determined by the pH. Iron dissolution can proceed by a number of paths namely protonation, complexation, reduction (Fe(III) – Fe(II)), photochemical and biological paths.

2.6.2.1 Protonation.

In general the reaction between protons and iron(III) oxides can be written as **reaction 18**.

$$FeOOH_{aq} + 2H^{+} \rightarrow [Fe(OH)]^{n+}{}_{aq} + H_2O \text{ ----- (18)}$$

A detailed dissolution mechanism has been has been proposed[67] and is shown in **Scheme 1**.

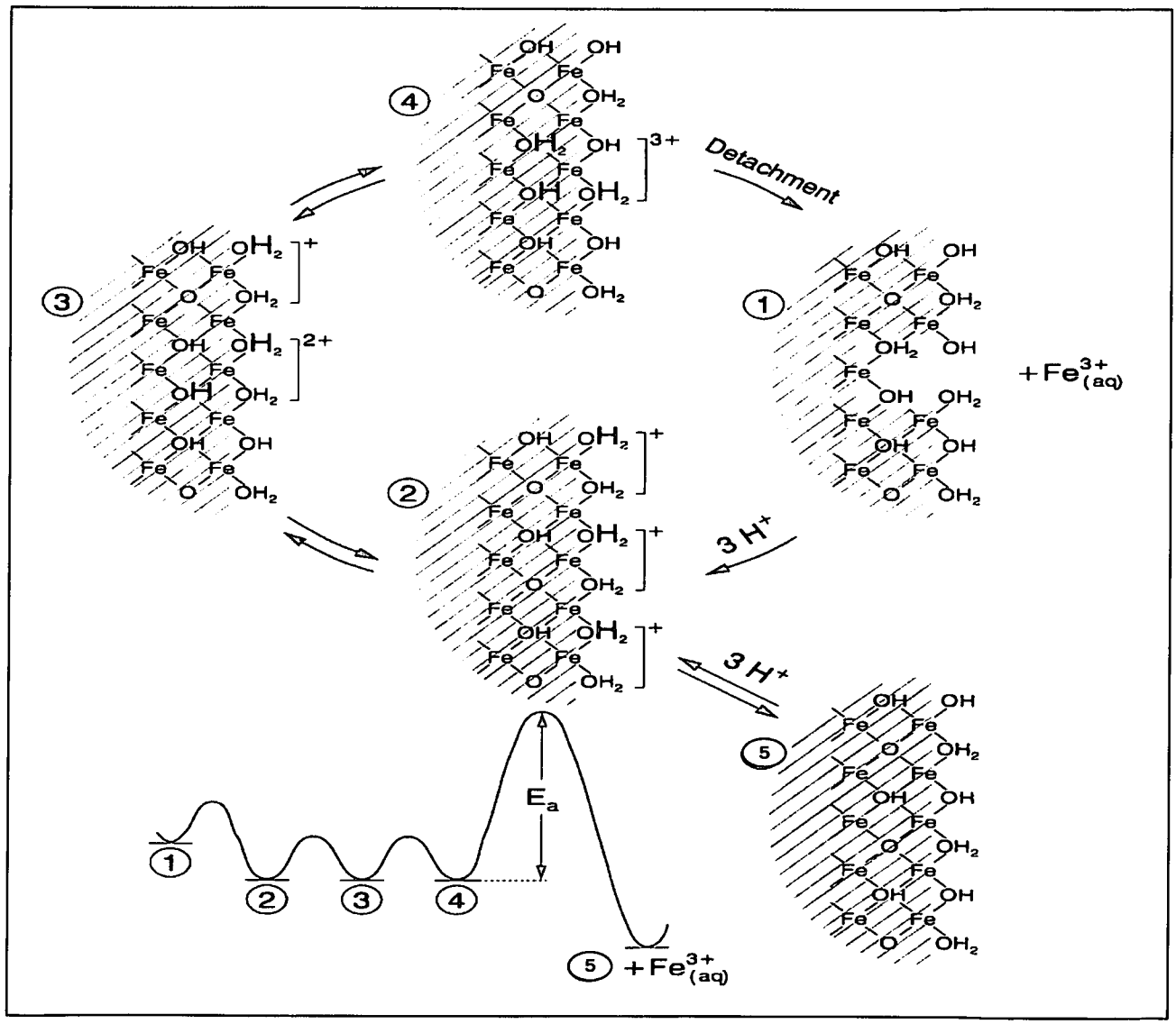

Scheme 1. Representation of the consecutive steps of dissolution by protonation. (Adapted from Stumm & Furrer[59]). The shaded area represents the solid particle cluster in the iron oxide bulk.

The dissolution process is started by observing a surface Fe atom on a iron oxide particle that is coordinated at alternating OH and OH_2 surface ligation pattern spacings creating neutral charge

see position 1, **Scheme 1**. The proton bonds to the OH group changing the surface structure from a neutral surface species, $s\text{-}FeOHOH_2$, to a positively charged $s\text{-}Fe(OH_2)_2$ group as shown in position 2. Subsequently two more protons can be adsorbed per iron atom. The proton adsorption weakens the interior Fe-O bond probably by polarization and so promotes H^+ transfer form the particle surface to the interior; see section labelled 3 and 4 (**Scheme 1**). Further bond polarisation promotes detachment of the iron from the bulk oxide. Included in **Scheme 1** are the relative activation energies for the various steps. Activation energies for the proposed mechanism show the detachment step is rate limiting as it has the highest activation energy.

The initial dissolution rate can be very high and then the rate drops to a steady state. The initial high rate has been shown to often only involve 1% of the solid.[68,69] The rate of dissolution by protonation can often be described by the relationship

$$r = k[H^+_{aq}]^n$$

Here *n* ranges between 0 and 1 and *k* is a constant. The above equation arises from the relationship between H^+ and adsorbed protons.

The same principal may hold for the anion associated to the proton when the anion replaces surface OH groups and thereby assists in the release of iron cations. Cl^- ions have a strong dissolution promoting effect whereas ClO_4^- has a much lower affinity with the oxide surface and therefore has little effect.

2.6.2.2 Complexation.

Organic and inorganic ligands with a suitable functional group can substantially increase the rate of dissolution of iron oxides. Ligands can enhance, retard or even block dissolution. Ligands can aid in dissolution by adsorption or by complexation with Fe in solution.[70]

The first mechanism involves ligand adsorption on the surface of the Fe oxide. This weakens the Fe-O bond to neighbouring atoms that leads to the detachment of the Fe^{3+} complex. Examples include the oxalate-promoted dissolution of goethite, hematite and ferrihydrite over the pH range 3 – 5, (**Figure 3**). In the absence of the ligand, dissolution at $3 < pH < 5$ is essentially zero.[55]

Stumm and Furrer[55] proposed that the dissolution of an M^{3+} oxide by an organic ligand through a surface reaction involved three consecutive reactions, namely ligand adsorption, metal detachment and proton adsorption/surface restoration. Protons therefore facilitate the process by protonating the OH groups. The protonated OH_2 group then weakens the Fe–O bond and acts by increasing

the positive charge of the oxide surface and promoting ligand adsorption. On the other hand, as the pH falls, protonation of the ligands in solution increase and therefore the extent of both ligand adsorption and complex formation in solution falls. This leads to a reduction in the dissolution rate. The balance between surface protonation and ligand protonation means that there is often a specific pH at which optimum dissolution is obtained. For example the optimum pH for the dissolution of hematite in citric acid is pH 4 – 5 whereas for oxalic acid the maximum is at pH 1.5.[71] Ligands which promote dissolution are thought to form mononuclear surface complexes, whereas those that inhibit the process form binuclear surface complexes. The former will promote detachment whereas the latter forms a stronger bond to the surface.

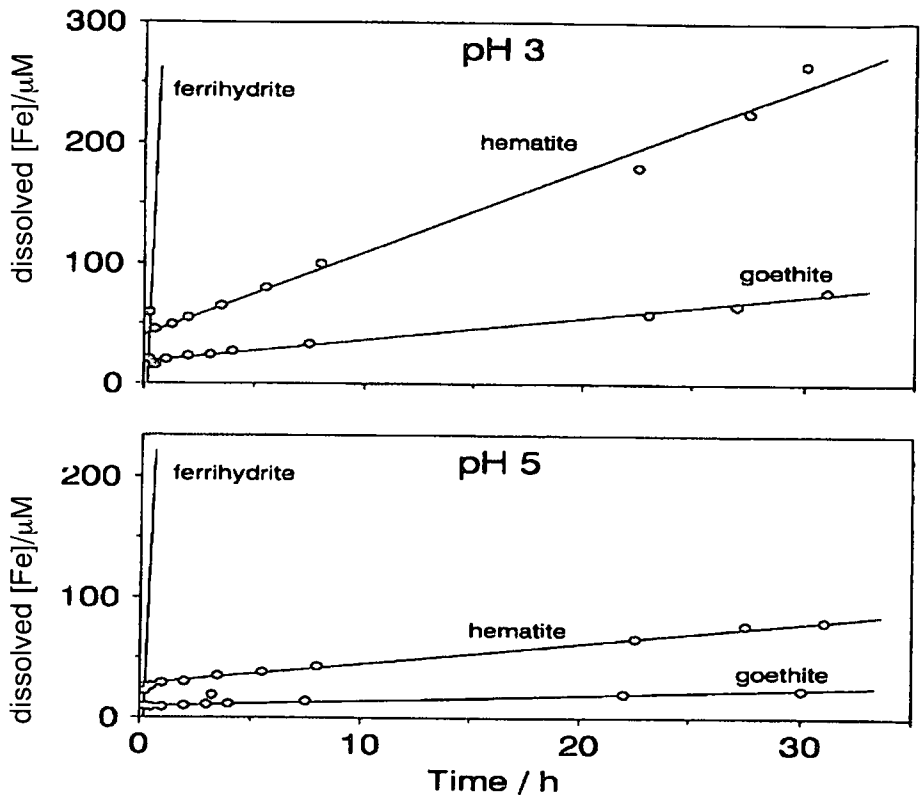

Figure 3. Initial stage of dissolution of ferrihydrite, goethite and hematite in the presence of *$10^{-3}M$* Oxalate at pH 3 and 5 (adapted from Stumm[72], 1985).

2.6.2.3 Reduction.

The covalent bond between iron(III) cations and oxygen ligands can also be weakened by Fe(III) reduction to Fe(II). In biological processes, reductive dissolution is by far the most important dissolution method.[1] Reductive dissolution is also often used for the removal of corrosion products from piping in industrial equipment and the bleaching of kaolin.[1] Reductive dissolution of iron has

therefore been widely studied. Reductants investigated include dithionite, thioglycolic acid, thiocyanate, hydrazine, ascorbic acid, dihydrogen sulphide, gaseous hydrogen, fulvic acid, fructose and sucrose. The formation of Fe(II) by Fe(III)) reduction to promote iron cation dissolution can be enhanced by the adsorption of an electron donor, on a surface of the Fe(III) oxide cluster particle. Similar enhancement is found by cathodic polarization of an electrode supporting the iron oxide and by transfer of an electron from within the bulk to a iron oxide cluster surface. Reduction from Fe(III) to Fe(II) destabilizes the coordination sphere of the iron cluster both due to a loss of charge and because of the larger size of the bivalent Fe(II) (0.078 nm cation diameter *vs.* 0.064 nm cation diameter for Fe(III)) and therefore aids in the detachment of the Fe(II) species from the solid iron oxide cluster. Detachment of the structural iron will again be facilitated by protonation. The reducing ligand is often a charged species and therefore pH will often have a strong effect on the rate of dissolution. The rate will be determined by both ligand concentration and pH.

Reduction can also be promoted by light of the appropriate wavelength in supplying the energy for charge transfer among the surface $Fe^{3+}OH$ groups. Frequently ligands such as oxalate, citrate and thioglycolate which assist in complexation dissolution can dissolve iron oxide reductively if photo chemically activated.

Systematic studies of the photochemical dissolution of hematite[73], lepidocrocite[74] and goethite[75] have been carried out and some of the results are shown in **Figure 4.** The combined effect of light, organic complexing and pH on the dissolution of iron from lepidocrocite as determined by Waite & Morel[65] is apparent.

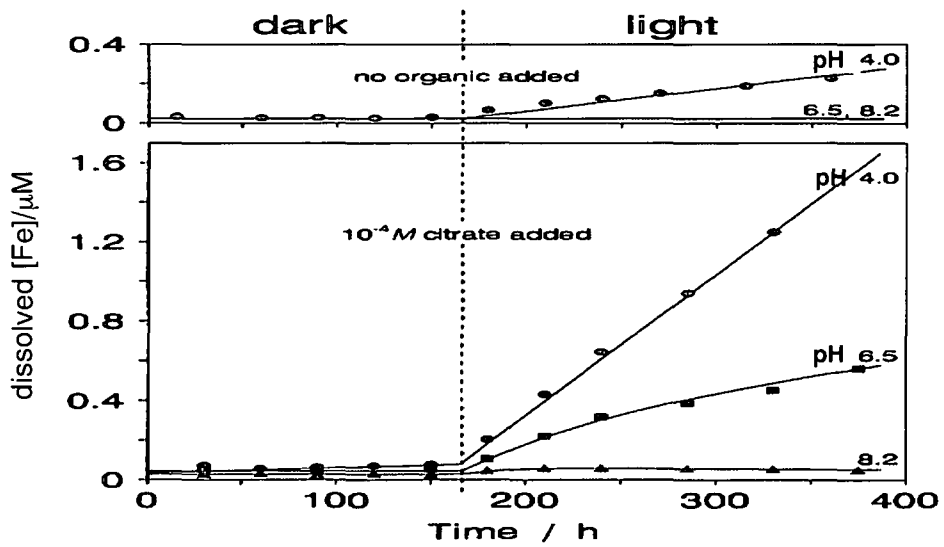

Figure 4. Dissolution–time curves for lepidocrocite in dark and light (300μE $cm^{-1}.min^{-1}$) conditions at different pH values in 10^{-4} *M* citrate (adapted from Waite and Morel[61], 1984).

It can be seen that light is the main accelerant but the process is also enhanced by the presence of citrate and protons.

2.6.3 Comparison of the three types of dissolution reactions.

There have been some studies where the dissolution of iron oxides by all three processes have been done under comparable conditions[76]. From these studies it was shown that at pH = 3 the rate of dissolution of hematite increased in the order: photon assisted dissolution < complexation < reduction with a factor of 350 between the extremes. A dissolution enhancement factor of 400 was found for goethite.[77] A study was also done on hematite at typical biological pH and it was shown that simple protonation was slow but Fe(II) complexing ligands were very effective. It can be concluded that reduction particularly when assisted by protonation and complexation is the most effective mechanism for iron dissolution.

2.6.4 Dissolution characteristic for different phases.

As mentioned before characteristic dissolution rates cannot as yet be assigned to different iron oxide phases. This is most probably due to the varying consistency within a specific iron oxide sample. There are, however, some trends observed between oxides with considerable stability differences.

2.6.4.1 Goethite.

- **Un-substituted (pure) goethite.**

When the dissolution of synthetic goethite was studied in HCl (0.5*M*) it was seen that the dissolution rate depended on crystal morphology[78]. Lowest dissolution rates were observed for acicular (flat, plate-like) crystals. Twinned crystals dissolved more rapidly initially because the twin boundaries acted as preferential dissolution sites. Investigations showed that although needle like goethite crystals retained their basic shape during dissolution the dissolution was not isotropic. Crystals initially became pointed at the domain ends but the subsequent acid attack led to preferential attack along the grain boundaries and diamond shaped holes were formed. The holes led to a large increase in surface area and subsequent increase in dissolution rate. Similar experiments showed a different dissolution rate and the main cause was due a large variation in

crystal sizes. The complete dissolution of the smaller crystals outweighed the area increase due to the development of holes in the larger crystals. It is therefore clear that under similar experimental conditions differences in dissolution rates of different samples can be attributed to differences in crystallinity and surface area. Goethite samples were prepared and some of the samples were heat treated. The untreated goethite samples had highly serrated edges and dissolution was comparative rapid. For the heat treated samples the serrated edges were absent and subsequently the dissolution rate was significantly slower. Crystals were therefore less prone to acid attack and more stable due to the heat treatment. Therefore the dissolution rate of an specific sample depends on a number of different parameters. The combined effect of all these factors is measured and it is difficult to identify to what extent the dissolution rate depends on each of the various parameters separately.

- **Substituted goethite.**

Goethites containing aluminium compounds of various concentrations were submitted to dissolution studies.[79] It was shown that samples containing less Al had much higher dissolution rates. One would expect that substitution by foreign compounds would accelerate dissolution due to crystal defects and vacancies. This is true for most "impurities" but not for V, Al and Cr.[79] It would seem that the bond strengths in particles consisting of iron oxides and V, Al and Cr are stronger than in the pure iron oxide particles. Infra red studies could concur that the bonds were indeed stronger by evaluating the bending mode frequencies.[79] In contrast Mn-goethites showed a decrease in bending mode frequencies and a subsequent increase in dissolution rate with higher Mn substitution.

- **Natural goethite and hematite.**

The leaching of ores has prompted investigations into the dissolution characteristics of natural occurring goethites and hematites.[80,81] From the results it was shown that the presence of SO_2 increased the dissolution rate. It was also noted that chloride, sulphate and bisulphate anions accelerated the dissolution process. Poorly crystalline goethite / ferrihydrite ores from Finnish lakes indicated that the ferrihydrite fraction dissolved faster that the goethite.[82]

2.6.4.2 Lepridocrocite.

Only a few investigations into the dissolution behaviour of lepridocrocite have been carried out. Being thermodynamically less stable than goethite or hematite it dissolves more rapidly.[83-85] The dissolution of lepridocrocite was studied in *0.5M* HCl at 76 °C.[86] TEM showed that the crystals maintained their shape for most of the dissolution process by preferentially dissolving at the edges which became strongly corroded, except for obvious surface imperfections where holes developed. The acid attack on the main crystal face (001) appeared very limited. The dissolution was also accompanied by the precipitation of goethite.

2.6.4.3 Ferrihydrite.

Only 2-line ferrihydrite has to date been investigated. Fisher[73] dissolved ferrihydrite in *0.2M* oxalate solution and found that dissolution was faster for a sample of ferrihydrite that was formed *via* quick precipitation. Adsorbed silicate reduced the dissolution rate in oxalate possibly due to blocking of the iron sites.[87]

2.6.4.4 Hematite.

The dissolution of hematite has been studied in more detail. Synthetic hematites with different morphologies have been synthesized and studied. In broad terms it was always found that the dissolution rate was linearly related to the initial surface area of the samples. More crystalline hematite prepared synthetically dissolved slower than hematite prepared by heat treating of goethite. The number of surface defects are probably the deciding factor here.[88] For most morphologies, the dissolution was shape preserving with no preferential attack for a specific crystal face. The rate of reductive dissolution in ascorbic acid was increased at lower pH. Aluminium substitution suppressed the rate of reductive dissolution. Copper substitution did not influence the rate of hematite dissolution in acid (the copper was released along with the iron[76]).

2.6.4.5 Magnetite and Maghemite.

Magnetite usually dissolves quicker than Fe(III) oxides due to the Fe(II) content and also because in these samples some Fe(III) exists having a octahedral coordination sphere and other Fe(III) cations exist having a tetrahedral coordination sphere.

2.6.5 Comparisons of different oxides.

Although specific dissolution rates are difficult to assign even to samples of the same oxide phase due to all the different parameters that influence the dissolution process, some studies have shown that certain general rules apply. In strong acids, ferrihydrite dissolves much quicker than goethite and hematite.[89] Similar results were also obtained for oxalate dissolution at pH 3 and pH 5. For more crystalline oxides, dissolution data is shown in **Figure 5**.

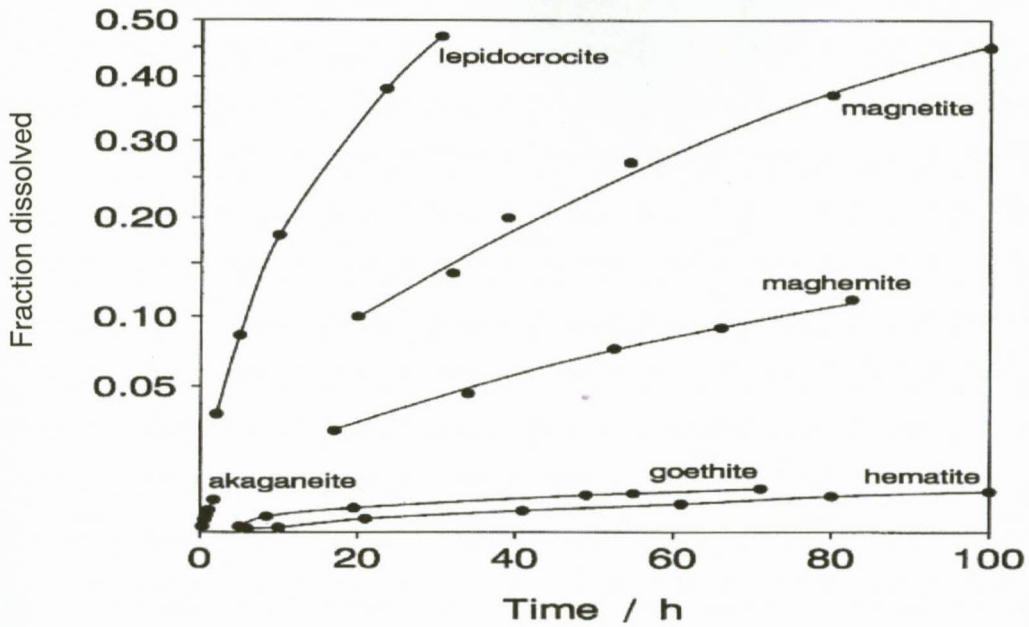

Figure 5. Dissolution-time curves of various Fe oxides in 0.5 *M* HCl at 25 °C.

Lower dissolution rates in HCl were also found for goethite over hematite by another study.[80] Goethite and hematite have very similar thermodynamical stabilities and other factors such as surface area may cause these phases to dissolve at different rates depending on the conditions. A study where dissolution was evaluated in ascorbic acid also showed that ferrihydrite dissolved 1000 times quicker than the other phases.

In hydroquinone at pH 1.9 – 13.8 goethite dissolved a 100 times quicker than hematite.[90] With sulphide as a reductant, ferrihydrite and lepidocrocite were significantly more reactive towards dissolution than goethite and hematite.[91]

2.6.6 Transformations.

A characteristic of iron oxide systems is that phases can transform from one to the other depending on the conditions. For instance under oxygen rich conditions goethite and hematite are

thermodynamically the most stable, they tend to be the end phase of many transformations. Some of the transformations that can take place between iron oxides are summarized in **Table 5**. The most important transformations to consider for this study are the transformation of ferrihydite to magnetite, maghemite and hematite. During catalyst reduction in syngas a mixture of iron oxides and iron carbides are formed. When the catalyst is removed from the reactor the relative amounts of these phases may be different but all will be present. Oxidation is inhibited by the wax layer coating the catalyst. The wax coated catalyst will therefore look much like the working catalyst unless exposure to air has led to some oxidation. Various wax removal methods will result in the formation of different iron oxide phases. The dissolution characteristics will be strongly influenced by the iron phases present as well as the available surface area.

Transformations due to elevated temperatures are of importance for this study as well as transformations in a reducing environment (organic matter). The polymorphs of FeOOH and also ferrihydrite can be dehydrated to those of Fe_2O_3 under the influence of either heat or mechanical stress[1]. This type of transformation can take place in solution but has been extensively studies in the "dry" state.

Thermal transformations have been found in nature where fires transform goethite or ferrihydrite to maghemite in the presence of organic matter. In the absence of organic matter hematite is formed.

The interconversions between maghemite and hematite have been studied in the dry state. Depending on the foreign ion content, maghemite transforms to hematite in the temperature range 370 – 600 °C.[92] The transformation involves the change of a cubic closest packing (ccp) anion arrangement to a hexagonal closest packing (hcp) arrangement. This involves considerable rearrangement and hence a fairly high temperature is required. The transformation to hematite from maghemite in samples containing ≤ 0.01 mol/mol of Co, Ni, Zn, Cu, Al, V and Cr was slower than for pure maghemite.[93] These metals were also ejected during heating and were concentrated on the surface[94]. Another study concluded that the crystallite size also plays an important part in the transformation[95]. Dry grinding of hematite led to transformation forming magnetite and wüstite.

Table 5. Inter-conversions among iron oxides (Adapted from Schwertmann[1]).

Precursor	Product	Type of transformation	Preferred medium
Goethite α-FeOOH	Hematite α-Fe_2O_3	thermal or mechanical dehydroxylation	gas/vacuum
		hydrothermal dehydroxylation	solution
	Maghemite γ-Fe_2O_3	thermal dehydroxilation	air + organic material
Lepridocrocite γ-FeOOH	Maghemite, Hematite	thermal dehydroxilation	gas/vacuum
	Goethite	dissolution/reprecipitation	alkaline solution
	Magnetite Fe_3O_4 ($Fe^{II}Fe^{III}_2O_4$)	Reduction	alkaline solution with Fe^{2+}
Akaganéite β-FeOOH	Hematite	thermal dehydroxilation	gas/vacuum
	Goethite	dissolution/reprecipitation	alkaline solution
	Hematite	dissolution/reprecipitation	acid solution
	Magnetite	dissolution/reduction	alkaline solution with N_2H_4
δ - FeOOH	Hematite	thermal dehydroxilation	gas/vacuum
Feroxyhyte δ' - FeOOH	Goethite	dissolution/reprecipitation	alkaline solution
Ferrihydrite $Fe_5HO_8 \cdot 4H_2O$	Hematite, Maghemite	Thermal dehydration/dehydroxylation	gas/vacuum
	Goethite	dissolution/reprecipitation	aqueous solution pH 3 – 14
	Akaganéite	dissolution/reprecipitation	acidic medium + Cl^-
	Lepridocrocite	dissolution/reprecipitation	pH 6 presence of cysteine
	Hematite	aggregation, short-range crystallization within ferrihydrite aggregate	aqueous solution at pH 6 – 8.
	Substituted magnetite	dissolution/reprecipitation	alkaline solution with M^{2+}
Hematite	Magnetite	Reduction	reducing gas
		reduction-dissolution reprecipitation	alkaline solution with N_2H_4
Magnetite	Maghemite, Hematite	Oxidation	air
Maghemite	Hematite	thermal conversion	air
$Fe(OH)_2$	Magnetite	Oxidation	N_2, alkaline solution
	Goethite		alkaline solution
	Lepridocrocite		
	Magnetite		
	Maghemite		
FeO	Magnetite	Disproportionation	air

2.7 Analysis Methods.

The analysis methods presented in this section will deal with methods and techniques used to investigate the iron oxide precursors and dissolution products as well as with synthesis performance evaluations during the course of this study.

To evaluate the phase of the iron precursors and of un-desolved metal oxides two techniques were employed namely Mössbauer Adsorption Spectroscopy (MAS) and X-Ray Diffraction (XRD). These methods are ideally suited for the analysis of iron-containing materials. Compositions of reagents and products were determined with the aid of Inductive Coupled Plasma (ICP). Surface area was determined using BET surface area equipment. Catalyst performance was evaluated by determining reactor inlet and outlet gas compositions employing Gas Chromatography (GC).

2.7.1 Mössbauer Adsorption Spectroscopy (MAS).

The Mössbauer adsorption spectroscopy technique is not widely used in catalysis. The technique can only be applied to elements that exhibit the Mössbauer effect.[96] Iron, tin, iridium, ruthenium, antimony, platinum and gold are elements that can be evaluated and are relevant for catalysis. Mössbauer spectroscopy provides valuable information on oxidation states, magnetic fields, lattice symmetry and lattice vibrations. Several books have been written on the technique[97-99] and reviews were published on the application thereof for catalysts.[100-102]

Mössbauer is a nuclear technique. Because the nucleus is at the heart of the atom knowing information about the nucleus tells one exactly what the chemical environment and the atoms are. The technique analyzes the energy levels of the nucleus with very high accuracy. The energy level reveals the oxidation state of the nucleus as well as how large the magnetic field is. By knowing this information it can be determined to what type of compound the atom belongs. The great advantage of Mössbauer is that it uses γ-radiation and therefore has high penetrating power. The technique can also be applied *in situ*.

When an exited iron nucleus decays to the ground state it emits a photon with energy typically between 10 – 100 keV. This photon strikes the nucleus of a second atom but the second atom is not exited because of the recoil energy involved. The first atom recoils when the photon is emitted and some energy is lost. When the second atom recoils as the photon hits it, even more energy is lost. The second atom therefore fails to adsorb enough energy to become exited and nothing is achieved. In a solid lattice, however, the atom cannot recoil as if it was free and the recoil energy is

taken up by vibrations of the whole lattice. Lattice vibrations are quantized and the quantum measured is called a *phonon*. If the recoil energy is larger than the phonon energy the lattice will adsorb the energy and nothing can be measured. If, however, the recoil energy is smaller that the phonon energy, a number of recoil-free events takes place. In short, if one places two atoms in a crystal lattice and perform an experiment under conditions where recoil energy of the photon emission and absorption are significantly smaller than the energy of the lattice vibrations, a number of the photons emitted by the source nucleus will be adsorbed by the second nucleus, the absorber. This is the Mössbauer effect and named after Rudolf L. Mössbauer who discovered it in 1957 and received a Nobel price for it in 1961.[103]

Surface atoms have a greater freedom to vibrate than the internal atoms in a crystal and this has to be taken into account when results are interpreted. In order to observe the Mössbauer effect one needs nuclei in the exited state as a source of γ – photons. This is achieved most frequently by using the ^{57}Fe isotope. This isotope is made in a nuclear accelerator, and decays with a half-life of 270 days.

In order to observe the Mössbauer effect the energy of the photons need to be varied to match the energy difference between nuclei of atoms in different oxidation states. This is done by using the Doppler Effect. The radiation source is therefore moved i.e. it is not stationary during measurements, in order to change the energy. For iron, the speed of either the sample or source must be between -1 to +1 cm/s (**Figure 6**).

A Mössbauer spectrum is a plot of the γ – ray intensity transmitted by the sample, against the velocity, *v,* of the source. The four most common type of Mössbauer spectra for iron containing samples are shown in **Figures 7(a) – (d)**.

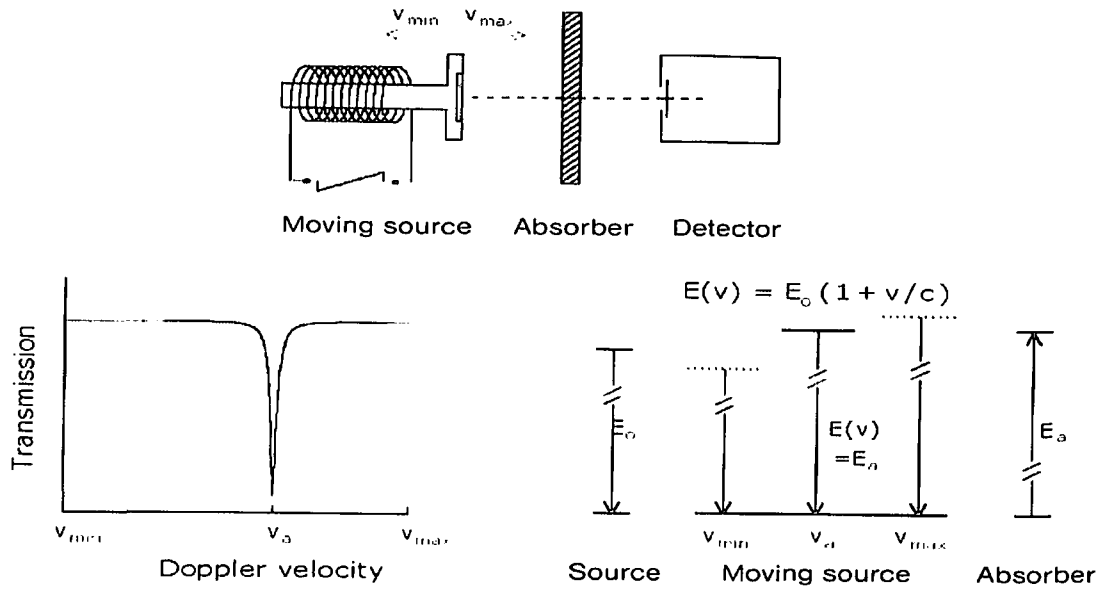

Figure 6. Simplified presentation of Mössbauer technique. E(V) is the energy of the γ - quantum emitted by the source and v is the velocity of the source (Adapted from Spectroscopy in Catalysis, Niemandsverdriet J.W.[92]).

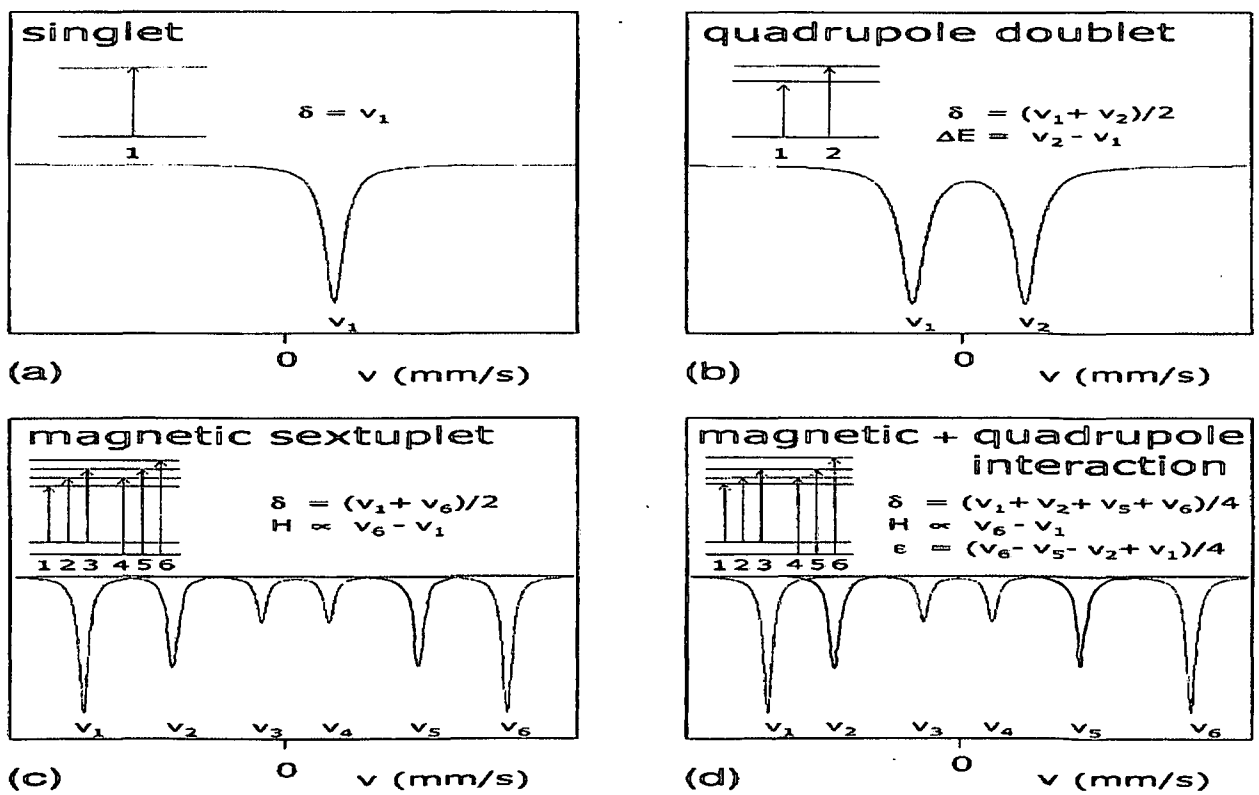

Figure 7. The four most common types of Mössbauer spectra observed for iron-containing materials. The corresponding nuclear transitions are also shown as well as how the Mössbauer parameters are derived from the spectra. The effect of the quadruple interaction can be seen a shift in peak v_2 on figure 7(d). (Adapted from Spectroscopy in Catalysis, Niemandsverdriet J.W.[92]).

2.7.1.2 Isomer Shift.

The isomer shift (δ) is the consequence of the Coulomb interaction between the positively charged nucleus and the negatively charged s-electrons. Due to the size change in the nucleus when it is exited, Coulomb interactions of the exited nuclei are also different. The isomer shift is therefore a measure of s-electron density at the nucleus and can give useful information as to the oxidation state in the absorber. Typical isomer shifts for iron are shown in **Table 6**.

Table 6. Mössbauer parameters for common iron compounds.

Compound	δ (mm s^{-1})	ΔE_Q (mm s^{-1}) Electric Quadrupole Splitting	ε' (mm s^{-1})	H (T) Refer to Figure 7
α - Fe_2O_3	0.43	-	- 0.10	51.5
α - FeOOH	0.35	-	0.13	38.4
Fe_3O_4	0.30	-		49.2
	0.63	-		45.5
FeO	1.08	0.55	-	-
FeS_2	0.28	0.60	-	-
α - Fe	0.00	-		33.0
θ - Fe_3C	0.19	-		20.8
SNP*	- 0.26	1.70	-	-

2.7.1.3 Electric Quadrupole Splitting.

Electric quadrupole splitting is caused by the interaction of the electric quadropole moment of the nucleus with an electric field gradient. The nucleus of iron in the ground state has a spherical distribution and hence no moment. When exited, the nucleus has the shape of an ellipsoid and possesses an electric quadrupole moment. This means the nucleus can orientate itself in two ways in an electric field gradient. This means that now two transitions from the ground state are possible. For randomly orientated samples such as catalyst powders the probabilities of having both are equal. On the Mössbauer spectra two peaks are observed and the splitting is proportional to the magnitude of the electric field gradient at the nucleus.

2.7.1.4 Magnetic Hyperfine Splitting.

Magnetic hyperfine splitting – the Zeeman effect – arises from the interaction between the nuclear dipole moment and the magnetic field at the nucleus. This interaction gives rise to six transitions; the separation between the peaks in the spectrum is proportional to the magnetic field at the nucleus. When discussing the spectra this is often referred to as the sextuplet or magnetic sextet.

2.7.1.5 Intensity.

The intensity of a Mössbauer spectrum depends not only on the recoil free fractions of the source and the absorber and on the number of absorbing nuclei, but also on the line width of the absorption lines and whether or not saturation effects occurred. Saturation effects come into play with heavier samples. It is therefore better to have very thin samples if sharper spectra are desired. This enables better quantitative interpretation.

2.7.1.6 Mossbauer Spectroscopy in Catalyst Characterization.

Mossbauer spectroscopy is particularly useful in:

- Phase identification
- Determination of oxidation states
- Structure information
- Determination of particle (crystallite) size.
- Kinetics of bulk transformations.

Lower analysis temperatures reduce the recoil energy and therefore much better resolution can be obtained at liquid nitrogen and liquid helium temperatures as depicted for a typical Ruhrchemie iron-based catalyst in **Figure 8(a) and Figure 8(b)**.

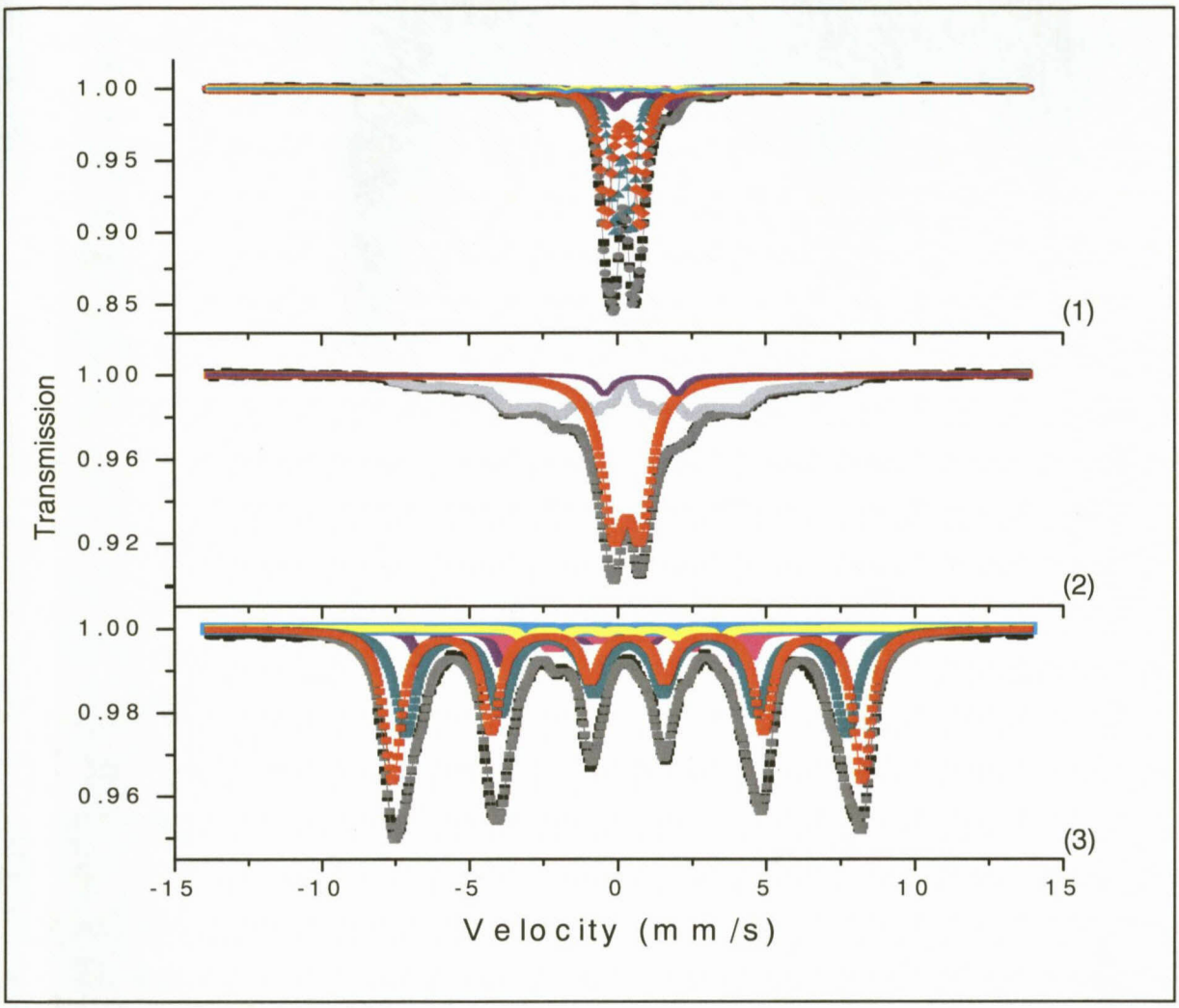

Figure 8(a). Mössbauer adsorption spectra of an iron-based catalyst measured at room temperature (1), 77 K (2) and 4 K (3). For these spectra the black points represent the data measured experimentally and the grey line fitted through these points represents the spectrum that is generated from them. It is important to realize that the experimentally determined spectrum is the compliment of all iron phases present in the sample. Other lines in each diagram (yellow, green, purple, red, etc.) represent the theoretical quantity of each phase present in the sample that will together give the experimental grey curve. For clarity Figure 8(b) shows the ideal theoretical spectrum of each of these phases separated from each other.

Due to the overlapping spectra it is difficult to distinguish the various phases easily. Therefore the spectra are also depicted for the various iron phases in **Figure 8(b)**.

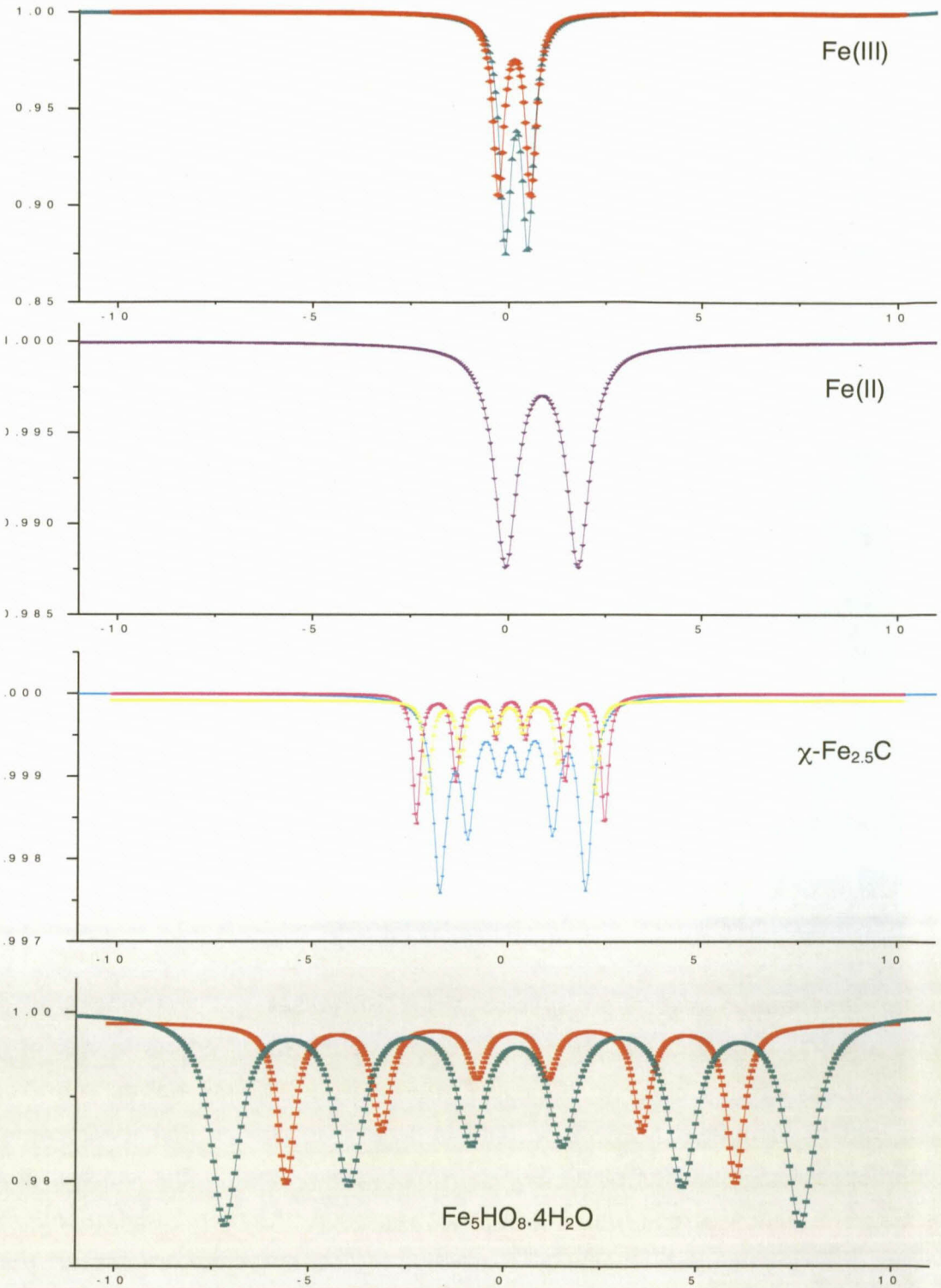

Figures 8(b). Theoretical Mossbauer spectra of Fe(III) (top), Fe(II) (2nd from top), Hägg carbide and ferrihydrite (bottom). Two forms of Fe(III) are detected, because within the structure of the sample, two different iron atoms with different environments exist in the same unit cell. Similarly, three signals are detected for Hägg carbide (χ-$Fe_{2.5}C$) and two for ferrihydrite.

The benefit gained from lower temperature Mössbauer experiments, as mentioned in **Section 2.7.1.6**, is that the recoil free interaction is enhanced and iron phases not easily distinguished at higher temperatures can be resolved as in the case of ferrihydrite which cannot be quantified at higher temperature Mössbauer analysis.

2.7.2 X–Ray Diffraction (XRD).

Broadly speaking the X-Ray diffraction method entails the study of structural properties of surfaces by means of interference effects in scattered radiation. XRD is one of the oldest and most frequently applied techniques in catalysis.[104] XRD is used to identify crystalline phases inside catalysts by means of lattice structural parameters. It can also be used to determine crystallite size. The technique depends on the constructive interference of radiation that is scattered by relatively large particles in the sample. As a consequence, the technique requires long range order. Related to XRD is Low – Energy Electron Diffraction (LEED), Extended X–ray Absorption Fine Structure (EXAFS) and X-ray Absorption Near Edge Spectroscopy (XANES). The latter methods were, however, not employed for this study.

X-rays have wavelengths in the Ångstrøm range and have energy to penetrate solids and probe their internal structure. Therefore XRD can be used to determine the average phase of the bulk material. A further benefit of the technique is that it can be applied *in situ*. The theory of XRD is provided in textbooks of solid state physics.[105-109]

A conventional X-ray source consists of a filament that is bombarded with high energy electrons. X-rays are then emitted and are the result of two processes. Electrons slowed down by the target emit a continuous background spectrum of Bremsstrahlung. Superimposed on this are characteristic, narrow lines; the Cu Kα line, with an energy of 8.04 keV and a wavelength of 0.154 nm. This arises due to an primary electron creating a core hole in the K shell. This gap is then filled by an electron from the L shell and so on. Every time this happens radiation is emitted. The process is also called X-ray fluorescence. X-ray diffraction is the elastic scattering of the X-ray photons by the elements present in the lattice. The X-rays that are in phase produce constructive interference. **Figure 9** explains the process graphically.

If one measures the angles, 2θ, under which constructively interfering X-rays leave the crystal, the Bragg relationship ($n\lambda = 2d \sin\theta$; n = 1,2,...) gives the corresponding lattice spacings, which are characteristic for specific compounds (**Figure 9**).

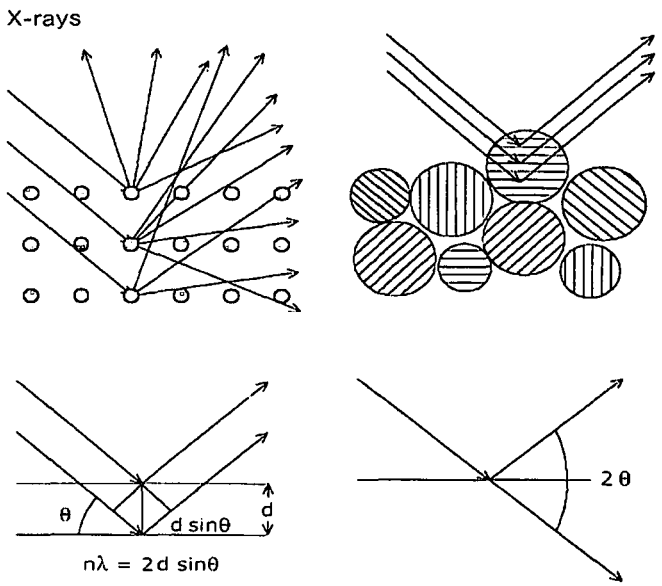

Figure 9. Schematic of how electrons are scattered by lattice atoms.

The diffraction pattern will be formed by only a small part of the sample shown in **Figure 9** by the top right drawing. It is therefore useful to rotate the sample during analysis, thereby increasing the number of atoms contributing to the spectrum.

The XRD pattern of a powdered sample is measured with a moveable X-ray source and a moveable detector, which scans the intensity of the diffracted pattern as a function of the angle 2θ between the incoming and diffracted beams. Only particles with crystal phases at the correct angle will give useful diffraction. By rotating the sample during analysis the fraction of particles that can attribute is increased. XRD is therefore mainly used to identify crystallographic phases that are present in the catalyst. XRD has one important limitation and that is that diffraction peaks are only observed when the sample processes sufficient long range order. The advantage on the other hand is that the shape of the diffraction peaks carries information on the dimensions of the reflecting planes. Diffraction lines from perfect crystals are very narrow and can be very accurately identified. When the crystallite size is less than 100 nm, line broadening occurs. This is due to incomplete interference (destructive) in scattering directions where the X-rays are out of phase. Therefore peak broadening can give a quick, but not always accurate estimation of crystallite size. Fourier transform methods have greatly increased the accuracy in determining crystallite size. A further advantage of XRD is that a fairly large part of the sample is evaluated as opposed to for instance, with electron microscopy.

In situ XRD has become more popular and is an extremely powerful method to investigate phase changes while the catalysts is under reducing or synthesis conditions.

Although bulk phase changes can be extensively studied with XRD the surface of the catalyst is where reaction takes place and hence for the study of catalytic surfaces the method may be less suited.

Figure 10 illustrates the changes for CuO when reduced in a CO atmosphere. Valuable data is generated with regards to the rate and extent of reduction.

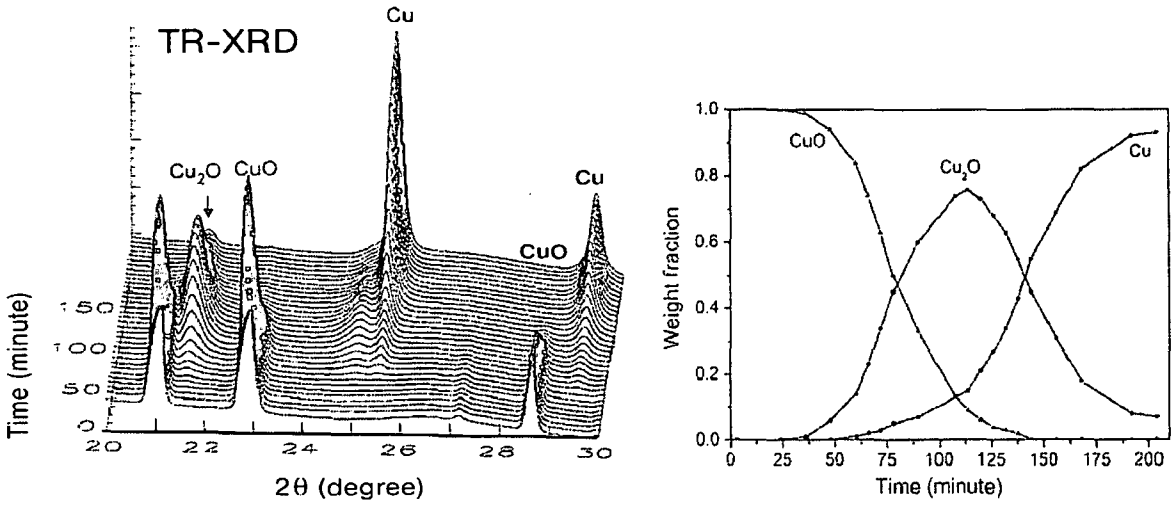

Figure 10. Phase changes taking place during the reduction of CuO powder in CO atmosphere.

From **Figure 10** it can be seen that with time on line the CuO species concentration disappears with the evolution of Cu_2O and the eventual reduction of the material to metallic copper.

2.7.3 BET Surface Area.

BET theory describes the physical adsorption of gas molecules on a solid surface and is the basis for an important analysis technique for the measurement of the specific surface area of a material. In 1938, Stephen Brunauer, Paul Hugh Emmett, and Edward Teller (BET) published an article about the method.[110] Theoretically the concept is an extension of the Langmuir theory, which is a theory for monolayer molecular adsorption, to multilayer adsorption with the following assumptions:

1. Multi-layer adsorption of adsorbent molecules is possible i.e. not only a monolayer of adsorbed molecules is formed, successive layers are also possible.
2. Adsorption takes place on a non-porous, uniform surface.
3. The heat of adsorption for the first surface adsorbed layer is higher than the heat of adsorption for successive layers.

4. Heat of adsorption for second and successive layers equals the heat of condensation of the adsorbent gas.
5. Lateral interactions of adsorbed molecules on each other (such as surface tension) are ignored.

Adsorption isotherms can be plotted as a straight line with $1 / v [(P_0 / P) - 1]$ (v = adsorbed volume) on the y-axis and $\varphi = P / P_0$ on the x-axis according to experimental results. This plot is called a BET plot. The linear relationship of this equation is maintained only in the range of $0.05 < P / P_0 < 0.35$.

The BET method is widely used in surface science for the calculation of surface areas of solids by physical adsorption of gas molecules and the process can be described by the following steps:

1. Molecules from the gas phase strike the surface and adsorb.
2. At equilibrium conditions (pressure, temperature dependant) the molecules adsorb, loses the heat of adsorption (q), and subsequently desorbs from the surface when the equilibrium conditions of the sample are changed.
3. At equilibrium the rate of condensation = rate of desorption.
4. Constant surface coverage of adsorbent molecules is achieved at equilibrium.

Important factors when BET data is interpreted:

1. Surface features change the adsorption potential at localized areas.
2. Surface area models neglect the effects of this localized phenomenon.
3. Curved surfaces or roughness provide enhanced adsorption potential.
4. As the system pressure is increased (gas concentration also increases) multiple layers adsorbs to the surface.
5. The monolayer coverage, a densely packed single adsorbed layer, is used for determining surface area.
6. As pressure is further increased and adsorption proceeds, gas condenses in the pores and this volume of condensed adsorptive is used for characterizing porosity.
7. Isotherms are the most often used graphs for analysis of materials. Graphs depict the quantity adsorbed as a specific pressure or relative pressure and the pressure is normally varied from vacuum to near atmospheric and performed at constant temperature. Quantities adsorbed are then normalized for adsorbent mass. Isotherms are classified according to shape and fall with the six classifications shown in **Figure 11**.

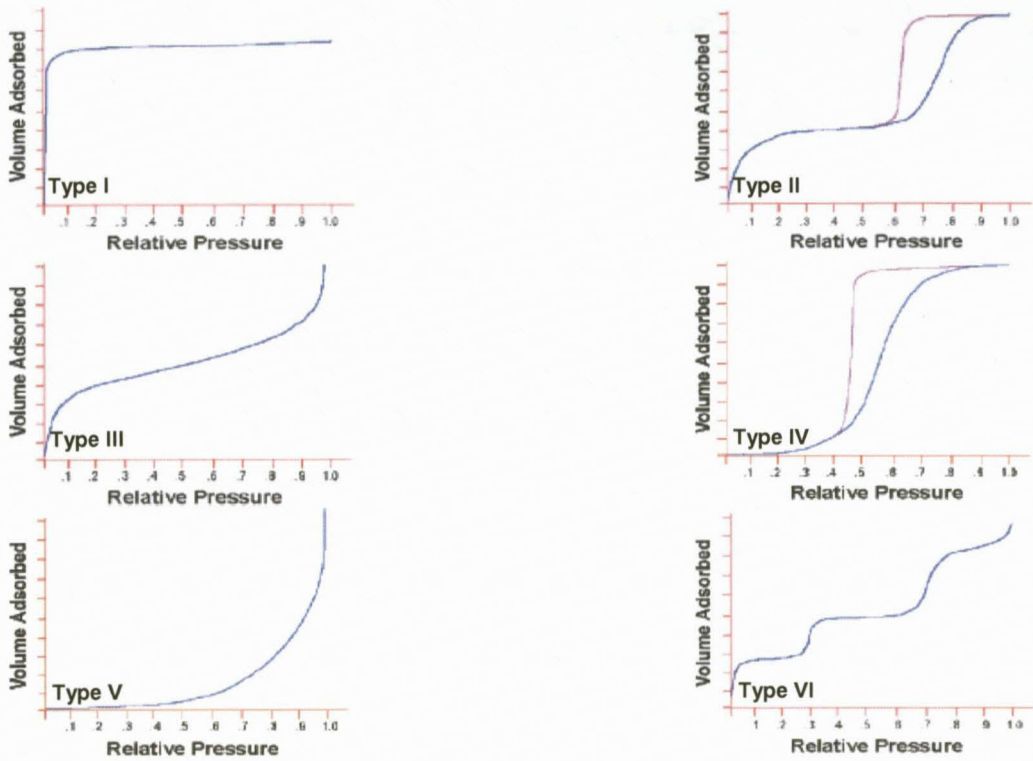

Figure 11. Different types of isotherms found for materials with different characteristics. (Types I, II and IV – most materials, Type III – uncommon, Type V – rare, Type VI – highly uniform surface)

The BET calculation is best suited for the determination of meso-porous samples between 2–50 nm.

2.7.4 Inductive Coupled Plasma (ICP).

Inductively Coupled Plasma (ICP) is an analytical technique used for the detection of trace metals in mostly aqueous solutions.[111,112] The ICP is used to emit characteristic wavelength specific light for elements which can then be measured. The technology for the ICP method was first employed in the early 1960's with the intention of improving upon crystal growing techniques.

Since then, ICP has been refined and used in conjunction with other procedures for quantitative analysis. ICP hardware is designed to generate a plasma, which is a gas in which atoms are present in an ionized state. A basic ICP consists of three concentric tubes, most often made of silica. These tubes, termed outer loop, intermediate loop, and inner loop, collectively make up the torch of the ICP. The torch is situated within a water-cooled coil of a radio frequency (r.f.) generator. As flowing gases are introduced into the torch, the r.f field is activated and the gas in the

coil region is made electrically conductive. This sequence of events forms the plasma. The formation of the plasma is dependent upon an adequate magnetic field strength and the pattern of the gas streams follows a particular rotationally symmetrically pattern. Plasma is maintained by inductive heating of the flowing gases. The induction of a magnetic field generates a high frequency annular electric current within the conductor. The conductor, in turn, is heated as the result of its resistance. In order to prevent possible short-circuiting as well as meltdown, the plasma must be insulated from the rest of the instrument. Insulation is achieved by the concurrent flow of gasses through the system. Three gases flow through the system namely the outer gas, intermediate gas, and inner or carrier gas. The outer gas is typically argon or nitrogen. The outer gas has been demonstrated to serve several purposes including maintaining the plasma, stabilizing the position of the plasma, and thermally isolating the plasma from the outer tube. Argon is commonly used for both the intermediate gas and inner or carrier gas. The purpose of the carrier gas is to convey the sample to the plasma.

An ICP typically includes the following components:

1. Sample introduction system (nebulizer).
2. ICP torch.
3. High frequency generator.
4. Transfer optics and spectrometer.
5. Computer interface.

An ICP requires that the elements which are to be analyzed be in solution. An aqueous solution is preferred over an organic solution, as organic solutions require special manipulation prior to injection into the ICP. Solid samples are also discouraged, as clogging of the instrumentation can occur. A nebulizer transforms the aqueous solution into an aerosol and the light (electromagnetic waves) emitted by the atoms of an element in the ICP must be converted to an electrical signal that can be measured quantitatively. This is accomplished by resolving the light into its radiation component (nearly always by means of a diffraction grating) and then measuring the light intensity with a photomultiplier tube at the specific wavelength for each element line. Light emitted by the atoms or ions in the ICP is converted to electrical signals by the photomultiplier in the spectrometer. The intensity of the electric signal is compared to previous measured intensities of known concentration of the element and a concentration is computed. Each element will have many specific wavelengths in the spectrum which could be used for analysis. Thus, the selection of the most appropriate wavelength for the analytical application at hand requires considerable experience of ICP wavelengths.

Advantages of using an ICP include its ability to identify and quantify all elements with the exception of Argon; since many wavelengths of varied sensitivity are available for determination of

any one element, the ICP is suitable for all concentrations from ultratrace levels to major components; detection limits are generally low for most elements with a typical range of 1-100 $\mu g.l^{-1}$. Probably the largest advantage of employing an ICP when performing quantitative analysis is the fact that multi-elemental analysis can be accomplished, and quite rapidly. A complete multi-element analysis can be undertaken in a period as short as 30 seconds, consuming only 0.5 ml of sample solution. Although, in theory, all elements except argon can be determined using and ICP, certain unstable elements require special hardware to maintain the plasma. Also, an ICP has difficulty handling halogens, for halogens require special optics for the transmission of the very short wavelengths.

In this study, due to the high concentration of iron in the liquid and solid samples a volumetric method was also used in some cases along with ICP.

2.7.5 Gas Chromatography (GC).

2.7.5.1 Introduction.

Gas-liquid chromatography (GLC), or generally gas chromatography (GC), is a method to determine the concentration of gasses and liquids in a sample.[113,114] Chromatography dates back to 1903 and the work of the Russian scientist, Mikhail Semenovich Tswett. German graduate student Fritz Prior developed solid stationary chromatography in 1947. Archer John Porter Martin, who was awarded the Nobel Prize for his work in developing liquid-liquid (1941) and paper (1944) chromatography, laid the foundation for the development of gas chromatography and later produced liquid-gas chromatography (1950).

A gas chromatograph is a chemical analysis instrument for separating chemicals in a multi component sample. A gas chromatograph uses a flow-through narrow tube known as the *column*, through which different chemical constituents of a sample pass in a gas stream (carrier gas, the so called *mobile phase*) at different rates depending on their various chemical and physical properties and their interaction with a specific column filling, called the *stationary phase*. As the chemicals exit the end of the column, they are detected and identified electronically. The function of the stationary phase in the column is to separate different components, causing each one to exit the column at a different time (this means column *retention time* differs for each component). Other parameters that can be used to alter the order or time of retention are the carrier gas flow rate, and the temperature.

In a GC analysis, a known volume of gaseous or liquid sample is injected into the "entrance" of the column, usually using a micro syringe or auto sampler (an automatic gas source switching system). As the carrier gas sweeps the analyte molecules through the column, the movement of the analyte through it is inhibited by the adsorption of the analyte molecules either onto the column walls or onto packing materials in the column. The rate at which the molecules progress along the column depends on the strength of adsorption, which in turn depends on the type of molecule and on the stationary phase materials. Since each type of molecule has a different rate of progression, the various components of the analyte mixture are separated as they progress along the column and reach the end of the column at different times (retention time). A detector is used to monitor the outlet stream from the column; thus, the time at which each component reaches the outlet and the amount of that component can be determined. Generally, substances are identified (qualitatively) by the retention time after which they emerge (elute) from the column.

2.7.5.2 Sample inlet.

Column inlets or injectors provide the means to introduce a sample into a continuous flow of carrier gas. The inlet is a piece of hardware attached to the column head and the most common inlet type is the Split/Splitless (S/SL) injector and this was also used for gas analysis pertaining to this study. Samples are introduced into a heated small chamber via a syringe through a septum - the heat facilitates volatilization of the sample and sample matrix. The carrier gas then either sweeps the complete (splitless mode), or a portion (split mode), of the sample into the column. In split mode, a part of the sample/carrier gas mixture in the injection chamber is exhausted through the split vent.

2.7.5.3 Columns.

Two types of columns are used in GC namely:

1. *Packed columns* are 1.5-10 m in length and have an internal diameter of 2-4 mm. The tubing is usually made of stainless steel or glass and contains a *packing* of finely divided, inert, solid support material (e.g. diatomaceous earth) that is coated with a liquid or solid stationary phase. The nature of the coating material determines what type of materials will be most strongly adsorbed. Thus numerous columns are available that are designed to separate specific types of compounds.
2. *Capillary columns* have a very small internal diameter, in the order of a few tenths of millimeters, and lengths between 25-100 meters are common. The inner column walls are

coated with the active materials (WCOT columns), some columns are quasi solid filled with many parallel micropores (PLOT columns). Most capillary columns are made of fused-silica with a polyimide outer coating. These columns are flexible, so a very long column can be wound into a small coil.

The rate at which a sample passes through the column is directly proportional to the temperature of the column. The higher the column temperature, the faster the sample moves through the column. However, the faster a sample moves through the column, the less it interacts with the stationary phase, and the less the analytes are separated.

In general, the column temperature is selected to compromise between the length of the analysis and the level of separation.

A method which holds the column at the same temperature for the entire analysis is called "isothermal." Most methods, however, increase the column temperature during the analysis, the initial temperature, rate of temperature increase (the temperature "ramp") and final temperature is called the *temperature program.*

A temperature program allows analytes that elute early in the analysis to separate adequately, while shortening the time it takes for late-eluting analytes to pass through the column.

2.7.5.4 Carrier gas.

The choice of carrier gas (*mobile phase*) is important, with hydrogen being the most efficient and providing the best separation. However, helium has a larger range of flowrates that are comparable to hydrogen in efficiency, with the added advantage that helium is non-flammable, and works with a greater number of detectors. Therefore, helium is the most common carrier gas used.

2.7.5.5 Detectors.

A number of detectors are used in gas chromatography. The most common are the flame ionization detector (FID) and the thermal conductivity detector (TCD). Both are sensitive to a wide range of components, and both work over a wide range of concentrations. While TCDs are essentially universal and can be used to detect any component other than the carrier gas (as long as their thermal conductivities are different than that of the carrier gas, at detector temperature), FIDs are sensitive primarily to hydrocarbons, and are more sensitive to them than TCD. However,

an FID cannot detect water. Both detectors are also quite robust. Since TCD is non-destructive, it can be operated in-series before an FID (a destructive detection method), thus providing complementary detection of the same analytes.

2.7.5.6 Data processing and analysis.

Qualitative analysis - Generally chromatographic data is presented as a graph of detector response (y-axis) against retention time (x-axis). This provides a spectrum of peaks for a sample representing the analytes present in a sample eluting from the column at different times. Retention time can be used to identify analytes if the method conditions are constant. Also, the pattern of peaks will be constant for a sample under constant conditions and one can identify complex mixtures of analytes. In most modern applications, however, the GC is connected to a mass spectrometer (MS) or similar detector that is capable of identifying the analytes represented by the MS peaks.

Quantitive analysis - The area under a peak is proportional to the amount of analyte present. By calculating the area of the peak, the concentration of an analyte in the original sample can be determined. Concentration can be calculated using a calibration curve created by finding the response for a series of known concentrations of analyte, or by determining the relative response factor of an analyte. The relative response factor is the expected ratio of an analyte to an internal standard (or external standard) and is calculated by finding the response of a known amount of analyte and a constant amount of internal standard (a chemical added to the sample at a constant concentration, with a distinct retention time to the analyte).

In most modern GC-MS systems, computer software is used to draw and integrate peaks, and match MS spectra to library spectra.

For this study detailed selectivity performance of the catalyst was not important and therefore only a TCD detector was used. The analysis of H_2, CO_2, Ar, N_2 and methane were performed on a GOWMAC gas chromatograph. The GC is equipped with two split/splitless injectors and two TCD detectors. Two packed columns and a valve system was used (2m $^1/_8$" molecular sieve 5Å; 2 meter $^1/_8$" Restek Shincarbon column)

One channel was used to analyze for CO, CO_2, N_2 and Ar with helium as the carrier gas. The other column was used to determine the H_2 and methane with Ar as the carrier gas. The GC was operated under isothermal conditions (110 °C). Gas samples were purged through the sample loop for approx. 5 min and then injected online and splitless. The GC was calibrated daily by the

analysis of a known standard with gas composition and concentration similar to those sampled as part of this study.

2.8 References

[1] Schwertmann, U., Cornell, R.M., in *The Iron Oxides – Structure, Properties, Reactions, Occurrences and Uses*, **1998**, Second Edition, Wiley – Vch.

[2] Ertl, G., Knözinger, H., Weitkamp, J., in *Handbook of Heterogeneous Catalysis*, **1997**, vol. 4, 1697.

[3] http://www.steelonthenet.com/commodity_prices.html

[4] (a) Boudart, M., *Top Catal.*, **1994**, 1, 405.

(b) Jennings, J.R., in *Catalytic Ammonia Synthesis: Fundamentals and Practise, Fundamental Applied Catalysis*, **1991**, Plenum Press, New York.

(c) Gunze, M., in *The Chemistry and Physics of Solid Surfaces and Heterogeneous Catalysis*, **1982**, Elsevier, 4, Amsterdam.

(d) Nielsen, J., in *Ammonia Synthesis*, **1995**, Springer, New York.

[5] Bartholomew, C.H., Farrauto, R.J., in *Fundamentals of Industrial Catalytic Processes*, **2005**, Wiley, Second Edition, 371.

[6] Mittasch, A., *Adv. Catal.*, 1950, 2, 81.

[7] Mittasch, A., in *Geschichte in der Ammoniaksynthese*, **1951**, Verlag Chemie, Weinheim.

[8] Schlögl, R., in *Catalytic Ammonia Synthesis, Fundamental and Practice*, **1991**, Plenum, New York, 19.

[9] Rayment, T., Schlögl, R., Thomas, M.M., Ertl G., in *Nature*, **1985**, 315, 311.

[10] http://www.researchandmarkets.com/reports/606126

[11] Global Insight, *Economic Primer on Formaldehyde*, **2006**.

[12] Supp, E., in *Rohstoff Kohle*, **1987**,Verslag Chemie, Weinheim, New York, 136.

[13] Bridger, G.W., Chinchen, G. C., in *Catalyst Handbook*, **1970**, Wolf Scientific Books, London, 97.

[14] Jennings, J.R., Twigg, M.V., in *Selected Developments in Catalysis*, **1985**, Oxford, 4, 102.

[15] Hawker, P.N., in *Hydrocarbon Processing*, **1982**, 183.

[16] Thomas, C.L., in *Catalytic Processes and Proven Catalysts*, **1970**, Academic Press, New York, 104.

[17] Newsome, D.S., in *Catal. Rev. – Sci. Eng.*, **1980**, 21, 275.

[18] Trimm, D. L., in *Methane conversion, Studies is Surface Science and Catalysis*, **1988**, Elsevier, Amsterdam, 36, 39.

[19] Duprez, D., in *Appl. Catal.*, **1992**, 82, 111.

[20] Ertl, G., Knözinger, H., Weitkamp, J., in *Handbook of Heterogeneous Catalysis*, **1997,** 4, 1831.

[21] Thomas, C.L., in *Catalytic Processes and Proven Catalysts*, **1970**, Academic Press, New York, 39.

[22] Chinchen, G. C., Logan, R.H., Spencer, M.S., in *Appl. Catal.*, **1984**, 12, 89.

[23] Gonzales, J.C., Gonzales, M.C., Laborde, M.A., Moreno, N., in *Appl. Catal.*, **1986**, 20, 3.

[24] Newsome, D.S., in *Catal. Rev. Sci. Eng.*, **1980**, 21, 275.

[25] Tamaru, A., Oshima, Y., Honda, K., in *German Pat. Appl. DE 3853345 Al*, **1984,** Mitsubishi Kasai Co., Tokyo, Japan.

[26] Schneider, M., Kochloefl, Pohl, J., Bock, O., in *Euro. Pat. Appl., 0126425*, **1984**, SüD CHEMIE AG, München, Germany.

[27] Andreev, A., Idakiev, V., Mihajlova, D., Shopov, D., in *Appl. Catal.*, **1985**, 22, 385.

[28] Huang, D.C., Braden, J. L., Eurp., in Pat. Appl. 0353453, **1969**, United Catalyst Inc., Louisville, USA.

[29] Rao J. R., Sant, B.R., in *Chem. Age India*, **1973**, 24, 695.

[30] Singh, G. P. A., Saraf, D. N., in *Ind. Eng. Chem.*, **1980**, 16, 313.

[31] Keiski, R. L., Salmi. T., in *Appl. Catal.*, **1992**, 87, 185.

[32] Chinchen, G. C., in *Europe. Pat. Appl., A 0062410,* ICI PLC, London, **1982**.

[33] Kochloefl, K. Ladebech, J., in *Preparation of Catalysts VI*, in *Studies in Surface Science and Catal.*, **1995**, Elsevier Sci. Publ B. V., Amsterdam, 91, 1079.

[34] Bartholomew, C.H., Farrauto, R.J., in *Fundamentals of Industrial Catalytic processes*, **2005**, Wiley, Second Edition, 398.

[35] Williamson, H.F., Andreano, R.L., Daum, A.R., Klose, G.C., in *The American Petroleum Industry, The age of energy 1899 – 1959*, **1963**, North-western University Press, Evanston.

[36] Sabatier, P., Senderens, J. B., in *C. R. Acad. Sci.*, **1902**, Paris, 134, 514.

[37] Orlov, E. I., in *Zhur Russ. Khim. Ob-za*, **1908**, 40, 1588.

[38] *German patent 293787*, **1913**, BASF.

[39] Fischer, F., Tropsch, H., in *Bennstoff-Chem.*, **1924**, 4, 276.

[40] Steynberg, A.P., Dry, M.E., in *Fischer Tropsch Technology, Studies in Surface Science and Catalysis*, Elsevier, **2004**, 533.

[41] Dry, M. E., in *Catalysis Science and Technology*, Springer-Verlag, **1981**, 159.

[42] Anderson, R. B., in *Catalysis*, **1956**, Reinhold, 4.

[43] Dry, M. E., Shingles, T., Botha C. S., in *J. Catal.*, **1970**, 17, 341.

[44] Baulok, W., Hellbrugge, J., in *Brennst. Chem.*, **1942**, 23, 87.

[45] Dry, M. E., in *Hydrocarbon Process*, **1980**, 59, 92.

[46] Hasll, C. C., Gall, D., Smith, S. L., in *Inst. Petrol*, **1952**, 38, 845.

[47] Arnold, J. H., Keith, P. C., in *Amer. Chem. Soc. Adv. Chem. Ser.*, **1951**, 5, 120.

[48] Frohning, C.D., in *Fischer Tropsch Synthese aus Kohle*, **1977**, Stuttgart, Thieme.

[49] Malherbe, J.A., *The effect of catalyst pre-treatment on the mechanical integrity and synthesis performance of an iron-based Fischer Tropsch catalyst.*, **2006**, MSc. thesis UCT, Cape Town.

[50] Jager, B., Espinaza, R. L., in *Catal. Today*, **1995**, 23, 17.

[51] Bukur, D. B., Norwicki, L., Manne, R. K., Lang, X., in *J. Catal.*, **1995**, 155, 366.

[52] Bukur, D. B., Norwicki, L., Patel, S. A., in *Canadian J. Chem. Eng.*, **1996**, 74, 399.

[53] Bukur, D. B., Lang, X., Ding, Y., in *Applied Catal.*, **1999**, 155, 255.

[54] Davies, B. H., O'Brien, R. J., Xu, L. G., Spicer, R. L., in *Eng & Fuels*, **1996**, 10, 921.

[55] Duvenhage, D.J., *An investigation of the physical and chemical changes occurring in a Fischer Tropsch fixed bed catalyst during hydrocarbon synthesis.*, **1991**, PhD. Thesis, WITS, Johannesburg.

[56] Anderson, R.B., in *Catalysis*, **1956**, 4.

[57] Niemela, M.K., Krause, T., Backman, A.O., in *Appl. Catal.*, **1997**, 156, 319.

[58] Iglesia, E., Soled, S.L., Fiato, R.A., *Fisher Tropsch Synthesis on Cobalt and Ruthenium. Metal Dispersion and Support Effects on Reaction Rate and Selectivity,* in *J. Catal.*, **1992**, 137, 212.

[59] Dry, M.E., *The Fischer Tropsch Synthesis*, in *Catalyst Science and Technology.*, **1981**, Springer-Verlag, New York, 159.

[60] Tramm, H., in *Chem. Ing. Techn.*, **1952**, 24, 237.

[61] Storch, H.H., Golumbic, N., Anderson, R.B., in *The Fischer Tropsch and Related Synthesis.*, **1951**, Wiley, New York.

[62] Kolbel, H., Ralek, M., in *Chemierohstoffe aus Kohle*, **1977**, Verlag, Stuttgart, 232.

[63] Bloom, P.R., Nater, E.A., *Kinetics of Dissolution of Oxides and Primary Silicate Minerals,* in *Soil Sci. Soc. Am. Spec.*, **1991**, 21, 151.

[64] Blesa, M.A., Morando, P.J., Regazzoni, A.E., in *Chemical Dissolution of Metal Oxides*, **1994**, CRC Press, London, 104.

[65] Casey, W.H., *Surface chemistry during the dissolution of oxide and silicate materials,* in *Mineral Surfaces. Min. Soc.*, **1995**, Chapman & Hall, London, 5, 231.

[66] Blesa M.A., Maroto, A.J.G., *Dissolution of metal oxides.,* in *J. Chim. Phys.*, **1986**, 83, 757.

[67] Stumm, W., Furrer, G., *The dissolution of Oxides and Aluminium Silicates,* in *Aquatic Surface Chemistry*, **1987**, Wiley & Sons, New York, 197.

[68] Cornell, R.M., Posner, A.M., Quirk, J.P., *Crystal Morphology and the Dissolution of Goethite,* in *J. Inorg. Nucl. Chem.*, **1974**, 36, 1937.

[69] Maurice, P.A., Hochella, M.F., Parks, G.A., Sposito, G., Schwertmann, U., *Evolution of Hematite surface microtopography upon dissolution by simple organic acids,* in *Clays Clay Min.*, **1995**, 43, 29.

[70] Salfity, J.A., Regazzoni, A.E., Blesa, M.A., in *Interfacial Chemistry of Dissolving metal Oxide particles: Dissolution by Organic Acids*, **2000**, 14, 513.

[71] Zhang, Y., Kallay, N., Matijevic, E., in *Interactions of metal hydrous oxides with chelating agents, VII., Hematite – Oxalic and Citric systems*, **1985**, 1, 201.

[72] Stumm, W., Furrer, G., Wieland, E., Zinder, B., in *The effects of complex-forming ligands on the dissolution of oxides and aluminosilicates. The chemistry of weathering*, **1985**, Dortrecht, 55.

[73] Waite, T.D., *Photo-redox Chemistry of Colloidal Iron Oxide,* in *Geochemical Processes at Mineral Surfaces*, **1986**, Washington, ACS Symp. Ser. No. 323, 426.

[74] Waite, T.D., Morel, F.M.M., *Photoreductive dissolution of colloidal iron oxide: Effect of citrate*, in *J. Colloidal Interface Sci.*, **1984**, 102, 121.

[75] Cornell, R.M., Schindler, P.W., *Photochemical dissolution of goethite in acid/oxalate solution,* in *Clays Clay Min.*, **1987**, 27, 347.

[76] Banwart, S., Davies, S., Stumm, W., *The role of oxalate in accelerating the reductive dissolution of hematite by ascorbate,* in *Colloids & Surfaces,* **1989**, 39, 303.

[77] Zinder, B., Furrer, G., Stumm, W., *The coordination chemistry of weathering, Dissolution of Fe(III) oxides,* in *Geochim. Cosmoshim*, **1986**, 50, 1861.

[78] Cornell, R.M., Posner, A.M., Quirk, J.P., *Crystal morphology and the dissolution of goethite,* in *J. Inorg. Nucl. Chem.,* **1974**, 36, 1937.

[79] Schwertmann, U., Kämpf, N., *The influence of aluminium on iron oxides., Dissolution of Al-goethites in 6M HCl,* in *Clay Min.*, **1984**, 19, 9.

[80] Surana, V.S., Warren, I.H., *The leaching of goethite., Mineral Process.,* in *Extr. Metall.*, **1969**.

[81] Warren, I.H., Roach, G.I.D., *Physical aspects of the leaching of goethite and hematite.,* in *Trans. Inst. Min. Metall.*, **1971**, 152.

[82] Schwertmann, U., Carlson, L., Murad, E., *Properties of iron oxides in two Finnish lakes in relation to the environment of their formation,* in *Clays Clay Min.*, **1987**, 35, 297.

[83] Sidhu, P.S., Gilkes, R.L., Cornell, R.M., Posner, A.M., Quirk, J.P., *Dissolution of iron oxides and oxyhydroxides in hydrochloric and perchloric acids,* in *Clays Clay Min.*, **1981**, 29, 269.

[84] Canfield, D.E., Berner, R.A., *Dissolution and pyritization of magnetite in anoxic marine sediments.,* in *Geochim. Cosmochim,* **1987**, 15, 645.

[85] Fischer, W.R., in *Standard potentials of iron(III)oxides under reducing conditions., Z. Pflanzenernähr. Bodenk.,* **1987**, 150, 286.

[86] Cornell, R.M., Giovanoli, R., *Acid dissolution of Akaganeite and Lepridocrocite: The effect on crystal morphology,* in *Clays Clay Min.,* **1988**, 36, 385.

[87] Schwertmann, U., Thalmann, H., *The influence of Fe(II), Si and pH on the formation of lepridocrocite and ferrihydrite during oxidation of aqueos $FeCl_2$ solutions,* in *Clay Min.*, **1971**, 11, 189.

[88] Cornell, R.M., Giovanoli, R., *Acid dissolution of hematites of different morphologies,* in *Clays Clay Min.*, **1993**, 28, 223.

[89] Cornell, R.M., Posner, A.M., Quirk, J.P., *Crystal morphology and the dissolution of goethite,* in *J. Inorg. Nucl. Chem.,* **1974**, 36, 1937.

[90] LaKind, J.S., Stone, A.T., *Reductive dissolution of goethite by phenolic reductants,* in *Geochim. Cosmochim.*, **1989**, 53, 961.

[91] Canfield, D.E., *Reactive iron in marine sediments,* in *Geochim. Cosmochim*. **1989**, 53, 612.

[92] Bernal J. D., Dasgupta, D.R., Mackay, A.L., *The oxides and hydroxides of iron and their structural interrelationships,* in *Clay. Min.,* **1959**, 4, 15.

[93] Sidhu, P.S., *Transformations of trace elements-substituted maghemite and hematite,* in *Clays Clay. Min.*, **1988**, 36, 31.

[94] Sidhu, P.S., Gilkes, R.J., Posner, A.M., *The behaviour of Co, Ni, Zn, Cu, Mn, and Cr in magnetite during alteration to maghemite and hematite,* in *Soil Sci., Soc., Am. J.*, **1980**, 44, 135.

[95] Feitknecht, W., Lehman, H.W., *The oxidation of magnetite to* γ *-* Fe_2O_3*., Helv. Chim.*, **1959**, 42, 2035.

[96] Niemantsverdriet, J. W., in *An Introduction to Spectroscopy in Catalysis,* **2007**, Wiley-VCH, Weinheim, 121.

[97] Wertheim, G.K., in *Mössbauer Effect: Principals and Applications*, **1964**, Academic Press, New York.

[98] Greenwood, N. N., Gibb, T. C., in *Mössbauer Spectroscopy*, **1971**, Chapman & Hall, London.

[99] Cranshaw, T. E., Dale, B. W., Longworth, G. O., Johnson, C. E., in *Mössbauer Spectroscopy and its Applications*, **1985**, Cambridge University Press, Cambridge.

[100] Dumesic, J. A., Topsøe, H., in *Adv. Catal.*, **1977**, 26, 121.

[101] Topsøe, H., Dumesic, J. A., Mørup, S., in *Applications of Mössbauer Spectroscopy*, **1980**, Academic Press, New York, 55.

[102] Van der Kraan, A. M., Niemantsverdriet, J. W., in *Industrial Applications of the Mössbauer Effect,* **1985**, Plenum, New York, 609.

[103] Mössbauer, R. L., in *Z. Phys.,* **1958**, 151, 538.

[104] Niemantsverdriet, J. W., in *An Introduction to Spectroscopy in Catalysis*, **2007**, Wiley-VCH, Weinheim, 147.

[105] Ashcroft, N.W., Mermin, N.D., in *Solid State Physics*, **1976**, Holt-Saunders, Philadelphia.

[106] Cullity, B.D., in *Elements of X-ray Diffraction*, **1978**, Addison-Wesley, Reading.

[107] Cohen, J.B., Schwartz, L.H., *Diffraction from Materials*, **1987**, Springer-Verlag, New York.

[108] Hammond, C., in *The basics of Crystallography,* **1998**, Oxford University Press, Oxford.

[109] Als–Nielsen, J., McMorrow, D., in *Elements of Modern X-ray Physics,* **2001**, Whiley, Chichester.

[110] Brunauer, S., Emmett, P.H., Teller, E., in *J. Am. Chem. Soc.,* **1938**, 60.

[111] Montaser, A., Golightly, D.W., in *Inductive Coupled Plasma in Analytical Atomic Spectrometry,* **1992**, VCH Publishers, New York.

[112] Alcock, N.W., in *Flame, flameless, and plasma spectroscopy, Analytical Chemistry*, **1995**, 67.

[113] Scott, P.W., in *Quantitative Chromatographic Analysis*, **2007**, Library4Science.

[114] Ettre, L.S., Hinshaw, J.V., in *Basic Relationships in Gas Chromotography,* **1993**, Advanstar, Cleveland, USA.

Chapter 3 - Results and Discussion

3.1 Introduction.

Spent, iron-based, high and low temperature Fischer-Tropsch catalysts are generated from fixed bed (FB), slurry bed (SB) and fluidized bed reactors at both Sasolburg and Secunda operations.

These spent iron-based catalysts are a mixture of wax (C_{18} +), and primarily, various iron phases including oxides, oxy-hydroxides and iron carbides. The spent catalysts as unloaded from the different reactors are in a reduced state and are partly or surface-oxidized when unloaded under water spray or water submersion. Although the catalysts are referred to as "spent" they are in fact still partially active, but the activity has diminished due to various deactivation mechanisms. For some applications the catalyst is unloaded to maintain an average catalyst age inside the Fischer-Tropsch synthesis reactors, implying the unloaded catalyst consists of a range of catalyst ages.

In all cases, the catalyst was used to promote hydrogenation and chain expansion of CO (Fischer-Tropsch process) to give methane, liquid paraffins, olefins and oxygenated hydrocarbons and heavy hydrocarbons such as waxes. Depending on the type of reactor used the wax that formed in the reactor will cover catalyst particles when these are removed from the reactor. Spent catalysts can be associated with 30 -60 % by mass wax.

In the case of the low temperature fixed bed reactor, spent iron-based catalyst particles consist of pellets roughly 6 mm in length with a diameter of 2.5 mm. These catalysts normally retain a higher degree of activity upon unloading because upon cooling the wax congeals and protects the catalyst from oxidation and the water used to unload the catalyst mostly causes surface oxidation only. Due to the size of the pellets the surface oxidation therefore accounts for a smaller percentage of total catalyst deactivation. Fixed bed reactors are shut down and unloaded completely. The reactor tubes are emptied using high pressure water jets. The catalyst is therefore soaked with water during the unloading process. This is desired as the oxidation that is caused, negates the pyrophoric nature of the spent "active" catalyst. The wax-coated spent catalyst pellets are then blended into a fine coal stream and burned for steam generation. After combustion, the mixed metal oxide residue is disposed of along with the ash generated from coal combustion. In comparison to the generated coal ash stream, the spent catalyst stream is small and the dilution factor is therefore high. As a result the residue can be disposed of within environmental legislation.

In contrast, the low temperature iron-based slurry bed catalyst has an "un-loaded" mean particle size of less than 250 μm and is filtered and / or sprayed from the Fisher Tropsch synthesis reactor while dousing with water. The degree of iron oxidation achieved during unloading is somewhat

higher due to the small catalyst particle size. The slurry bed reactor (SBR) is operated with an average catalyst age. This means that catalyst is unloaded and loaded regularly to maintain the average age. The spent catalyst is filtered from the slurry in order for the plant to maximize recovery of the associated high value reactor wax. In the past the filter cake was allowed to cool and congeal and the product was crushed *via* a hammer mill to smaller particles and blended into the fine coal stream used as combustion medium for steam generation purposes. Currently, due to filter constraints the catalyst and wax mixture is directly unloaded from the reactor. The slurry is sprayed through a nozzle with a water jet to produce a finely divided catalyst-wax mixture which is removed from site and land filled by an industrial waste disposal company. The composition of a typical Ruhrchemie iron-based catalyst precursor before activation and synthesis is shown in **Table 1.**

High temperature Fischer-Tropsch (FT) iron-based catalysts are also unloaded in water and then exposed to the atmosphere. It contains very little wax, but contains significant amounts of elemental or free carbon. Although the main focus of this study does not concern the high temperature catalyst, some of the knowledge gained will determine the suitability of this catalyst as a feedstock for the low temperature catalyst if successfully digested in acid. Spent catalyst for the high temperature iron-based Fischer-Tropsch process (the Synthol catalyst) is also loaded and unloaded from the reactor to maintain an average catalyst age. This catalyst is unloaded from the reactor under nitrogen and then quenched in water. Catalyst is disposed of through mixing with gasification coal ash and water and utilized as landfill material. The spent synthol catalyst contains very little wax. **Table 2** shows the approximate analysis of spent synthol catalyst.

Table 1. Approximate analysis of fresh Ruhrchemie type low temperature Fischer-Tropsch catalyst.

Analysis	Units	Results
Fe	mass %	56.0
Cu	/ 100g Fe	5.0
K_2O	/100g Fe	5.0
SiO_2	/100g Fe	24.0

Table 2. Approximate analysis of spent high temperature Fischer-Tropsch catalyst.

Analysis	Units	Results
Fe	mass %	57.8
C^{total}	mass %	20.3
C^{total}	/100gFe	35.1
Wax	mass %	3.8
Wax	/100gFe	6.5

3.2 Opportunity.

From the introductory information given it can be seen that a large amount of iron-based material is being disposed of during reactor unloading of "old" or "spent" catalyst that could potentially be recovered. The aim of any recovery project should be focused towards metal (Fe, Cu) recovery as iron and copper nitrate after nitric acid dissolution and subsequent re-use to produce "new" catalyst precursor. It would be advantageous if any wax that congealed around catalyst particles could also be recovered.

Figure 1 summarizes the strategies that were investigated in this study to recover catalytic metals and wax from spent iron-based Fischer-Tropsch catalysts. Two main recovery routes were investigated. The first involves the direct dissolution of the wax coated catalyst. In the second approach, the spent catalyst was subjected to various wax removal processes before metal recovery by acid dissolution was attempted.

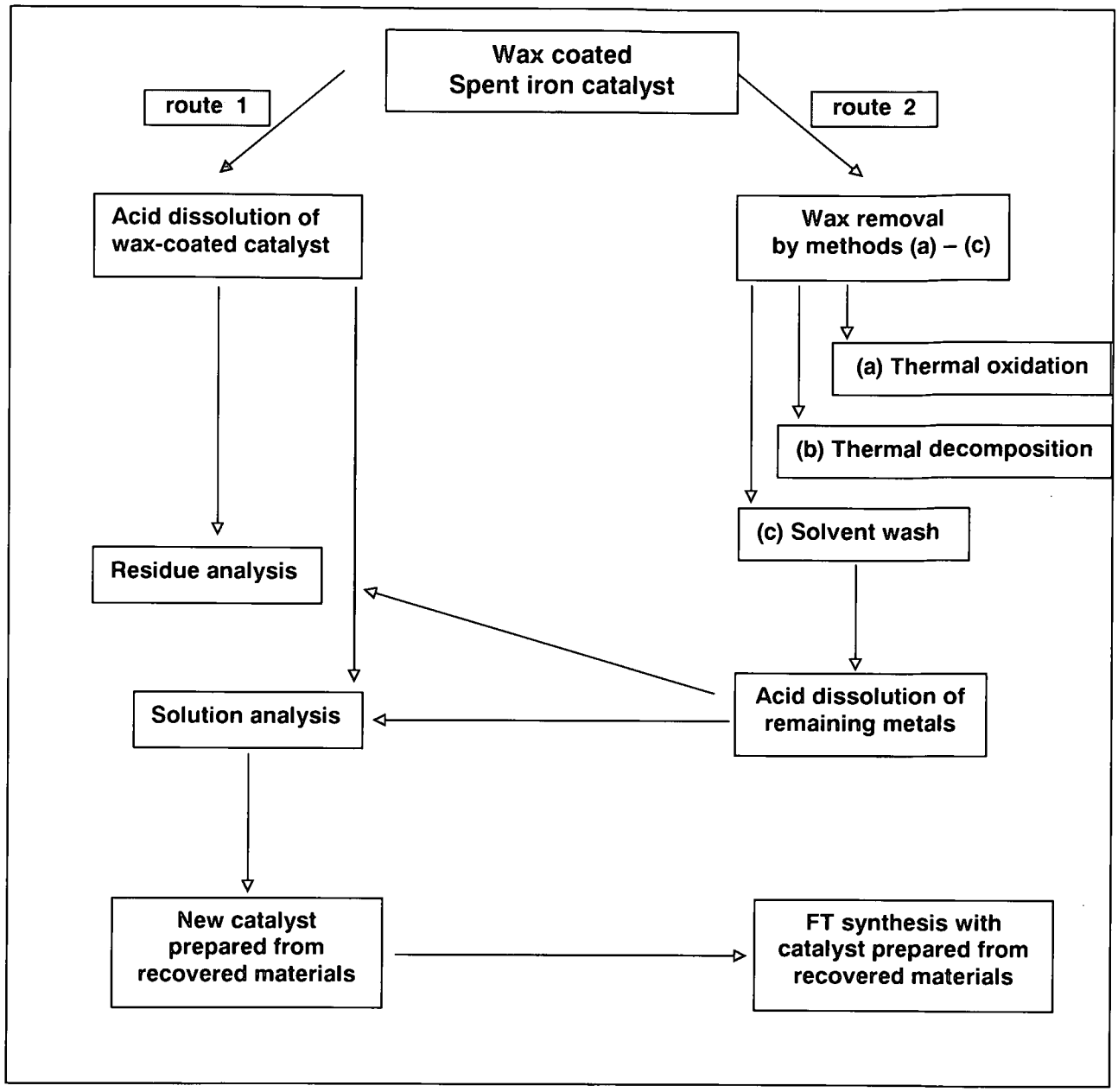

Figure 1. Schematic of project scope showing the various process under investigation.

3.3 Wax-Coated Spent Catalyst Recovery.

As previously noted, from a process simplification point and also for ease of integration with current commercial operations, recovering the metals from the wax coated catalyst rather than removing the wax first will be beneficial. Currently iron and copper metal is added to a concentrated nitric acid solution, manually, to prepare the Fe/Cu nitrate solution used to precipitate the iron bearing slurry. First a concentrated solution of > 100 g/l of iron in solution is prepared. The solution is then diluted to ca. 40 g/l of iron bearing ca. 2 g/l of copper. Adding the wax-coated catalyst to the same "dissolution" vessel will therefore have little cost implication although by-product separation in terms of the wax and acid insoluble material will have to be addressed. Preliminary experiments were conducted investigating this approach by using spent wax coated Ruhrchemie type iron-

based catalyst used for the low temperature slurry bed operations. All dissolution experiments, unless otherwise noted, were performed in a fume cupboard with PVC gloves and eye protection as a minimum precaution. The acidic nature of the experiments, as well as the accompanying production of NOx gases[a] necessitates caution.

A known amount of wax coated iron-based catalyst with known iron content was added to the same amount of concentrated nitric acid as employed for preparation of the fresh catalyst. Including the wax content, the mole ratio of acid to wax-coated catalyst was 4:1. This is stoichiometrically more acid than required but excess acid ensures that the dissolved metal nitrate species do no reach saturation in solution. The acid solution was preheated to 80 °C which is similar to the dissolution temperature at which metals are added to nitric acid commercially. Experiments were performed in a 2000 ml glass beaker with mild agitation (120 rpm) by "propeller" type impeller from an overhead stirrer. The glass beaker was placed on a heating plate controlled by a thermocouple placed inside the solution. The liquid level was maintained by first marking the liquid level after spent catalyst addition and then correcting with deionised water. Losses occurred due to evaporation during the experiment at 80 °C. The experiment was conducted and 6 samples, taken hourly, were submitted for inductive coupled plasma analysis. Liquid samples were first filtered to remove all solid material. The analytic results are shown in **Table 3.**

Table 3. Solution composition results for wax coated spent iron-based slurry bed catalyst dissolved in nitric acid with samples taken hourly.

Sample time (hr)	Analysis	Results (g/l)
1	Fe	89.9
	Cu	4.9
2	Fe	91.5
	Cu	5.1
3	Fe	94.9
	Cu	5.4
4	Fe	102.1
	Cu	5.7
5	Fe	99.7
	Cu	5.6
6	Fe	97.2
	Cu	5.5

[a] NOx is the abbreviation that is industrially used for mixtures of NO, NO_2, N_2O_5 and other nitrogen oxygen gas mixtures.

Complete dissolution would have resulted in a solution containing 143 $g.l^{-1}$ Fe and 5.7 $g.l^{-1}$ of Cu. The results from **Table 3** shows, surprisingly, that the dissolution process is very rapid initially and that high copper and iron concentrations are noted after 1 hr of dissolution. The lower concentrations reported for hours 5 and 6 are because of previous sample volume removal and volume correction by adding deionised water. It is also important to note that the copper seems to dissolve more rapidly than the iron. Evaluation of the liquid sample revealed that approximately 68% of the loaded iron and almost all the copper were removed.

The following observations were made during the dissolution process

1. The exothermic dissolution reaction caused the solution to heat to boiling temperature (103 °C). The high temperatures lead to rapid evaporation of water vapour from the solution. Elevated temperatures also increase the safety risk of the process.
2. Large volumes of NOx gasses evolved during the process, as was expected, during the oxidation of the reduced iron species with HNO_3 as well as during the oxidation of associate wax (C_{20}+) coatings.
3. The escaping gasses caused foaming that reached 2,5 times the height of the original liquid level. The foaming caused initial experiments to be abandoned due to overflowing. Taller beakers were then used to be able to do the experiments.
4. Wax congealed on the surface of the resultant liquid upon cooling. The wax contained some un-dissolved catalyst particles and was in the form of a paste rather than a well defined wax layer.

The experiments showed that the reaction heat liberated could potentially be used to heat the solution thereby reducing the process energy requirement. The process was vigorous and the foaming problem would have to be addressed because the current commercial plant vessels would not be able to contain the volume increase due to the foaming. The rapid evolution of NOx would also be problematic to deal with commercially because the NOx is sent to a NOx recovery unit with fixed flow rate. A higher flow rate, due to the rapid dissolution initially might cause the unit to be ineffective. Most of these problems can be negated by adding smaller amounts of spent catalyst at a time. The NOx production and foaming could be controlled in this fashion. For this study, milder dissolution conditions were investigated to negate the problems. To reduce the rate of the reaction the acid concentration was reduced to 50% of the original 45 mass% nitric acid concentration. The experiment was repeated and samples after 4, 5 hours and 6 hours was submitted. The results are shown in **Table 4**.

Table 4. Solution composition results for wax coated iron-based slurry bed catalyst dissolved in nitric acid with samples taken hourly (27.5 mass% nitric acid concentration).

Sample time (hr)	Analysis	Results (g/l)
4	Fe	60.6
	Cu	3.8
5	Fe	61.2
	Cu	4.09
6	Fe	63.4
	Cu	4.3

From the results in **Table 4** as well as from the solution temperatures it could be seen that the lower nitric acid concentration led to a milder process with lower iron and copper recoveries after similar stirring times. In addition, using a lower acid concentration would complicate things in existing plants as the vessels on the existing plant would become too small to dissolve the required amount of metals to maintain production rates.

Subsequently spent iron-based fixed bed catalyst pellets were added to ambient temperature concentrated nitric acid with mild agitation (120 rpm). The lower starting temperature would reduce the initial reaction rate and the heat of dissolution generated would be able to heat the solution as opposed to external heating. Spent fixed bed catalyst pellets were used as opposed to the spent slurry bed catalyst of the previous experiment. The fixed bed catalyst was easier to work with because it is discrete particles. Slurry bed catalyst is also often in the form of "chunks" containing catalyst and wax of varying solid content. Fixed bed catalyst on the other hand has a much more uniform solid to wax ratio and the accuracy of the experiments would therefore be better. The larger particles, and hence lower outer surface area for the same mass of catalyst, would also dissolve slower and therefore be better for the initial investigation where excessive rates have shown difficulties.

The temperature of the solution increased during the fixed bed catalyst dissolution process but dissolution rates and metal recoveries were low (54 $g.l^{-1}$ Fe^{3+} from a possible 143 $g.l^{-1}$). Better recoveries were attained by increasing the retention time but the same final recoveries, as for the "high temperature" dissolution, was not attained. Due to the associated wax, contact between the acid and metal was insufficient. The wax layer "protects" the metal surface from being attacked by the acid solution. At lower temperatures the wax does not melt and results in poor acid-metal contact. The problem could be addressed by either elevated temperatures (above the wax melting point ~ 94-97 °C) or more vigorous agitation (breaking up and exposing the metal surface). Larger

fixed bed iron-based catalyst particles also had significantly lower external surface areas and would therefore already react slower than the finely divided spray dried spent catalyst.

The initial experiment (acid pre-heated to 80 °C) was repeated for the fixed bed spent wax coated catalyst and vigorous agitation (800 rpm) was introduced *via* high shear mixing. High shear mixing on the heated (80 °C) solution resulted in increased dissolution rates and rapidly heated the solution to boiling point. Positive results in terms of metal recoveries were obtained from this method, but the reaction rates were still excessive as was seen from solution temperatures and NOx production.

Thereafter spent catalyst was added to ambient nitric acid, to slow initial reaction rates, with high shear mixing. High shear mixing would increase reaction rates due to better acid to metal contact through wax particle break-up. Ambient nitric acid experiment with mild agitation did not yield high recoveries because the temperature of the liquid mixture did not increase significantly. High shear mixing however increased the temperature of the solution and led to higher dissolution rates. A typical temperature profile with time for this experiment is shown in **Figure 2**. Thus by utilizing the exothermic reaction energy rather than external heating the energy requirement for the process would be less. Within short reaction times (<1 h) temperatures reached around 80 °C with high, > 80%, iron and copper recoveries.

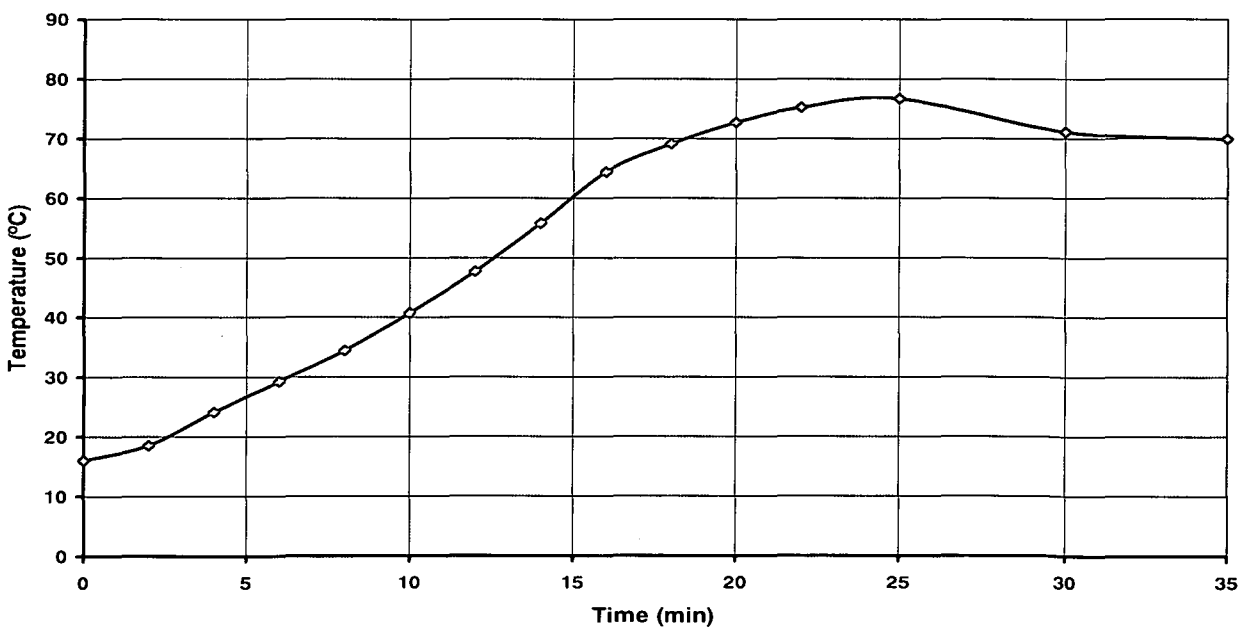

Figure 2. Typical time *versus* temperature profile attained with spent fixed bed wax coated catalyst loaded into ambient temperature nitric acid with high rate (800 rpm) mixing.

Without further optimization it was decided to first investigate the wax separation from the resultant solution in order to investigate the viability of further process steps. The next step therefore was to filter the resultant solution to separate the un-dissolved catalyst and wax from the liquid.

Filtration through acid resistant glass micro fibre filter material on a Buchner filter, with vacuum assistance, facilitated virtually no filtration. Pressure filtration (5 bar nitrogen) also showed extremely low filtration rates. Wax separation *via* filtration is difficult due to the large amount of wax. The malleable nature of wax leads to clogging of the filter medium. The wax particles formed an emulsion-like solution which was difficult to filter. The high pressure filtration method produced an acidic filter cake with high moisture content containing emulsion-like wax particles as well as some of the liberated silica and un-dissolved catalyst particles originally present in the spent catalyst.

In an attempt to increase wax separation during dissolution, thereby reducing the amount to be filtered, the reaction mixture was externally heated from 80 °C to 103 °C. The temperature increase was done after dissolution of the metal particles. This was done to ensure that the mixture was well above the congealing point of the wax (94-97 °C). Agitation was terminated after dissolution while the temperature was maintained at 103 °C. Wax separation was now aided as wax could float unhindered to the surface of the aqueous solution due to the lower density of the wax. The solution was then left to cool. Upon cooling the wax solidified in a solid layer on top of the solution and could be removed by hand. By utilizing this method substantially better wax separation was achieved and subsequent filtration of the solution was easier although filtration required residence times of more than 24 h under 5 bar nitrogen pressure to obtain a filtrate. The resulting filtrate contained Fe/Cu nitrates in suitable ratios and concentrations for the preparation of a new catalyst precursor. Small amounts of wax and silica was separated from the filtrate through centrifuge.

The solid wax product consisted primarily of wax although some associated silica and small amounts of iron and copper were also detected. The ratio of the Fe/Cu corresponds to the ratio in the spent catalyst, indicating un-dissolved catalyst particles trapped in the wax. These particles might be dissolved with better agitation or increased residence times thereby obtaining a cleaner wax fraction.

Removing the floating solidified wax fraction by hand experimentally, however, cannot be done on a commercial scale. Therefore after the wax layer formed and ambient conditions were reached, the stirrer was again started to see if the wax will break-up to more manageable fragments. The stirring, even at low rotation, rapidly formed an emulsion with similar filtration difficulties. The wax layer that was produced is mechanically weak probably due to the presence of moisture, acid and silica and catalyst particles.

A possible commercial solution would be to remove the molten wax fraction at ca. 102 °C by adding water to the bottom of the vessel as the metal nitrate solution is commercially also diluted later and will therefore not cause a undesirable effect on the metal nitrate solution. When the wax is decanted, the metal nitrate solution can be drained from the bottom of the vessel. The drained metal nitrate stream could pass through to a filter to remove un-dissolved spent catalyst particles. As a precaution draining only to a level well below the interface of the wax and metal nitrate solution is desirable to limit the waxy fraction from leaving the vessel. This process can be made cyclic because the correct nitric acid concentration may then be introduced through the same drain point and spent catalyst added to repeat the process. Periodically the vessel will probably have to be completely drained and cleaned. The process is illustrated in **Figure 3**.

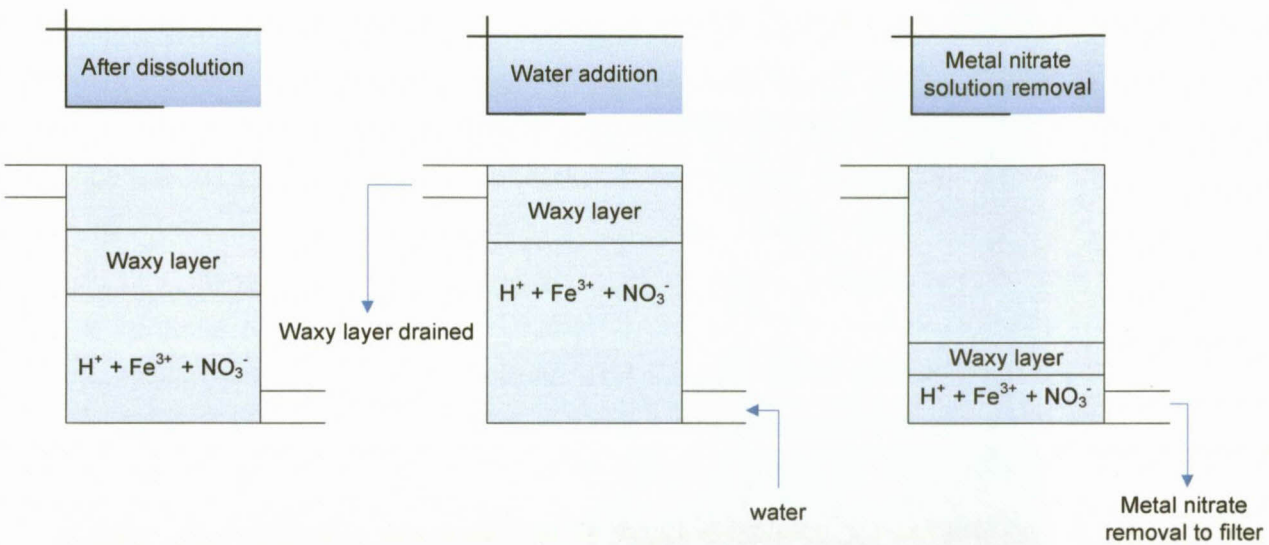

Figure 3. Possible commercial process of removing the molten wax fraction by adding water after acid dissolution. Thereafter, removal of the metal nitrate solution from the bottom of the vessel to a filter to removed un-dissolve spent catalyst particles is possible. The process can be made cyclic by repeating the process of adding nitric acid and spent wax coated catalyst for dissolution.

The following observations were made and conclusions drawn during the amended dissolution process.

1. The most encouraging results were obtained during high speed agitation. The high shear agitator not only serves as an agitator but also breaks up the spent catalyst particles thereby increasing the catalyst surface available for dissolution, particularly at low

temperatures where wax covers most of the catalyst. The mixing step will therefore have to be changed from the current commercial low shear mixing system to high shear mixing.

2. As the temperature of the solution increase more NOx gases are released at higher rates. These gases, and/or the action of the high shear mixer, causes excessive foaming. The foam rises in the vessel and might cause it to overflow. The cause of the foaming should be investigated and preventative measures taken. Mechanical means, such as an impeller above the liquid level, may also be used to reduce the foam and as mentioned before spent catalyst can be loaded in smaller batches. Smaller catalyst batches will probably require additional external heating as not enough heat will be produced by the smaller batches.
3. During longer experiments where no water was added to maintain a constant volume, crystallization took place during cooling. Attention will have to be given to concentrations were crystal formation may be problematic. During normal commercial operation crystallization never takes place. The crystallization may be propagated by the silica particles or the formation of different complexes.
4. The high temperatures needed for wax separation will cause evaporation and the vessel will have to be fitted with additional condensing capacity for the escaping vapours.
5. Wax separation was the single most important parameter when this process was evaluated. Wax recovery is inefficient and problematic mainly due to wax separation and filtration difficulties. Even limited amounts of wax, less than 5% cause severe filtration problems. Removing un-dissolved solids from the wax *via* filtration will also cause a filter cake associated with wax albeit significantly smaller amounts. From laboratory experimentation it was noted that wax separation in the liquid (molten) phase was never complete. Wax can be nitrated under these conditions which would increase the polarity of the wax. Polar components are more likely to form emulsions as was seen during the experiments. Emulsions would be increasingly difficult to filter. The improved separation obtained required high temperatures and process time was extended. This entails that wax remains a part of every subsequent stream and causes difficulties during further processing. The waxy filter cake that was produced also contains acid, catalyst particles and silica which means further processing of this stream is required before disposal or recovery of pure wax.

3.4 Wax Removal Investigations.

3.4.1 Introduction.

During the first part of the study, wax coated spent catalyst was used to study metal recovery because of process simplicity.It was seen that the recovery of catalytic metals showed promise but that the by-product streams, as well as process implications, such as filtration, makes effective metal recovery difficult. Removal of wax from the crude spent plant-recovered catalytic material would reduce the amount of material to be handled. It could also be seen that the recovered waxy product needs further purification from traces of metals before it can be utilized elsewhere commercially. Therefore the waxy product produced would require more process steps as opposed to less than was initially expected. It was decided to investigate other means of wax removal.

Wax can be removed from crude spent catalytic plant waste *via* various processes. Within the scope of this study, the following technologies were considered:

1. Solvent extraction – allows for the recovery of the wax without hydrocarbon chain length changes.
2. Thermal oxidation – destroys the wax to CO_2 and water
3. Thermal cracking – destroys the wax to shorter chain hydrocarbons.
4. Combinations of these technologies.

Solvent extraction - Solvent extraction involves an organic solvent, such as xylene or various paraffinic solvents, that is utilized to dissolve the wax and then drained from the spent metal-based catalyst containing especially iron and copper. This method fits well into the scope of catalyst recovery because lighter hydrocarbon streams that can be used as solvents are available from the Fischer-Tropsch Synthesis process.[1] The hydrocarbon streams generated could be integrated into the refinery section of current and future operations. Solvents such as xylene which are expensive and environmentally undesirable could be recovered and re-used. However, from previous experience it is known that it is very difficult to completely remove all the wax from recovered spent catalysts. The catalyst has a large internal surface area with extended porosity and the solvent does not penetrate to remove all the wax in the catalyst pores. Some wax will therefore remain in the interior of the catalyst particle. This must be considered during recovery of iron and copper from the spent catalyst resulting from solvent extraction.

Thermal oxidation - Thermal oxidation or burning off the wax in the presence of air can be done by technologies used for various other processes such as incineration, calcining, devolitization and oxidation. Wax also has a very high heating value and could make the process energy self sufficient and be used as heat source for alternative activities such as steam generation. Typical

heating values for slurry bed and fixed bed type spent catalysts are shown in **Table 5**. The heating values for wax removed (*via* solvent extraction) spent catalyst are also indicated. From these values the calorific contribution from the wax can be clearly seen. Since the wax is never completely extracted there is still a calorific contribution from the extracted catalyst because of the incomplete wax extraction. Wax also burns very "cleanly" to give off water and carbon dioxide as products (as determined by TGA/MS), as it consists almost exclusively of carbon and hydrogen.

Table 5. The calorific values for wax coated and solvent extracted samples from fixed as well as slurry bed operations.

Sample name	Analysis	Units	Results
Spent slurry bed catalyst	calorific value	kJ/kg	21478
Extracted spent slurry bed catalyst	calorific value	kJ/kg	4270[a]
Spent fixed bed catalyst	calorific value	kJ/kg	16840
Extracted spent fixed bed catalyst	calorific value	kJ/kg	2872[b]

[a] The wax remaining in the spent slurry bed catalyst after extraction is ca. $\frac{4270}{21478} X 100 = 20\%$

[b] The wax content remaining in spent fixed bed catalyst after extraction is ca. $\frac{2872}{16840} X 100 = 17\%$

The syngas feed stream to the reactors that are used for Fischer-Tropsch Synthesis is extensively cleaned of contaminants, such as sulphur, and these are therefore not present in the wax. This means that off-gas cleanup from the thermal oxidation process will be limited. Off-gas from the process could also be handled within the normal refinery product work-up as the composition will be similar to other process streams. Thermal oxidation has the advantage of simplicity but the disadvantage that a high value product (wax) is destroyed. In addition, the temperature reached during wax combustion determines the final iron oxide phase recovered.[7] Not all the oxide phases dissolve equally well or easily. Hence, the temperature of combustion may significantly influence the ease of dissolution of recovered iron oxide, and will consequently influence the dissolution properties. Results for this investigation are described in section 3.4.2.

Thermal cracking - Thermal decomposition or "cracking" of the wax under inert (i.e. oxygen-free) conditions will produce mostly gaseous short chain hydrocarbons that may also be recovered *via* the normal gas recovery system after the Fischer-Tropsch Synthesis reactors. Phase transformations will have to be carefully considered as some organic material, such as carbon, can function as a reducing agent under certain conditions.[4] It is expected that under certain experimental conditions graphitic carbon could also remain on the catalyst.[1] Results for this part of the study will also be presented in section 3.4.3.

3.4.2 Thermal oxidation as method to remove wax.

Experimental dissolution equipment used to recover iron and copper as soluble nitrate salts was not altered from the wax coated dissolution study described in section 3.3. The only difference was the removal of wax before metal dissolution by thermal oxidation. Spent fixed bed catalyst was thermally oxidized at 500 °C and also at 850 °C and the weight loss determined in each case. The results indicated that all the external wax is removed at 500 °C. The spent catalyst was then submitted for Thermo Gravimetrical Analysis (TGA) analysis to determine the wax burn-off profile. A catalyst sample was analyzed by heating a chamber containing the sample holder connected to a scale in the presence of air. The weight loss was then measured as a function of temperature. The profile is shown in **Figure 4.** From the analysis it can be seen that the wax self ignites and rapidly burns off at approximately 280 °C.

This means that the oxidation step does not require excessive temperature conditions and could possibly be energy self sufficient and generate additional energy from the combustion process. Due to the very small sample analyzed (< 1 g) the possible effect of higher temperatures generated by the burning wax is not seen here.

The fairly low burn-off temperature would impact positively on equipment costs and would prevent excessive sintering (loss of surface area) and phase transformations of the remaining metal oxides. As the catalyst is oxidized under inceasingly elevated temperatures, a more crystalline iron oxide phase such as hematite (Fe_2O_3) can be expected which would be much more resistant to acid attack during the dissolution process as was discussed in the literature[2] review (chapter 2, paragraph 2.6.5).

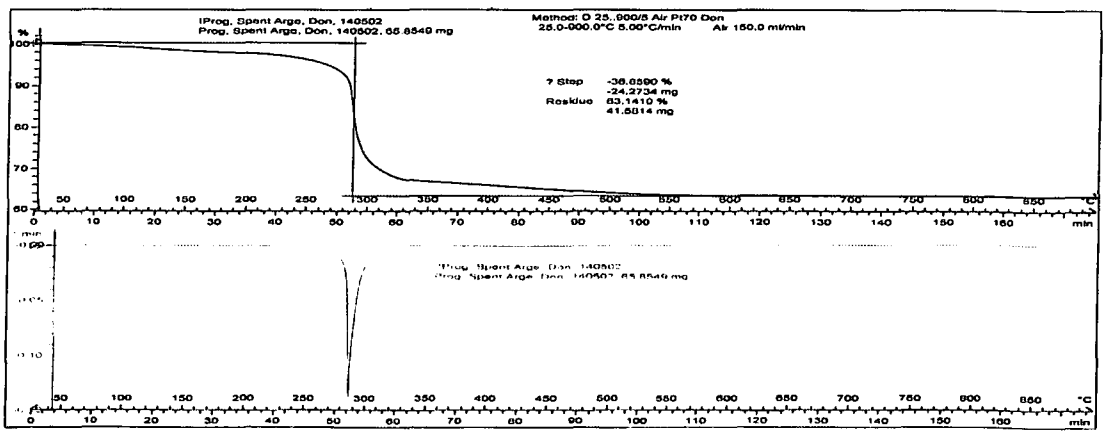

Figure 4. Top - Thermo Gravimetrical Analysis (TGA) of wax coated spent iron-based catalyst form Fisher Tropsch Synthesis operations heated at a rate of 5 °C.min^{-1} in the presence of a constant air flow. Mass loss was 36.9% Bottom – First derivative of TGA curve.

In a first experiment spent catalyst from a fixed bed reactor was oxidized in air at 500 °C. This burnt most of the wax. The remainder of the wax-free spent catalysts that was left after bulk thermal oxidation at 500 °C was then immersed in concentrated nitric acid at ambient temperature to investigate metal dissolution as described before (section 3.3). Only a very slight increase in solution temperature was observed which indicated a slow dissolution rate. This was to be expected given the higher oxidized form of the iron attained after thermal oxidation at 500 °C, and the absence of wax that could be oxidized.

The solution was subsequently heated externally to normal dissolution temperatures of 85 °C and maintained for 20 h. Approximately 75% of the solid oxidized spent catalyst particles were dissolved after 20 h. An important observation from the dissolution process was the negligible formation of NOx compounds. During the dissolution of the wax coated particles significant NOx production was observed. The reduced formation of NOx is the result of two changed factors in this experiment over that described in section 3.3. First the iron that is dissolved in the nitric acid is not Fe(0) anymore. It is already oxidized Fe(III). Secondly, there was no external wax left that could be oxidized. A reduction in NOx production would be very favourable from an environmental and off gas handling perspective.

In an attempt to increase the dissolution rate of the wax-free spent catalyst, the remaining residue after wax-removal was crushed with a mortar and pestle and the dissolution experiment repeated. It is important to note that the spent wax free catalyst is easily crushed and should not require expensive crushing equipment if crushing is required for commercial application. The slurry bed iron-based spray dried spent catalyst, already very fine, will also be utilized for recovery purposes; not just the fixed bed catalyst as in the above described process. The temperature of the dissolution experiment on the ground catalyst residue increased compared to the uncrushed catalyst but the final recovered amount was not altered much. Un-dissolved solids were again treated with concentrated nitric acid, in a similar experiment, but very little dissolution took place. The residue from the first dissolution was therefore very resistant to further dissolution by nitric acid, probably because the iron oxide was in a phase that was very resistant to dissolution.

Mössbauer spectroscopy was used to determine the phase identity of the iron oxide phases present in the spent catalyst before dissolution and the un-dissolved fraction after initial dissolution. Mössbauer spectra showed that the un-dissolved solid consists almost entirely of crystalline hematite (**Figure 5(c)**). Quantitative results are shown in **Table 6**. Crystalline hematite is known to be resistant to dissolution by mineral acids.[3] The use of organic acids such as oxalic acid, as well as other complexing ligands may prove to have higher dissolution efficiency but may be difficult to integrate into a commercial system suitable for dissolving oxidized spent iron-based catalyst from Fischer-Tropsch synthesis processes.

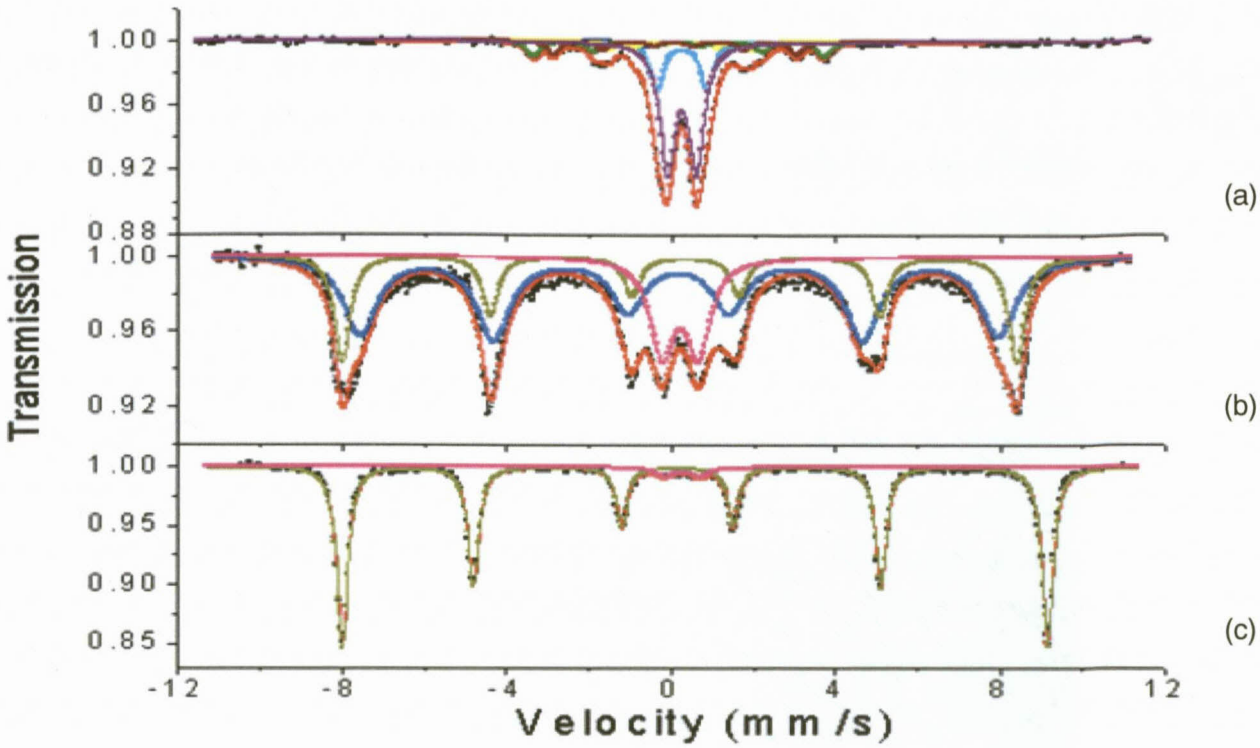

Figure 5. (a) Red line shows the experimentally determined Mössbauer spectra obtained, at room temperature analysis, from spent iron-based catalyst. (b), Red line shows the Mössbauer spectra obtained of spent catalyst oxidized in air at 500 °C (c) Redline obscured by green, hematite, line due to this being the predominant phase present in the residue after nitric acid dissolution of the sample described in (b). The other lines in (a), (b) and (c) were theoretical simulations of pure iron carbide, maghemite, Fe(III). Fe(II), ferrihydrite and hematite in the correct intensity to give the experimental determined spectrum as resultant when super-imposed on top of each other. The relative contribution of each iron phase is summarized in Table 6.

The Mössbauer analysis, of the wax coated spent iron-based catalyst (**Figure 5(a)**), shows the superposition of magnetic and superparamagnetic components. The magnetic components (three sextets – brown, green and yellow)) correspond to 26% of Hägg carbide (χ-$Fe_{2.5}C$). The doublet (purple) with isomeric shifts of 0.35 $mm.s^{-1}$ are identified as ferrihydrite (71%) and the doublet with isomeric shift of 0.96 $mm.s^{-1}$ (turquoise) has parameters typical of ferrous (Fe(II)) (pink) species of 3%. Mössbauer spectra of pure examples of each phase can be found in chapter 2 section 2.7.1.6. These results are in line with what is expected of a working iron-based catalyst removed from the reactor and coated in wax.[1]

From the second set of spectra (**Figure 5(b)**) the appearance of the sextets indicates the presence of maghemite (dark blue) and hematite (green). All the samples were fitted with a sharp sextet assigned to large crystallites of hematite (green), a broad sextet indicative of well crystallised maghemite (blue) and a doublet typical of superparamagnetic Fe(III) species (pink). The last spectra set (**Figure 5(c)**) consist almost entirely of a sharply defined sextet indicating large crystallites of hematite (green) with a small doublet representing Fe(III) species (pink). It can be deduced from the results that, with the exception of crystalline hematite, the other iron oxide phases are dissolved in nitric acid. Hematite and specifically very crystalline hematite show virtually no dissolution even when contacted with "fresh" nitric acid for a second time.

Table 6. Summary of the quantification results for selected iron-based spent catalyst samples analysed at 77 K.

Treatment	% Contribution (77K)					
	χ-$Fe_{2.5}C$ Iron Carbide (Hägg Carbide)	γ-Fe_2O_3 Maghemite	Fe^{3+}	α-Fe_2O_3 Hematite	Fe^{2+}	$Fe_5HO_8 \cdot 4H_2O$ Ferrihydrite
Spent catalyst[a]	26	-	-	-	3	71
Oxidized 500 °C	-	73	8	19	-	
Residue	-		4	96	-	

a Room temperature Mössbauer

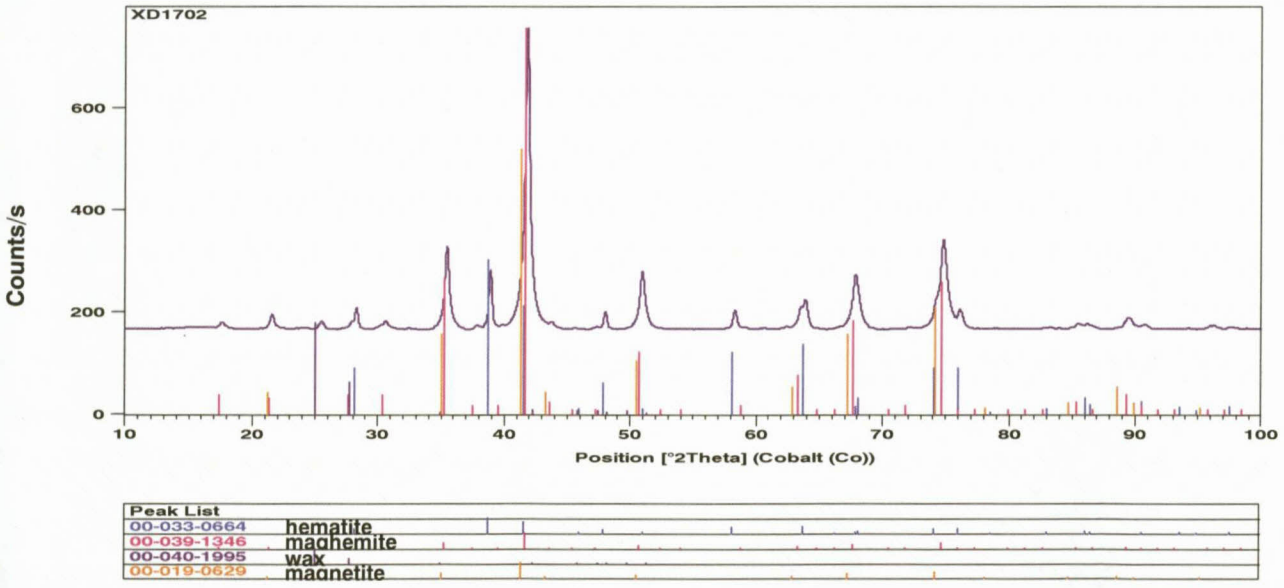

Figure 6. X-Ray diffractogram of the spent iron-based catalyst thermally oxidized at 500 °C in the presence of air before acid dissolution. Main phases identified are maghemite (73%), hematite (19%) and magnetite (2%). A weak fit for carbonaceous material was also performed to account for the remaining 6% which may have been due to incomplete combustion.

XRD analysis of the before-and-after dissolution in nitric acid experiments show that for the before dissolution sample the main phases identified were maghemite and hematite as was expected (**Figure 6**).

The XRD pattern for the remaining residue of the sample after dissolution (**Figure 7**) shows a very clear increase in crystalline material. Mainly the phase identified here is crystalline hematite. Sharper peaks, which correlate with pure hematite, can be clearly seen. The higher the degree of crystallinity the less the structure will be accessible for acid attack. An increase in crystallinity normally correlates with a loss in surface area which may lead to lower dissolution rates.

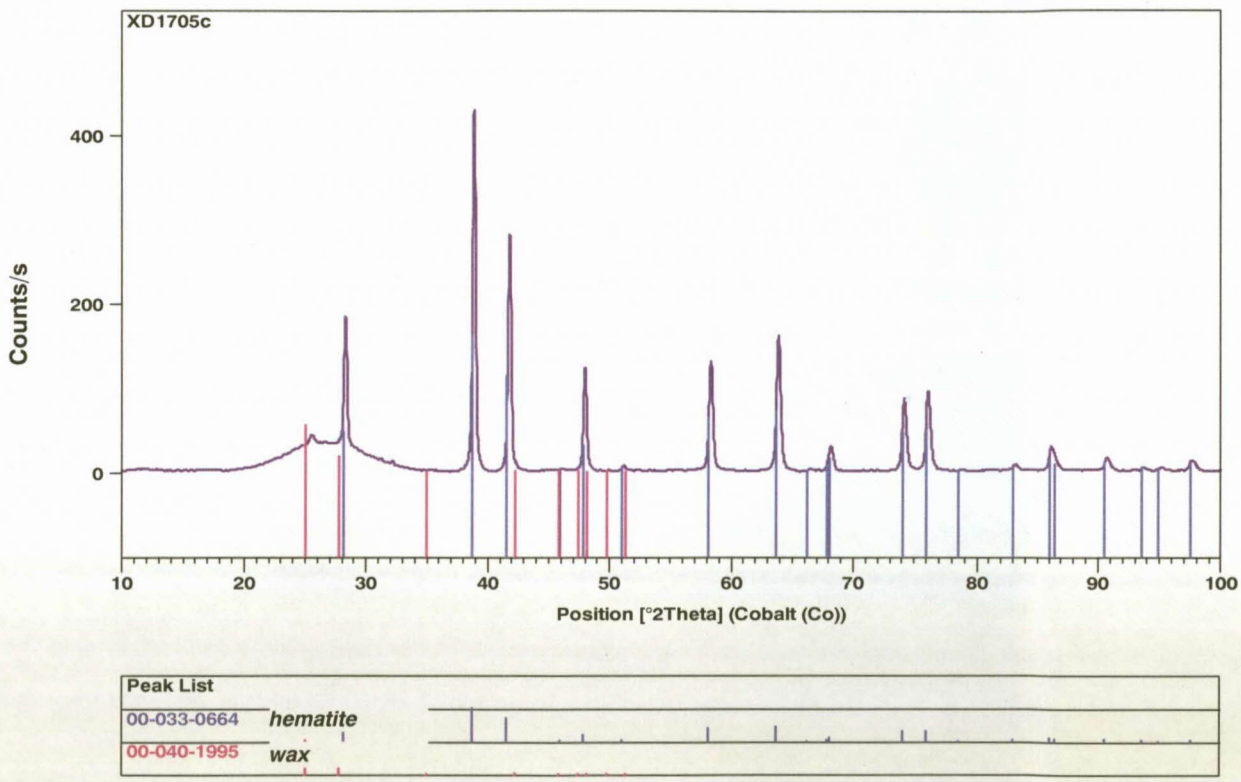

Figure 7. X-Ray diffractogram of the residue remaining after iron-based catalyst thermally oxidized at 500 °C in the presence of air and dissolution with nitric acid. The main phase reported was hematite (96%). A weak fit was also made for carbonaceous material (4%) which may have been left from incomplete combustion of the wax trapped inside the catalyst pores.

It was decided that before additional research was done on improving the dissolution yields a fresh catalyst precursor was to be prepared from the resultant iron/copper nitrate solution. The catalyst precursor should conform to standard catalyst precursor specifications. The catalyst precursor is to be activated and subjected to standard FT synthesis conditions to evaluate the performance of the catalyst. Similar performance to the standard low temperature iron-based catalyst under FT

synthesis conditions must be achieved to make the iron recovery experiment worthwhile. Only once proven that the newly prepared catalyst has similar physical and FT synthesis performance than commercial catalysts would the further optimization of dissolution rates be meaningfull.

3.5 Catalyst preparation and Fischer-Tropsch synthesis evaluation.

A larger scale dissolution experiment was conducted to produce enough of the concentrated Fe/Cu nitrate solution to prepare a batch of catalyst. The solution was diluted to the required specification of approximately 45 g/l of iron and a fresh catalyst precursor was prepared.

The larger scale prepared Fe/Cu nitrate solution was then precipitated with a standard Na_2CO_3 solution to produce an iron bearing slurry. The precipitation process was repeated three times to ensure that a constant precipitation product could be produced, see **Table 7**. The slurry was filtered from the solution and thoroughly washed with deionised water. The (150 °C dried) slurry is compared in **Table 7** to a normally prepared Ruhrchemie type catalyst at a similar production step.

Table 7. Component analysis of catalyst precursor produced from a standard metal nitrate solution compared to three catalyst precursors prepared from metal nitrate solutions generated by wax free oxidized spent catalyst dissolution in nitric acid.

Sample name	Analysis	Units	Results
Standard catalyst	Fe	mass%	65.40
	Na_2O	/100gFe	0.07
	Cu	/100gFe	5.55
Larger scale 1	Fe	mass%	65.37
	Na_2O	/100gFe	0.02
	Cu	/100gFe	4.91
Larger scale 2	Fe	mass%	64.04
	Na_2O	/100gFe	2.01
	Cu	/100gFe	4.73
Larger scale 3	Fe	mass%	67.18
	Na_2O	/100gFe	0.86
	Cu	/100Fe	4.74

From the results in **Table 7** it can be seen that a very similar precipitated iron-bearing slurry was produced using the Fe/Cu nitrate solution derived from the wax free oxidized spent catalyst. Sample larger batch 2 shows slightly higher Na_2O results which is a function of the washing

efficiency. This iron-based precipitate was therefore not washed sufficiently. The next step was to impregnate the catalyst with potassium waterglass (potassium silicate) and spray dry the resulting slurry in order to form spherical particles.

Due to the larger scale filter equipment available the impregnated catalyst had too much potassium compared to the standard catalyst precursor. The potassium is, however, still in a water soluble phase and therefore by washing the catalyst with deionised water, some of the potassium can be removed to produce a catalyst that is within specification. Care must be taken not to remove too much potassium as that would require re-impregnation of additional potassium. Therefore small quantities of water were used in each wash. The third wash resulted in a catalyst precursor of the required potassium promoter levels. The results for the final catalyst precursor produced and tested in a micro slurry reactor along with the standard specification are given in **Table 8**.

From **Table 8** it can be seen that the catalyst precursor, although not completely within specification, has a composition very close to that of a typical Ruhrchemie iron-based low temperature Fischer-Tropsch catalyst precursor.

The spray dried catalyst precursor was then calcined at 450 °C for 2 h and placed in a micro slurry reactor. Reduction and Fischer-Tropsch Synthesis conditions utilized for the comparison are shown in **Table 9**.

Table 8. Composition of catalyst prepared from the iron/copper nitrate solution generated by spent de-waxed catalyst dissolution in nitric acid.

Sample name	Analysis	Units	Results	Specification
Fresh catalyst after 3rd wash	Fe	mass%	52.23	54.0 – 60.0
	K_2O	/100g Fe	4.94	4.3 – 5.0
	Cu	/100g Fe	5.54	4.6 – 5.3
	Si	/100g Fe	28.8	22.0 – 26.0
	Surface area	m^2 / g	242	210 -260
	Pore volume	cm^3 / g	0.45	0.45 – 0.75

Table 9. Reduction and FT synthesis conditions employed on a micro slurry reactor to evaluate the performance of the catalyst produced from spent de-waxed catalyst.

Reduction with syngas		
	Value	**Unit**
Temperature	240	°C
Pressure	20	bar
Total space velocity	4800	(N)ml.g-cat^{-1}.h^{-1}
Syngas space velocity	4000	(N)ml.g-cat^{-1}.h^{-1}
Stirrer	450	rpm
Time	16	h
Synthesis with syngas		
Temperature	240	°C
Pressure	20	bar
Total space velocity	3600	(N)ml.g-cat^{-1}.h^{-1}
Syngas space velocity	3000	(N)ml.g-cat^{-1}.h^{-1}
Stirrer	450	rpm

In order to determine gas flows to and from the reactor and reagent conversions, roughly 10% argon flow (of known flowrate) is co-fed to the reactor. The argon is inert to the process and can therefore be used as an internal standard. The co-fed argon is the reason for the higher total space velocity as opposed to the syngas space velocity. **Figures 8-12** indicate the synthesis performance of the catalyst prepared. The graphs only describe the Fischer-Tropsch Synthesis performance of the catalyst and not the reduction procedure. The reduction procedure represents the procedure used to generate active catalyst in the reactor after it has been loaded as catalyst pre-cursor.

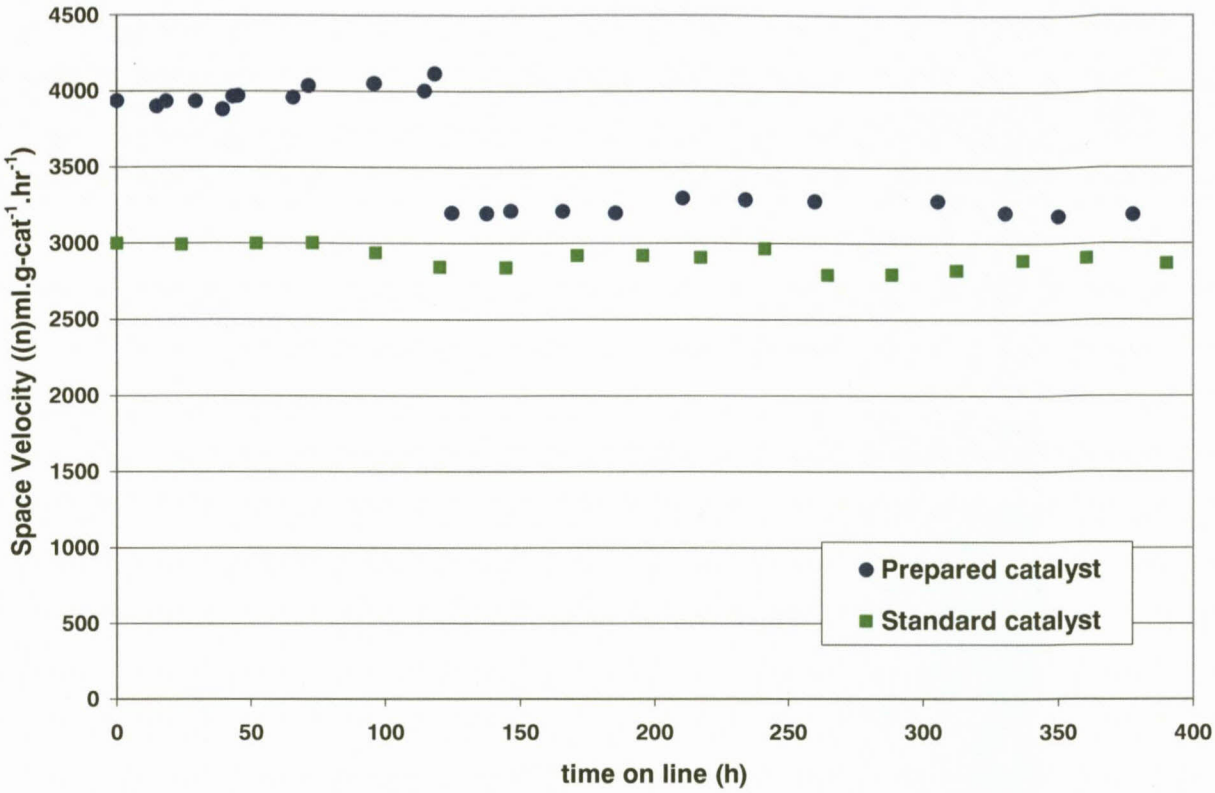

Figure 8. Gas Hourly Space Velocity for Fischer-Tropsch Synthesis of standard catalyst and the "prepared" catalyst. The data points up to 120 h represents the commissioning of the prepared catalyst. Thereafter the conditions were corrected to evaluation conditions.

Space velocity, in this case, is the gas flow fed to the reactor expressed per mass of catalyst loaded. This is very useful concept in evaluating catalyst performance as systems with different catalyst mass can be evaluated under similar conditions. From **Figure 8** it can be seen that the prepared catalyst was commissioned under higher space velocity but was corrected to the conditions under which the standard catalyst was evaluated. The higher space velocity initially led to lower conversions as the reactor residence time of the reagent gasses were lower for the higher space velocity. After the correction the space velocity was only slightly higher than that of the standard catalyst.

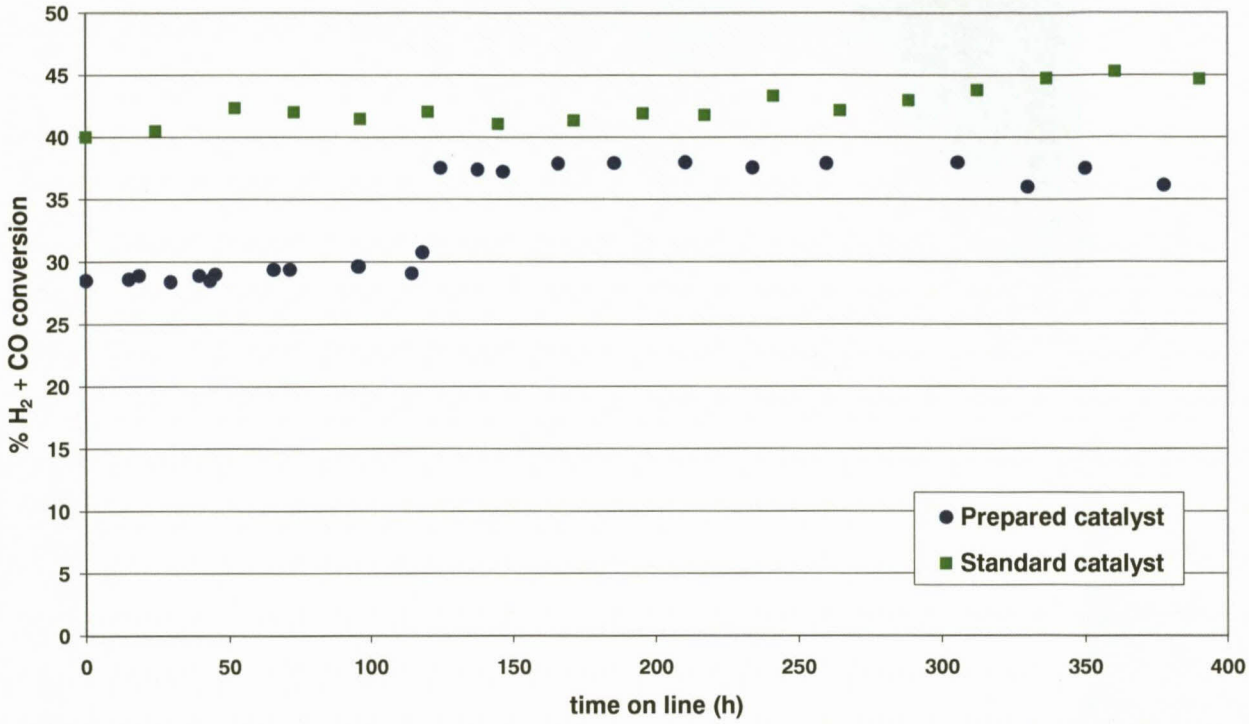

Figure 9. H_2 + CO conversion of standard catalyst and the "prepared" catalyst under Fischer-Tropsch synthesis conditions.

The H_2 and CO conversions are commonly used to evaluate the performance of FT catalysts. From the results it can be seen that at higher space velocity (< 120 hrs) the conversion of the prepared catalyst was lower than expected and after the correction the conversion results of the standard and prepared catalyst are similar. The actual difference is somewhat less as the prepared catalyst was evaluated at slightly higher space velocity. When evaluating H_2 + CO conversion the relative contributions of the Fischer-Tropsch synthesis and water-gas-shift rates are not evaluated. A relative change in the rate of the two reactions can give similar H_2 + CO conversions but the products produced would be different. For this reason, apart from H_2 +CO conversion, CO + CO_2 conversion is often used. The term CO + CO_2 could be confusing because the graph actually depicts total CO converted minus the CO that was converted to CO_2 and thereby including the effect of the water-gas-shift reaction. CO + CO_2 conversion data is shown in **Figure 10**.

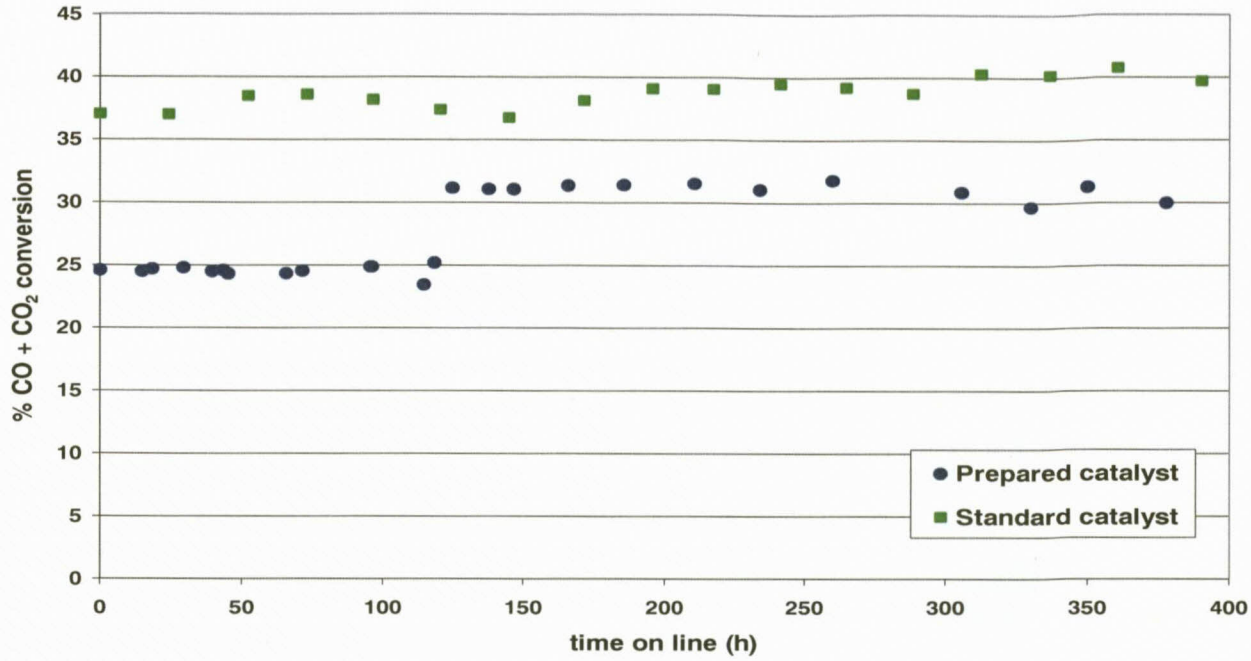

Figure 10. CO + CO_2 conversion for the standard and prepared catalyst under similar conditions. Although it is common to label the x-axis % CO + CO_2 conversion the number actually plotted represents total CO converted minus the CO that was converted to CO_2 and thereby including the effect of the water-gas-shift reaction.

The results in **Figure 10** also show that the prepared catalyst performs well when compared to a standard industrial catalyst. The increase in conversion after 120 h was a result of the decreased space velocity.

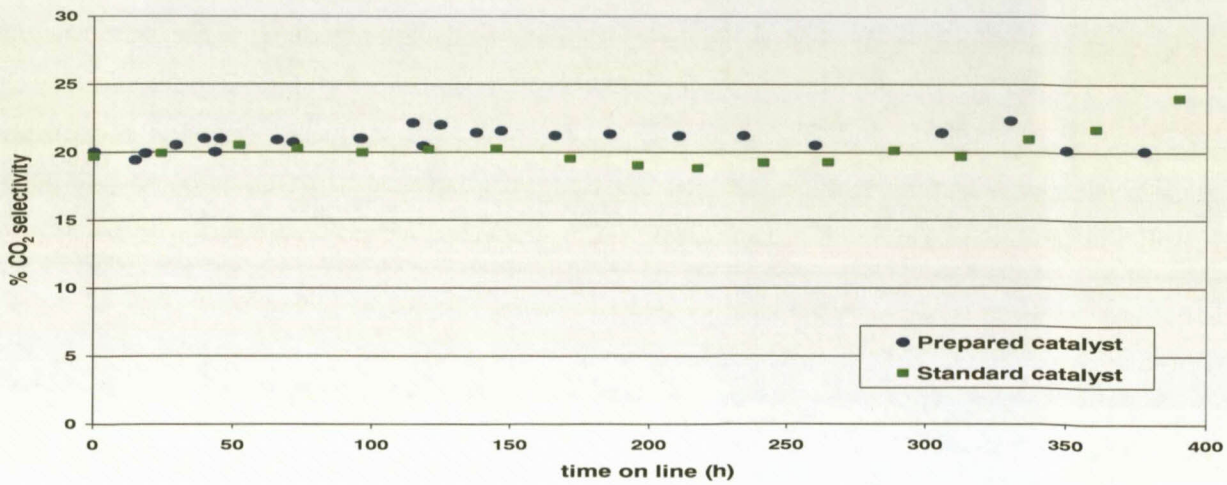

Figure 11. % CO_2 selectivity for the standard and prepared catalyst under similar conditions.

The CO_2 selectivity **(Figure 11)** is a direct indication of the contribution of the WGS reaction as CO_2 is only formed through this reaction. High WGS activity is not desirable because that means that CO is converted to CO_2 and not to hydrocarbon products. The CO_2 selectivity for the prepared catalyst does not show higher water-gas-shift activity than standard commercial catalysts.

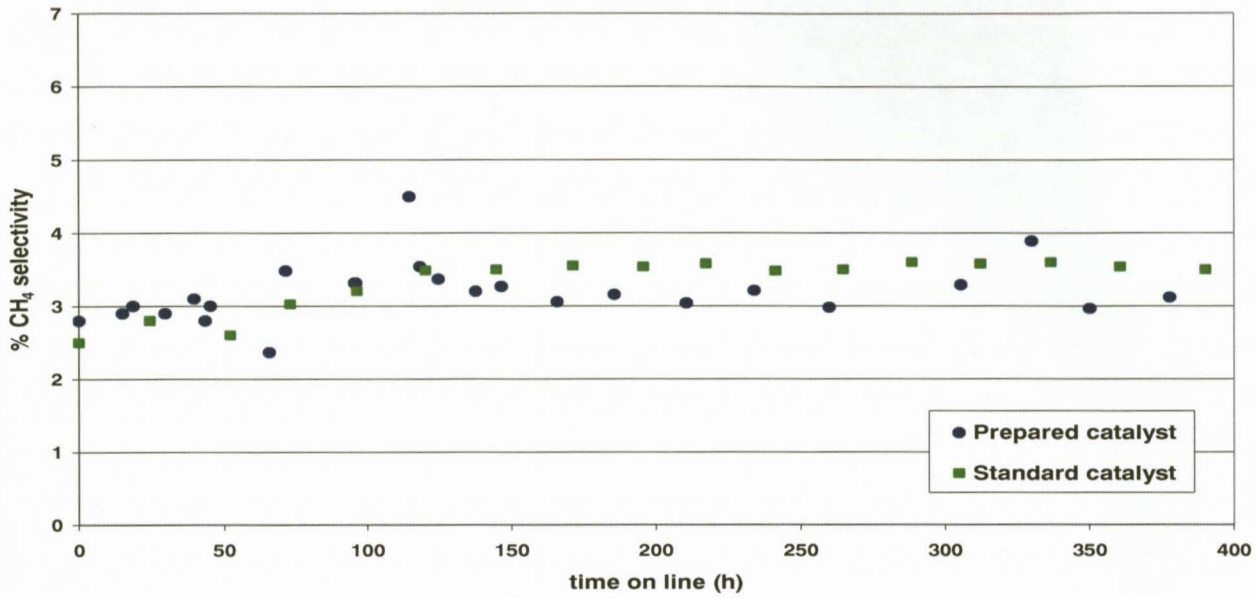

Figure 12. Methane selectivity for the standard and prepared catalyst under similar conditions.

Methane selectivity gives a good indication as to the FTS activity of the catalyst and is therefore closely monitored. High methane selectivity is, however, not desired as methane is of little commercial value. High methane selectivity can also indicate that that the product spectrum may consist of shorter hydrocarbon chain lengths which is also not desired if waxy products are targeted. The methane selectivity for the two catalysts compare well.

In conclusion the catalyst prepared from the metal nitrate solution generated by recovery of the iron and copper content of spent catalyst performs well when compared to a standard Ruhrchemie type iron-based catalyst with similar chemical composition under similar Fischer-Tropsch Synthesis conditions. This process is therefore viable and the focus was diverted to obtain maximum metal dissolution from the wax removed spent catalyst. This would not only affect the process economically favourably but would reduce the amount of by-products to be handled from the process.

The wax removal methods were now investigated in more detail. It is known from literature that iron will undergo phase changes with increasing temperature and it is also known that hematite, the thermodynamically most stable phase is the most difficult to digest with acid.[4] Should hematite be

the final phase, after transformations, it is likely to have the lowest surface area and further impact negatively on dissolution behaviour. Carbonaceous materials (wax) may also act as reducing agents under certain conditions and could influence the phase generated. It is therefore expected that the temperature at which combustion, or other treatments, take place and/or the time spent at said conditions could have a marked influence on the iron phase, available surface area and subsequently the dissolution characteristics. A clear correlation between iron phase and/or available surface area therefore also needs to be investigated. It may well be that a phase that is less prone to acid digestion but has a large available surface area is readily dissolved and *vice versa*.

3.6 Wax combustion temperature

During the course of the study various inconsistencies in iron phase analysis were found for samples oxidized in the presence of air at the same temperature. Wax combustion is a rapid and exothermic process and the temperature at which the oven is set may be exceeded at the catalyst surface. In an attempt to account for the inconsistencies a thermocouple was placed in the catalyst sample holder and another thermocouple was placed ca. 250 mm above the combustion area to more accurately control the oven temperature. This information would be crucial when a possible combustion technology is to be evaluated because removing the wax in a controlled fashion at specific conditions might be targeted.

The first test was done for a fresh catalyst precursor sample prior to activation with no wax added to it as a baseline experiment. Temperatures were logged with a logger that generates a temperature profile on a calibrated paper roll that runs at a fixed speed. The profile generated for the standard sample can be seen in **Figure 13**. The specific heating rate was chosen because it was the maximum heating rate the oven used could attain controllably. Commercially the process will probably be done in a rotary calciner where the heating rate would be high as slower heating rates would require larger equipment. The final temperature of 600 °C was maintained for one hour as this time was shown, from previous experiments, as adequate to ensure complete wax combustion.

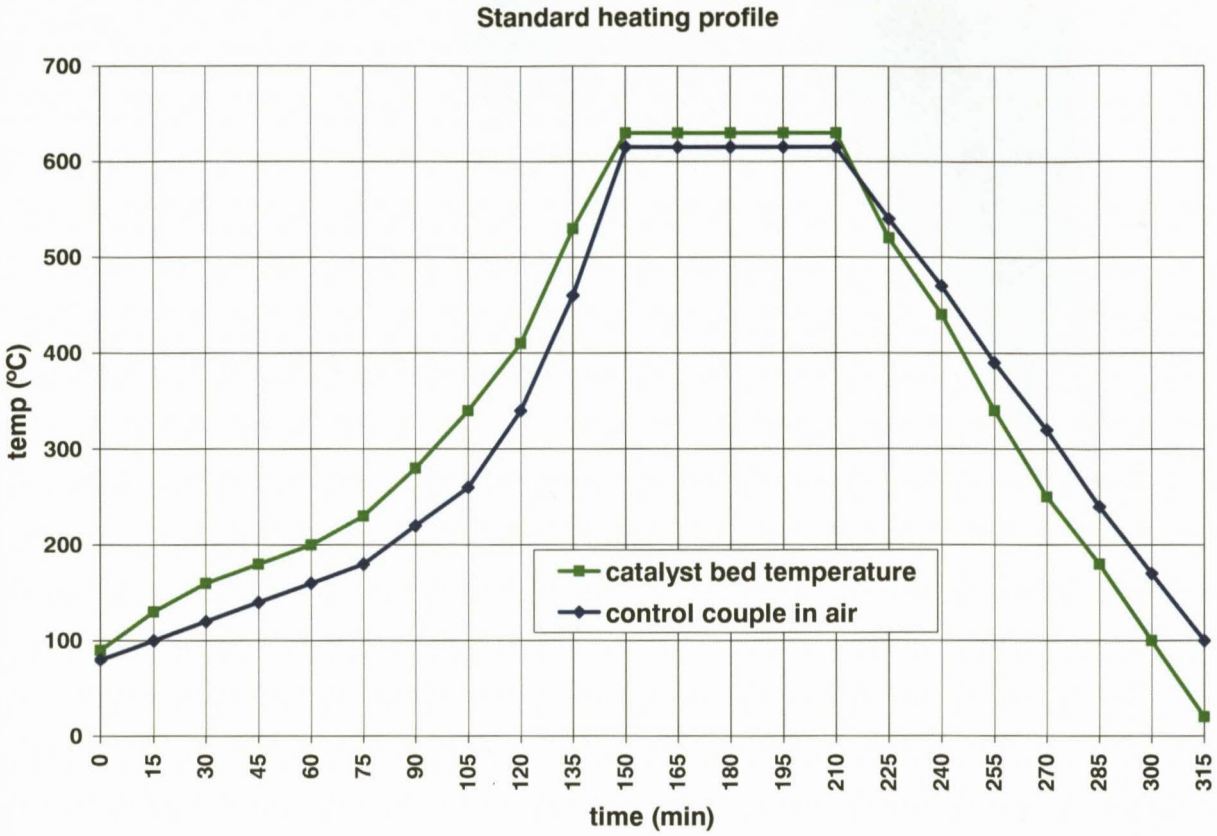

Figure 13. Standard heating profile of fresh calcined catalyst precursor with no associated wax measured by two thermocouples: one inside the catalyst bed (green line) and one well away from the combustion area. The second thermocouple (blue line) was used to control the oven temperature.

From **Figure 13** it can be seen that the temperatures the two thermocouples measured are close to each other, especially when steady state conditions are reached. During the initial stages the catalyst bed is at a slightly higher temperature due to better heat transfer through the metal base of the oven as opposed to the other thermocouple situated in air away from the heated surface. The maximum temperature differences noted amounted to 80 °C.

In order to evaluate the temperature effect of the bed height and volume, different sizes of square stainless steel sample containers were used. The bed height, volume as well as surface area were varied. This would also serve as an indication of the type of oxidation technologies that can be evaluated. **Table 10** lists the bed heights that were evaluated with stainless steel sample containers. The containers were manufactured so that the different bed heights could be evaluated in containers with fixed base dimensions. Thermocouple entry points that could be closed when not used were added at various heights and could therefore measure the catalyst bed surface temperature for different bed height experiments. A photograph of one of the stainless steel sample containers is shown in **Photograph 1.** The time reported was chosen as the time where

the differences in oven and bed temperatures were more than the 30 °C baseline. This means that differences higher than 30 °C was interpreted as significant. During all the evaluations the oven control temperature was set to 600 °C and similar temperature ramp rates were employed.

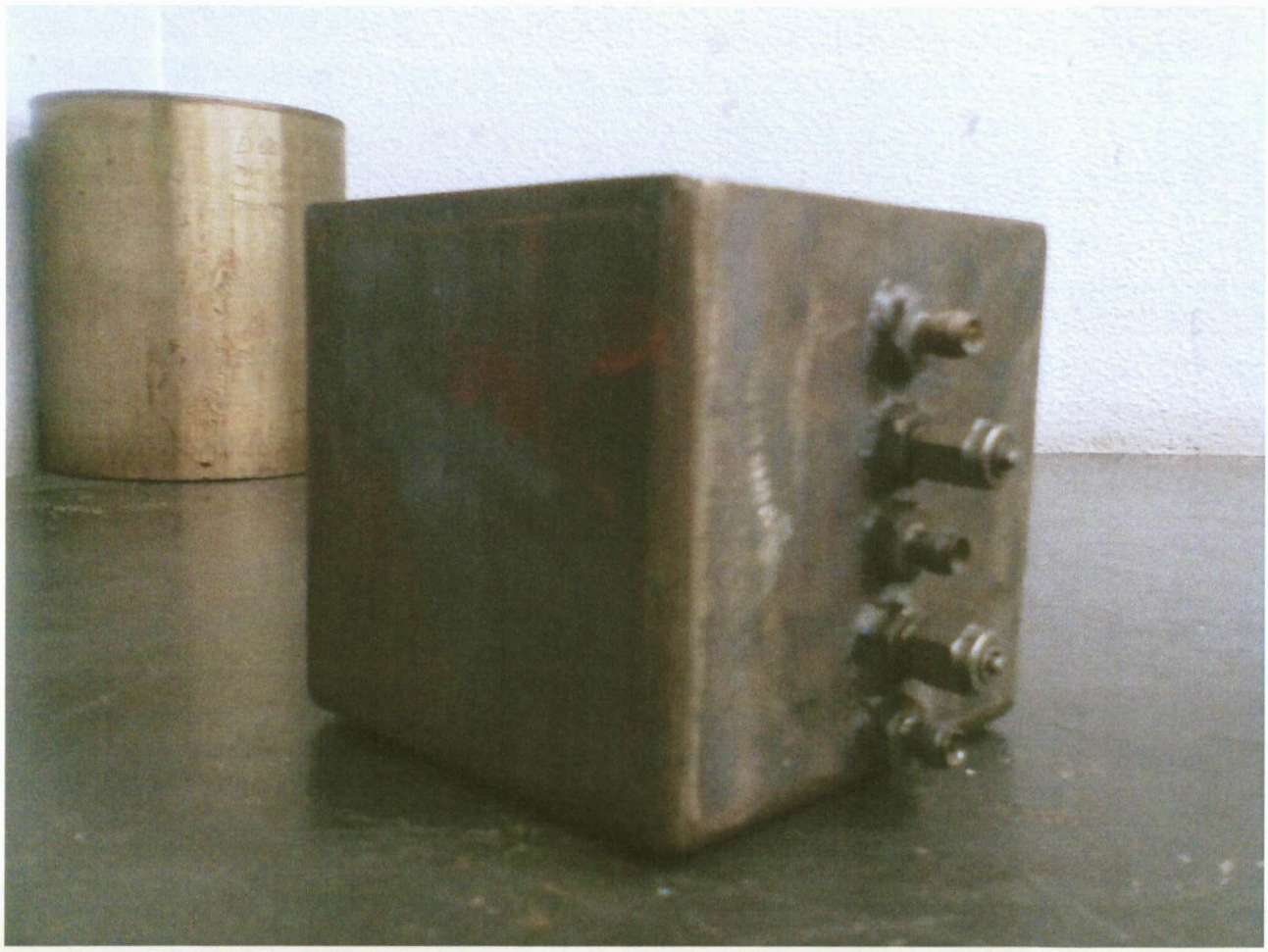

Photograph 1. One of the stainless steel sample containers used during different bed height and bed volume thermal wax oxidation experiments. Visible on the side is the connection points for a thermocouple at various bed heights.

From the results in **Table 10** it can be seen that the lowest difference in temperature is seen at a bed height of 10 mm. The most important difference between 20, 30, 50 and 90 mm of bed height is the time spent at the elevated temperatures. There is a marked difference between 10 and 20 mm. From 20 mm and up the process is possibly mass transfer limited in terms of available oxygen at the catalyst bed surface. Higher temperatures could possibly result if sufficient oxygen was available. Temperature differences do not go up significantly beyond the 20 mm bed height. Slow oxygen mass transfer could be due to a slower rate of oxygen introduction into the oven as well as a slower rate of oxygen transfer into the lower levels of the catalyst bed.

Table 10. The effect of bed height and volume on the exotherm experienced during the thermal oxidation of the wax-coated spent catalyst.

Catalyst bed and container dimensions (lxbxh = mm)	Maximum temperature difference above ΔT > 30 °C	Time (h) where ΔT > 30 °C
100 X 100 X 10	0	0
50 X 50 X 20	80	1
100 X 100 X 20	150	2
200 X 200 X 20	140	2
100 X 100 X 30	160	2
100 X 100 X 50	120	6
100 X 100 X 90	120	10

The result is that the process continues for much longer until the all wax is burnt off. If longer times are spent at elevated temperatures, it will result in lower surface area iron oxides as well as transformation to hematite which has poor dissolution properties. Results indicted in **Table 10** indicate that a maximum temperature deviation is seen between 20 and 30 mm bed heights but that samples with larger volumes and bed heights are exposed to the higher temperatures for longer. The results are intuitively correct and confirm that care has to be taken when a certain wax combustion time and temperature is aimed for.

The collected data for the 100 X 100 X 10, 100 X 100 X 20 and 100 X 100 X 30 sample bed heights are shown respectively in **Figures 14, 15 and 16**.

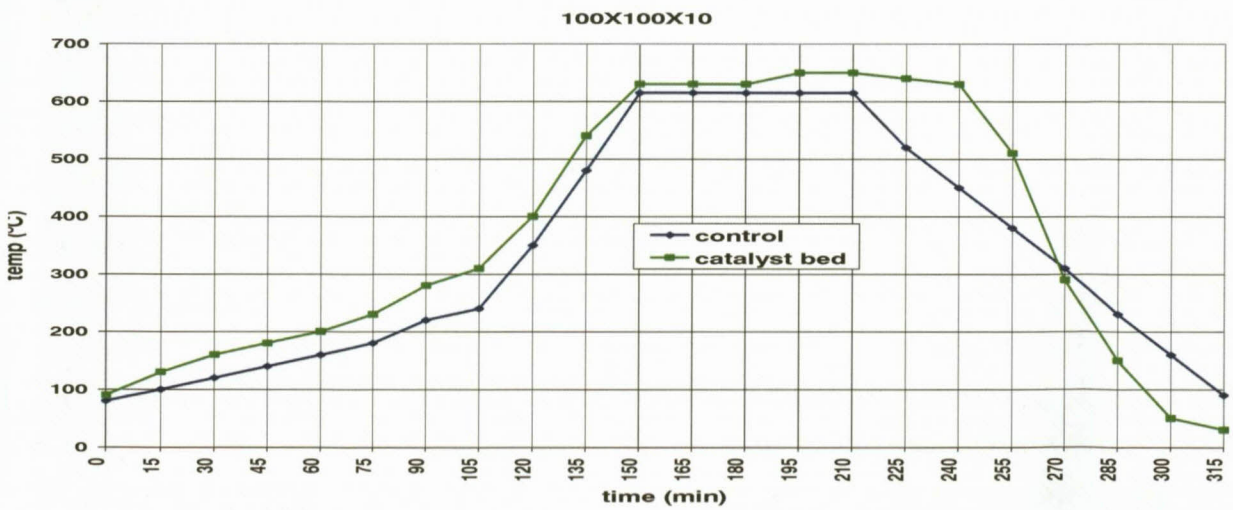

Figure 14. Temperature profile for 100X100X10 mm sample container with oven and sample temperatures plotted with time on line.

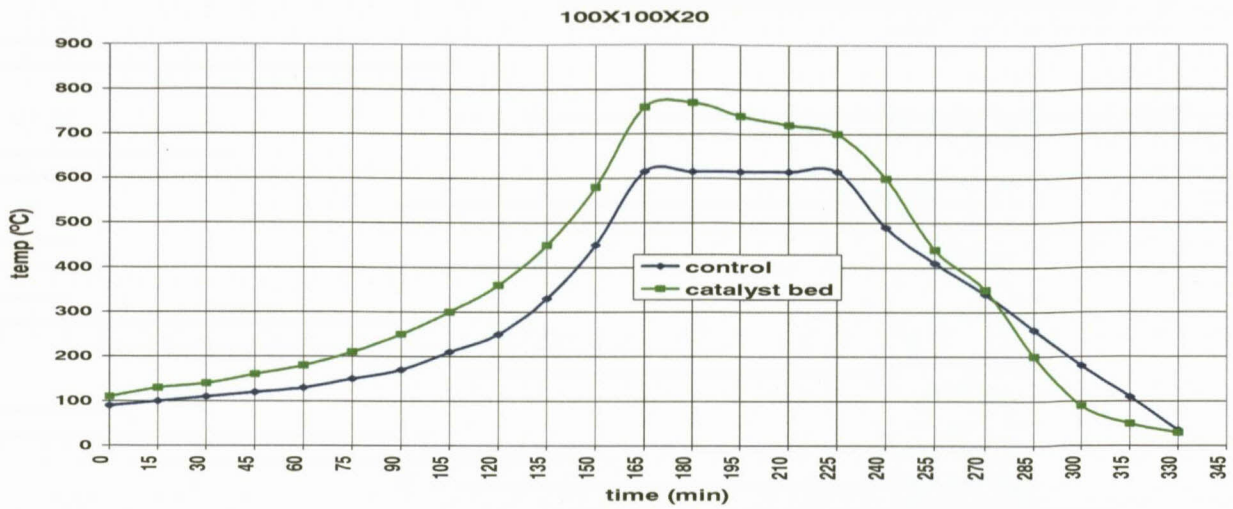

Figure 15. Temperature profile for 100X100X20 mm sample container with oven and sample temperatures plotted with time on line.

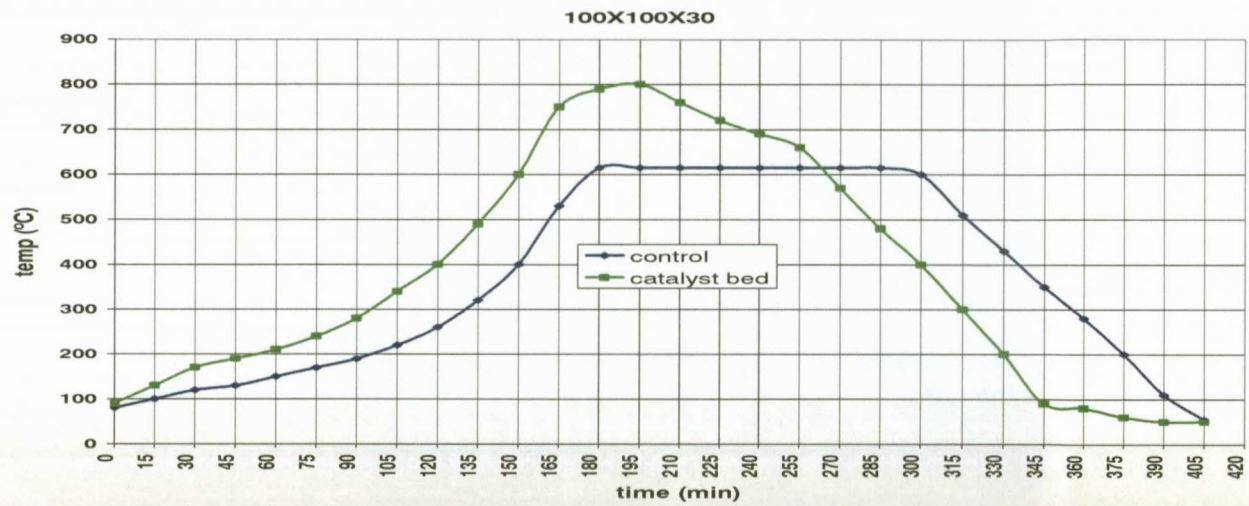

Figure 16. Temperature profile for 100X100X30 mm sample container with oven and sample temperatures plotted with time on line.

3.7 Dissolution behaviour of wax removed products.

Having determined optimum oven conditions, the effect of wax removal methods on acid dissolution of the remaining metals could be studied in detail. Three types of wax removal experiments were conducted namely thermal oxidation, thermal cracking and solvent extraction. Thermal oxidation is the simplest process but leads to the loss of valuable wax and may cause excessive temperatures. Thermal cracking may be a more controllable process (no excessive exotherm) and has the advantage that the wax may be recovered as lower chain length hydrocarbons. The reducing environment of thermal cracking due to the presence of carbon rich species, may also influence the final phase attained that could benefit the dissolution

characteristics. Solvent extraction has the benefit of recovering hydrocarbons without destruction as well as the low temperatures that could be employed. The solvent could be recovered or simply refined by the current down stream processes if a paraffin type solvent is used.

Thermal oxidation - The thermal oxidative removal of wax was done by placing an amount of spent wax coated spent iron-based catalyst in a muffle furnace at a bed height of 10 mm in the presence of air. The 10 mm bed height was chosen from the experiments conducted in the previous section where it was seen that higher beds either led to significantly higher temperatures or excessive times spent at elevated temperatures. The oven was then heated to the desired temperature in static air and then kept at the desired temperature for 2 hours. Thereafter the oven was cooled to room temperature and the sample was removed from the oven. The obtained sample was then sent for characterisation and tested for its dissolution behaviour.

Thermal cracking - The same oven configuration was used for the thermal cracking experiment with the exception that the heat treatment was performed inertly in the presence of a nitrogen atmosphere (oxygen was rigourlessly excluded) The same experimental temperatures were chosen as for thermal oxidation to be able to compare results.

Solvent washing – Wax coated spent iron-based catalyst was added to a pressurized filter system and the filter was heated to 90 °C. The filter rig consists of a 25 litre stainless steel vessel with filter material at the base of the vessel on a porous disc and a removable lid which is closed when pressure filtration is performed. An C_9-C_{11} paraffin was added to the filter and stirred for 30 minutes. The dissolved wax and paraffin solution was then filtered by pressurizing the filter with nitrogen. This procedure was repeated three times thereby removing most of the wax. Resultant spent catalyst cake was then pacified with dry ice as the catalyst is still partly reduced and rapid oxidation will lead to an exotherm that could influence the results. After the dry ice had sublimated the solid de-waxed spent iron-based catalyst was taken from the pressure filter and heated in the presence of nitrogen to 250 °C and kept there for 2 hours to render a free flowing solid. The heat treatment ensured that all the paraffin used evaporated and thus does not interfere with the subsequent treatments. A small amount of solvent extracted catalyst was then heated in a muffle furnace to 500 °C in a static air atmosphere and kept there for 2 hours. The mass of spent de-waxed catalyst left after this treatment was subtracted from the mass of loaded catalyst to obtain the amount of wax that was removed by the solvent extraction and temperature treatment method we employed. There was a mass loss of about 10% thus indicating that most of the wax was removed during the solvent extraction efforts. The 10% of wax is inside the pores of the spent catalyst and very difficult to remove *via* solvent extraction.

Characterisation - To obtain the optimal amount of information from the various samples generated from the wax removal experiments a number of characterisation techniques were employed. Firstly the iron phases present in the spent catalyst, encapsulated in wax, as unloaded from the synthesis reactor had to be identified so that the effect of any resulting treatments of the spent catalyst could be monitored. Mössbauer Absorption Spectroscopy (MAS) and X-Ray powder Diffraction (XRD) experiments were performed. Inductive Coupled Plasma (ICP) analysis was performed on the various solid and liquid fractions generated during the dissolution process to determine elemental composition. Surface area and pore volume (BET) determinations were necessary to conclude whether there is a relationship between the surface area and dissolution behaviour of the spent catalyst.

A sample of calcined (fresh) Ruhrchemie type iron-based catalyst was also tested in the dissolution process to verify that we can:

1. Recover all the metals from a fresh catalyst under the conditions used to test the dissolution behaviour of the various generated samples.
2. To test the effect of phase transformation on dissolution.

The dissolution behaviour of the samples were tested by adding 100 ml of ca. 45 mass% nitric acid to the small scale laboratory glass beaker and the acid was heated to 80 °C while stirring vigorously. Then 20 grams of various catalyst samples was added to the heated nitric acid. These ratios of solid to liquid were chosen as it is an approximation of the ratios used when pure iron is dissolved in nitric acid as per the standard Ruhrchemie iron-based catalyst preparation method. The spent catalyst and acid mixture was stirred for 24 hours after which the resultant solution was filtered, washed and dried at 120 °C. The solid obtained as filter cake was weighed after drying and hence the amount of solids that was recovered could be calculated. The solid and liquid fractions were also analyzed in order to obtain the amount of each metal (Fe, Cu, Na, K, Si) that has dissolved in the nitric acid. The spent, iron-based, wax coated, catalyst used as the starting material in the various wax removal studies were analyzed and from Mössbauer adsorption spectroscopy and X-ray diffraction measurements is was concluded the spent iron-based catalyst consists of 71% ferrihydrite, 26 % iron carbides and 3 % Fe(II) species in wax (**Figure 17**).

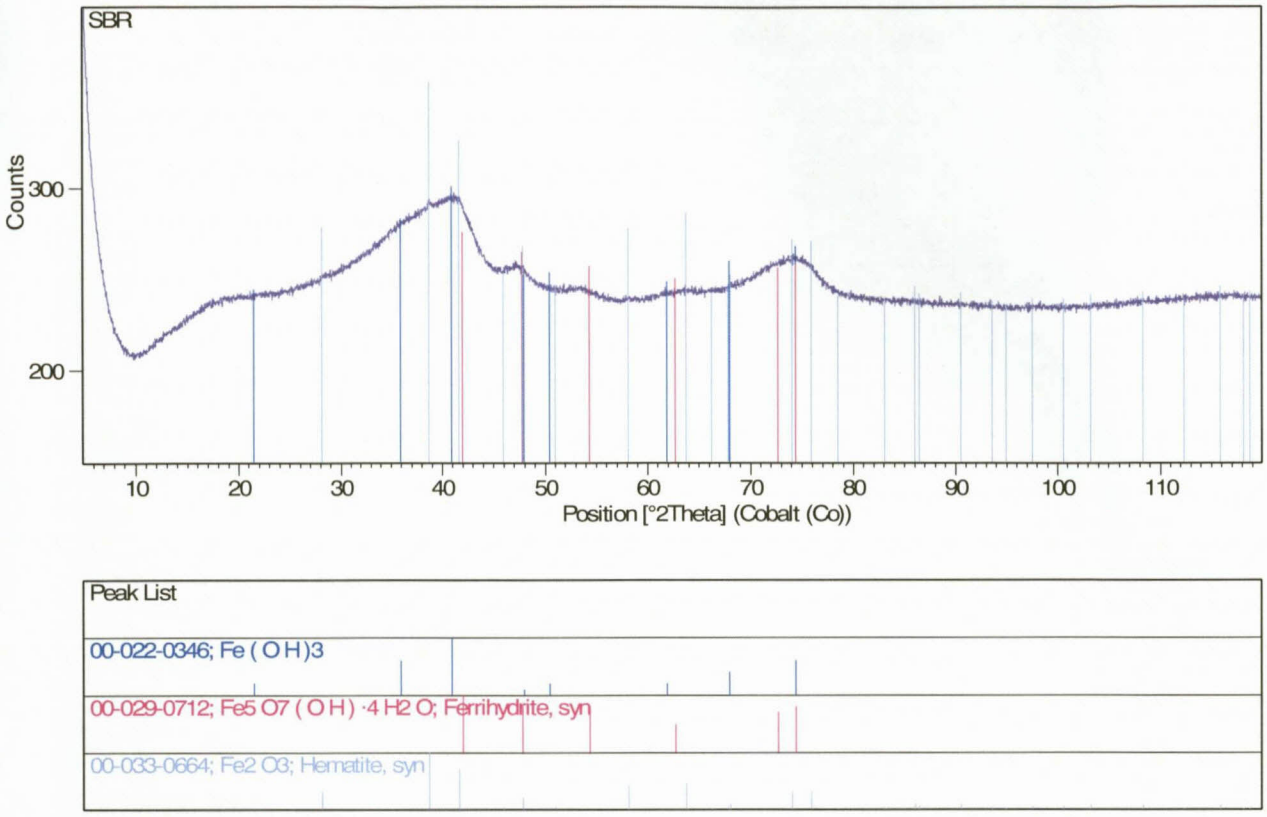

Figure 17. Powder X-ray diffractogram of wax coated spent iron-based catalyst and shows the presence $Fe(OH)_3$, ferrihydrite and hematite.

Table 11 gives a summary of the Mössbauer results (room temperature and 77K) of resultant iron phases formed after the various de-waxing treatments. Mössbauer spectra (**Figures 18 and 19**) are shown depicting the changes in phase composition occurring during the various wax removal techniques.

Table 11. Mössbauer-obtained analysis results for different samples of spent iron-based Fischer-Tropsch slurry bed samples exposed to different wax removal treatments.

SAMPLE	% Contribution							
	χ-$Fe_{2.5}C$ Hägg Carbide	γ-Fe_2O_3 Maghemite	Fe(III)	α-Fe_2O_3 Hematite	$Fe_5O_8 \circ 4H_2O$ Ferrihydrite	Fe(II)	Fe_3O_4 Magnetite	Iron nitride
Spent Slurry bed catalyst (1)	26	0	0	0	71	3	0	0
Thermally Cracked at 500 °C (2)	0	0	0	4	23	0	(66)*	7
Thermally Cracked at 750 °C (2)	0	0	0	49	7	0	(39)*	5
Thermally Cracked at 900 °C (2)	0	0	0	65	6	0	(24)*	5
Solvent Extracted (2)	0	57	0	2	41	0	0	0
Thermally Oxidised at 500 °C (1)	0	78	5	17	0	0	0	0
Thermally Oxidised at 900 °C (2)	0	24	4	72	0	0	0	0

(1) Mossbauer measurements performed at 77K

(2) Mossbauer measurements performed at 298K

* Under room temperature Mössbauer analysis conditions it is extremely difficult to distinguish between maghemite and magnetite as both phase appear at the same value (**Figure 17 (2),(3)**). Magnetite has been reported due to the presence of the secondary peak associated with magnetite (**Figure 12 (3)**) but could be a mixture of maghemite and magnetite.

From **Table 11** it can be seen that the various wax removal techniques result in a number of different iron phases. The temperature of wax removal also contributes to phase changes as can be seen when comparing the same technique at different temperatures. The iron carbides (here identified as χ-$Fe_{2.5}C$ - Hägg Carbide) which are present in the spent slurry bed catalyst are not present in any of the other samples that were heat treated or solvent washed with a C_9-C_{11} paraffin

fraction. This indicates that during all the wax removal techniques the iron carbides are oxidized or converted to hematite, maghemite and magnetite, or a mixture of maghemite and magnetite.

Ferrihydrite, the only iron oxide phase present in the spent wax-coated catalyst, is a poorly ordered material and therefore easily transforms. The amorphous nature of this material also explains the high surface area of the catalyst.[6] This poorly ordered structure can be dehydrated to magnetite, maghemite and hematite under the influence of either heat, mechanical stress or chemical environment. Magnetite differs from most iron oxides in that both divalent and trivalent iron is present. Magnetite is frequently non-stoichiometric in which case it has a cation deficient Fe(III) sublattice. For stoichiometric magnetite the Fe(II): Fe(III) ratio is 0.5. Maghemite which lends its name from a combination of the names magnetite and hematite, differs from magnetite in that all or most of the iron is in the trivalent state. Cation vacancies compensate for the oxidation state of the Fe(II). Hematite, the end product of various transformations, is usually much more structured and contains only iron in the trivalent state with limited crystal defects. Transformations in iron oxides from ferrihydrite to hematite therefore go through various stages where the relative amounts of divalent and trivalent iron determine the various structures.

Due to the number of iron phases simultaneously present in the samples generated by thermally cracking the wax the Mössbauer spectra that were obtained are visually complicated to interpret. In order to aid in the analysis of the results, all the pure iron phases theoretically present in the samples are separately depicted in **Figure 18 (a-h)**. Similar colours for the pure theoretical phases were used to aid with the identification of the iron phases present in the combined spectra. Some iron phases, such as magnetite, generate a dual signal because two different iron atoms (one Fe(II) and the other Fe(III)) with different environments exist in the same unit cell and therefore generate two characteristic Mössbauer signals. **Figure 18 (f-h)** depicts the experimentally measured data which reflects the compliment of all the pure iron phases present in their relative concentrations superimposed on top of each other in one experimentally determined spectrum. The complete spectra containing all the identified iron phases as well as the measured data representing the complement of all the phases are shown in **Figure 19**.

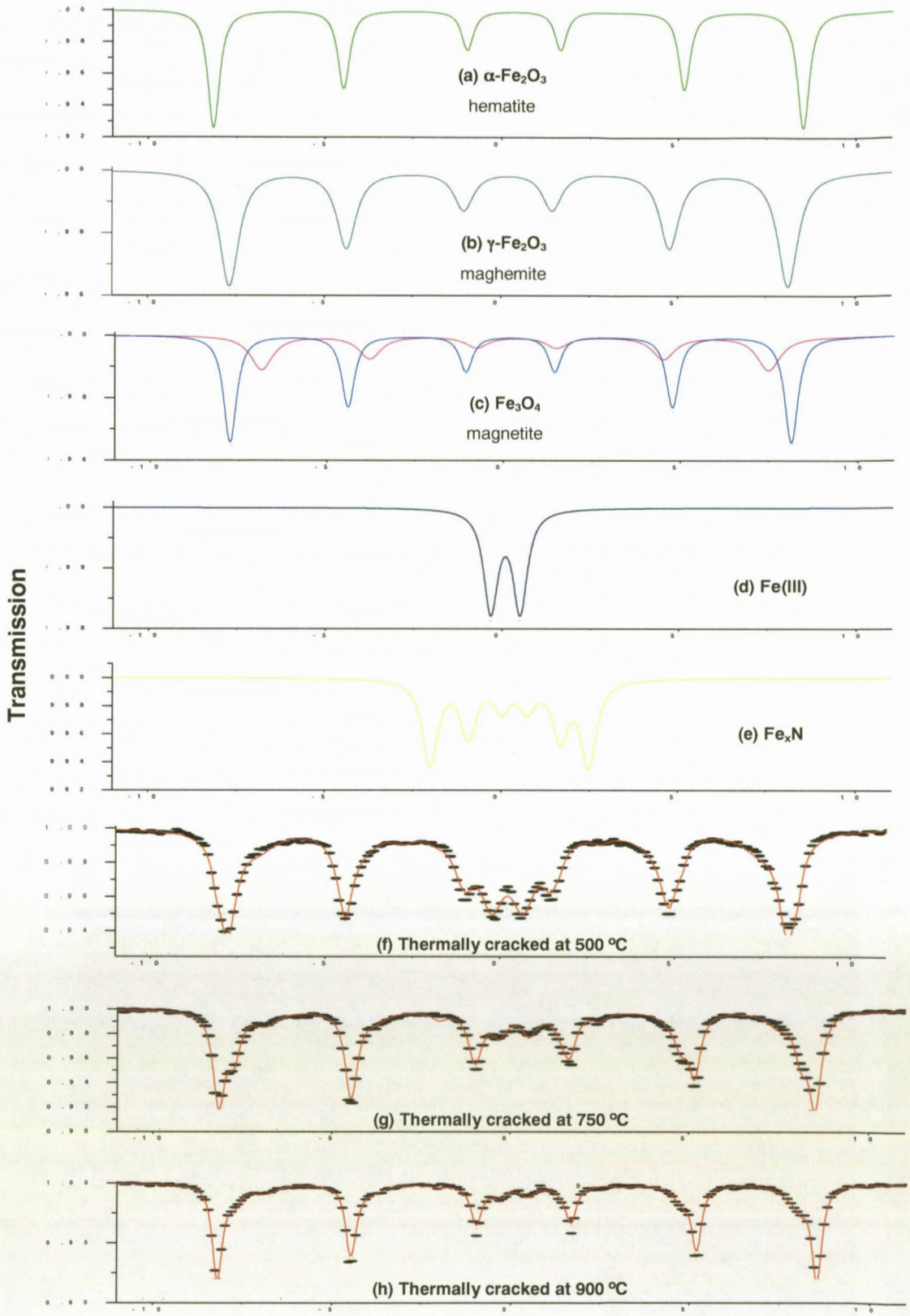

Figure 18. (a-e) Mössbauer spectra of pure iron phases that were found in thermally cracked spent FT catalyst. (f-h) The experimentally determined Mössbauer spectra of the thermally cracked FT catalysts at the indicated temperatures. These spectra are the final complement of the mixtures of all the iron phases present in the studied samples. Figure 19 shows what the relative contribution of each iron phase to the experimentally determined Mössbauer spectra must be.

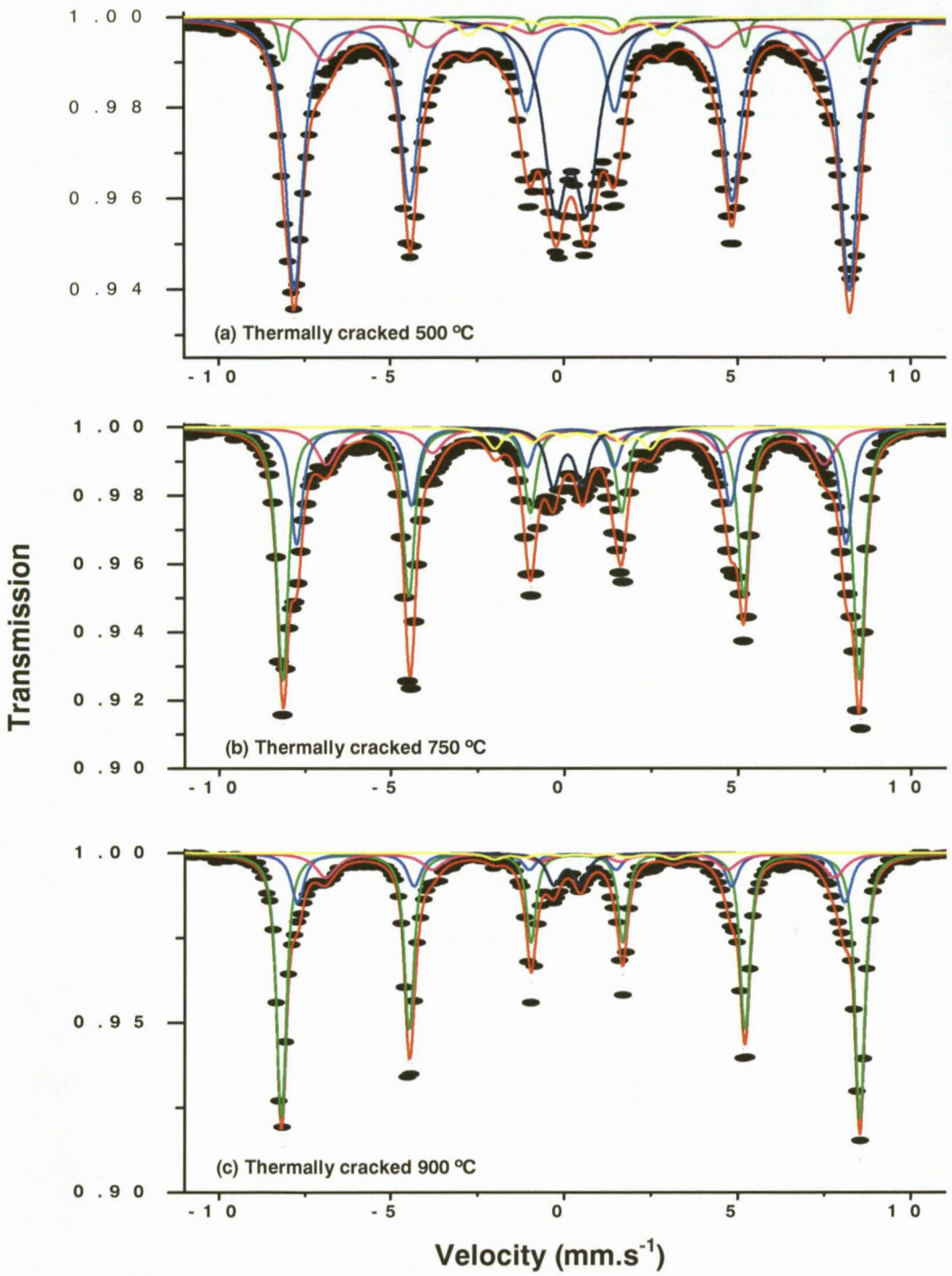

Figure 19. Mössbauer-obtained spectra for different samples of spent iron-based Fischer-Tropsch slurry bed samples exposed to different anoxic thermal cracking wax removal treatments. Red line: The experimentally determined Mössbauer spectra. Other colours: Relative contribution of different iron phases as listed in Table 11 to generate experimentally determined Mössbauer spectra.

When the wax is removed by thermal cracking (**Figures 18 and 19**) from the spent catalyst in the presence of a inert atmosphere (N_2), it can be seen that the amount of super paramagnetic Fe(III)

species (**Figure 18 (4)** and **Figure 19 (1)** (centre doublets, dark blue), which probably is ferrihydrite or iron silicates, decrease as the temperature at which the wax is cracked/decomposed increases (**Figure 19 (1) – (3)**). It can also be clearly seen that the hematite phase increases here depicted in green. The maghemite and magnetite phases appeared at very similar data points for room temperature Mössbauer analysis and can therefore not be assigned with certainty. It was decided to report the phase as maghemite due to the noticeable (pink) spectra assigned to magnetite (**Figure 18 (3)**) seen in the analysis data, although it must be stressed that some maghemite may be present in these samples. The amount of magnetite/maghemite (dark blue, pink) is converted to hematite as the temperature increases. As hematite is the more stable iron oxide than magnetite, these results are expected. When these results are compared to the thermally oxidized samples in **Table 11** it can be seen that for the thermally oxidized samples the transformation is rather from maghemite to hematite for the elevated temperatures indicating the more oxidizing environment of the procedure. Wax under anoxic conditions therefore influences the phases generated due to the reducing environment created by the presence of carbon.

Studies[4,5] have also noted that in the presence of organic matter, ferrihydrite is transformed to maghemite rather than hematite during heating. The high content of maghemite/magnetite in the thermally cracked spent catalyst is therefore plausible due to the large amount of organic matter (waxy paraffin's) in the spent wax coated catalyst. However, the hematite present in the thermally cracked samples could have resulted from the thermal transformation from maghemite/magnetite to hematite. Towards the end of the process when most of the carbon has been removed, and hence no reducing environment exists, this transformation can take place. The wax from the spent catalyst was thermally cracked at 500 °C, 750 °C and 900 °C in the presence of nitrogen which is above the temperature at which the transformation begins. It is also instructive to note that the transformation of maghemite/magnetite to hematite can be retarded by the presence of copper. It was also reported in the literature[6] that certain "contaminants" can retard the process while other can speed up the process or have no effect at all. Copper was reported as a retardant. The spent catalyst contains roughly 2.5 mass% of copper and could be the reason why only a small amount of the maghemite (blue and pink) was converted to hematite (green) at 500 °C and the hematite fraction increased as the temperature of thermal cracking/decomposition was increased. The copper, however, does not explain the presence of magnetite in the various samples.

A reason for the magnetite formation could be because ferrihydrite is converted to maghemite under reducing conditions. Under a reducing environment it is possible that an amount of the formed maghemite could be reduced to magnetite. It can also be seen that a small amount of the magnetite was transformed to hematite (4%) at 500 °C. As the temperature increased to 750 °C the rate of dehydration or dehydroxylation of ferrihydrite to maghemite increases but it seems that

the rate of reduction also increased at the elevated temperatures thus converting the initially formed maghemite to magnetite. At 750 °C it seems as if the rate of thermal transformation from maghemite to hematite is higher and thus an increased amount of the initially formed maghemite is transformed to hematite (49%). No maghemite was identified in this sample.

As the temperature is increased to 900 °C the amount of hematite increased to 65% and the amount of magnetite decreased to 24%. The reason for the increased amount of hematite and the lowering of the amount of magnetite is because the rate of thermal transformation from maghemite to hematite is greater than the rate of reduction of maghemite to magnetite at 900 °C. The sample also spends a longer time at elevated temperatures where the effect of carbon species will be negated.

The iron carbides which are present initially in the spent catalyst are not present after the various thermal treatments. When the wax is combusted in air the carbon will react with oxygen and form carbon dioxide. When a nitrogen atmosphere is employed the hydrocarbons on the surface thermally crack off (breaking the bonds to form shorter chain hydrocarbons) and are liberated as a hydrocarbon rich gas.

When the wax is removed by solvent extraction from the spent wax-coated catalyst, there is a temperature treatment after wax removal at 250 °C which potentially could transform some of the ferrihydrite to a mixture of magnetite and/or magnetite. We assigned the measured result to maghemite rather than magnetite because at the analysis temperature the phases cannot be accurately separated, as indicated from the Mössbauer results, see **Table 11**. The iron carbides were present initially but were not present after solvent extraction. This could be because the carbides were oxidised in air which could have entered the system during the various treatments combined with heat generated because of the pyrophoric nature of the spent catalyst. There is also a small amount of hematite which could be due to the temperature of the solvent extraction process resulting in the thermal transformation of ferrihydrite to hematite. As mentioned, when considering the method of phase transformation during the thermal cracked/decomposed samples, the decomposition of wax could cause a reducing atmosphere under which ferrihydrite could reduce to maghemite. This potentially could also occur during solvent extraction. This then explains the maghemite, observed in the solvent extracted sample, as seen from the Mössbauer results. From **Table 11** it is evident that the wax coated spent iron-based catalyst contains about 71% ferrihydrite and 26% iron carbides before any treatments are performed on the catalyst.

When combusting the wax at 500 °C in air (thermal oxidation at 500 °C) 78% maghemite is formed, 17% hematite and 5% Fe(III) compared to combustion at 900 °C in air where 24% maghemite, 72% hematite and 4% Fe(III) is formed. A large amount of the maghemite is therefore transformed to hematite when the oxidation temperature is elevated. These observations are supported by literature[7] findings where in the dry state, depending on its origin and content of foreign ions, maghemite transforms to hematite in the temperature range 370-600 °C. It is also known that hematite is thermodynamically the most stable iron oxide phase. The rate of the dehydration or dehydroxylation of ferrihydrite to maghemite and other iron oxide phases is faster at higher temperatures resulting in a decrease in the amount of ferrihydrite and subsequent increase in the amount of maghemite, hematite and magnetite (Fe(II)/Fe(III) spinel due to reduction). Unfortunately the low temperature Mössbauer technique (better resolution at lower analysis temperatures) could not be used in all instances but visually **Figure 20** shows the changes occurring in the material as higher oxidation temperatures were tested. By studying the spectra it is noticeable that the doublets in the middle of the spectra (**Figure 20 (b),(c)** - pink) become less pronounced and finally disappear (**Figure 18 (d)**) with increased temperatures. This portion of the spectra is assigned to small crystallites of Fe(III) which could be ferrihydrite but it is possible that it is also small crystallites of maghemite. The broad sextet (dark blue) is assigned to large crystallites of maghemite and can be seen for the solvent extracted and thermally oxidized 500 °C samples but disappears for the thermally oxidized 900 °C sample. The sharper (green) sextet is assigned to hematite and the increase of this phase can be seen as the temperature of exposure is increased. Except for the spent catalyst and the thermally oxidised (500 °C in air) spent catalyst the ferrihydrite phase is identified as a super paramagnetic Fe(III) species and is therefore regarded as ferrihydrite for the room temperature samples.

The above explanation could be why the various phases are formed during the different wax removal techniques. Although the effect of temperature and residence time on the phases formed is investigated further on, it is necessary to have knowledge of the phases and phase formation to conclude on the effect of the various phases on the dissolution behaviour of the various samples.

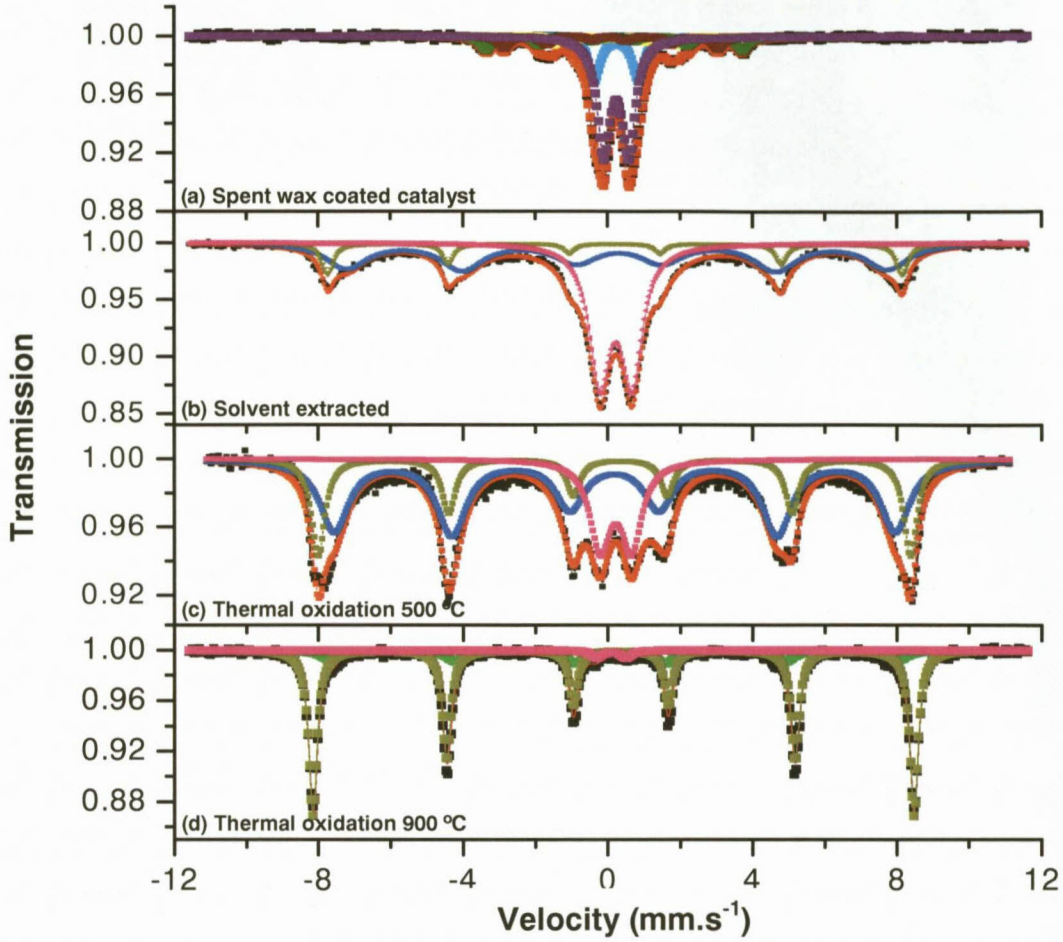

Figure 20 (a)–(d). Mössbauer spectra for different samples of spent iron-based Fischer-Tropsch slurry bed samples exposed to different wax removal treatments. For (a), (b) and (c) the red spectrum is the experimentally determined spectrum. Other coloured lines represent the theoretical relative contribution of different iron phases as listed in Table 11 to generate the Mössbauer spectra.

3.8 Iron Recovery by Acid Dissolution.

The iron phases in the various samples have an effect on the dissolution behaviour of the various samples. By performing inductive couple plasma (ICP) analyses on the samples prior to dissolution and comparing it with ICP analyses of the remaining solid after the dissolution experiments, it was possible to calculate the amount of metals that were recovered from the various samples investigated. **Figure 21** is a plot of the amount of iron that was recovered from the various samples that were investigated.

From **Figure 21** it can be seen that the fresh calcined Ruhrchemie iron-based catalyst (98.6%) and the solvent extracted sample (98.4%) had the highest iron recovery of the samples that were

investigated. By studying the Mössbauer adsorption spectroscopy results in **Table 11** it is evident that the solvent extracted sample has a large amount of ferrihydrite (41%) and a mixture of maghemite and magnetite (57%) whereas the calcined Ruhrchemie catalyst consists of only ferrihydrite. These phases should intuitively be more susceptible to dissolution as opposed to hematite. Various literature studies have also pointed out ferrihydrite dissolves quickest followed by magnetite and hematite.

The 500 °C thermally cracked sample also had a large recovery of iron (94.9%). This sample consisted of ferrihydrite (23%), maghemite (66%), hematite (4%) and a small amount of iron nitride (7%). The dissolution behaviour of iron nitride will be ignored at this stage. The high dissolution rate can be attributed to the amount of ferrihydrite as well as maghemite. Phase mixtures are bound to have a defective structure which will aid the dissolution process.

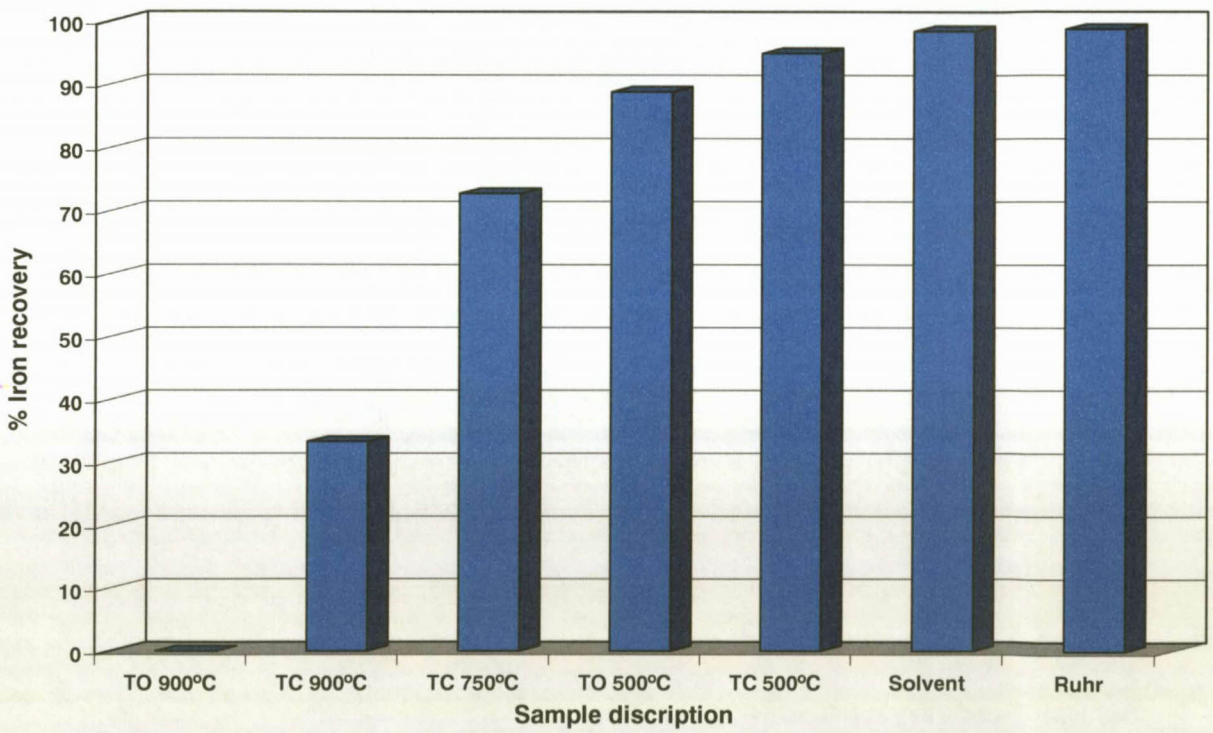

Figure 21. Iron recovered from various wax-removed samples. TO - Thermally oxidized, TC - Thermally cracked, Solvent - Solvent extracted, Ruhr - Ruhrchemie type iron- based catalyst precursor.

As the temperature at which the wax was removed increases the amount of iron recovered decreases, **Figure 21**. The amount of iron recovered from thermal oxidation at 500 °C, thermal oxidation at 900 °C, thermal cracking at 750 °C and thermal cracking at 900 °C were 88.8 %, 0%, 72.7% and 33.3% respectively.

By studying the various dissolution behaviours of the samples and potentially relating it to the presence of a certain phase or other property might be the key to recovering the metals from the catalyst. From the data presented thus far, it can be seen that as the amount of hematite increases iron recovery decreases. **Figure 22** is a plot of the percentage iron recovered as a function of the percentage hematite in the wax-removed sample before the dissolution experiments.

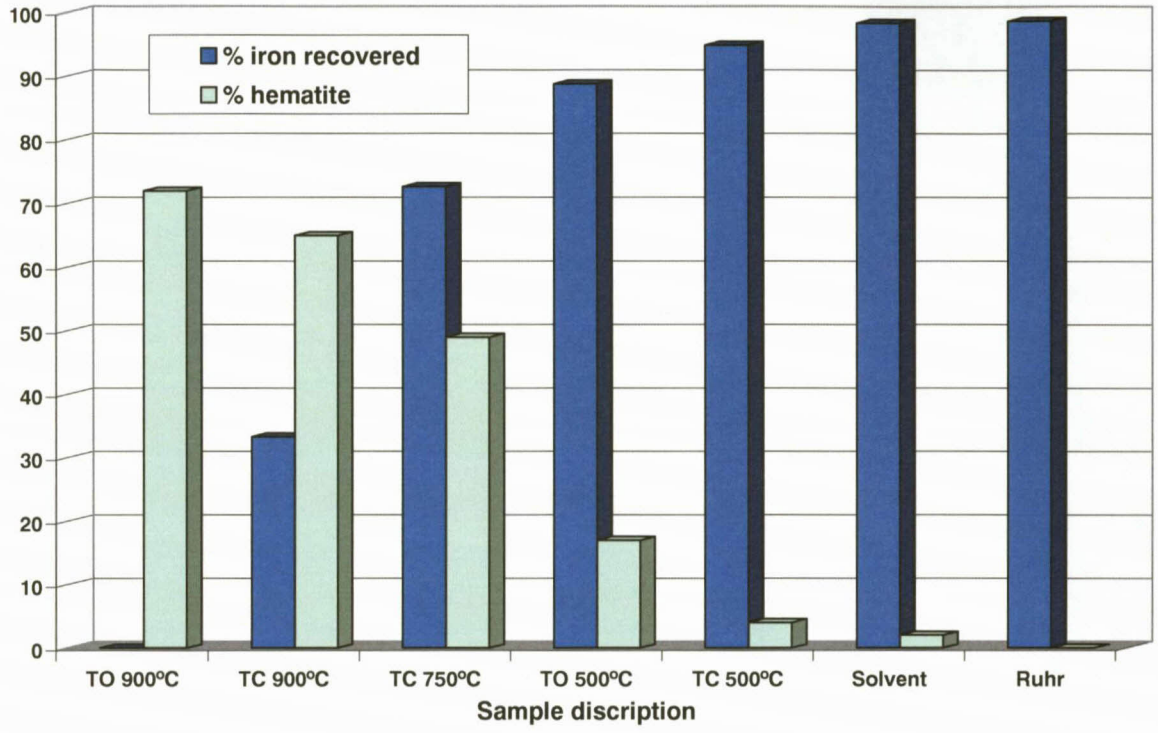

Figure 22. Percentage iron recovered as a function of the amount of hematite. TO - Thermally oxidized, TC - Thermally cracked, Solvent - Solvent extracted, Ruhr - Ruhrchemie type iron- based catalyst precursor

From the information in **Figure 22** it should be obvious that the wax removal endeavours should be tailored in such a fashion to minimise the amount of hematite formation. From the various wax removal techniques it is obvious that there are techniques which decrease the amount of hematite formed during wax removal. Both the solvent extraction and thermal cracking at 500 °C resulted in solids that had very small amounts of hematite (2% and 4% respectively). The amount of iron recovered from these samples was also the highest of the tested samples, 98.4% and 94.9%.

When comparing the two techniques it is obvious that the thermal cracking (500 °C) technique is the simplest and hence least expensive of the two methods. The potential to thermally decompose the wax at lower temperatures is also a possibility and could even lower the cost because of less energy that will be needed at lower temperatures.

By studying the effect of the calcination temperature of the various samples, on the amount of iron that can be recovered, a correlation could be seen between the temperature to which the catalyst is exposed to and the amount of iron that can be recovered.

To confirm that it is the presence of hematite that affects the recovery of iron negatively, a number of results have been studied relating the amounts of the various observed phases with the amount of iron that was recovered.

From **Table 11** it can be seen that the thermally oxidised 500 °C sample contains 78% maghemite and the thermally oxidised 900 °C contains 24 % maghemite. The iron that was recovered from these samples was 88.8% and 0% respectively. It can be deduced that the amount of iron that is recovered increases as the amount of maghemite increases. It can thus be concluded that the presence of maghemite is favourable for the dissolution of iron.

The amount of magnetite in the various samples can be obtained from **Table 11**. It can be seen that the amount of magnetite in the thermally cracked/decomposed 750 °C sample is 39% and 24% in the thermally cracked / decomposed 900 °C sample. Iron recovery was 72.7% and 33.3% respectively. The amount of magnetite in the sample may also favourably affect the recovery of iron from the investigated samples especially since there is no maghemite present in the two samples.

Figure 23 illustrates that the amount of iron that can be recovered is increased as the amount of ferrihydrite in the samples increase. Thus the manipulation of the wax removal method for maximum ferrihydrite composition should assist in maximum iron recovery to 100%.

From the above mentioned results and **Figure 23** the effect of the various iron phases on the recovery of iron is evident. It can be seen that only the presence of hematite significantly negatively affects the recovery of iron. The other phases seem to positively affect the recovery of iron.

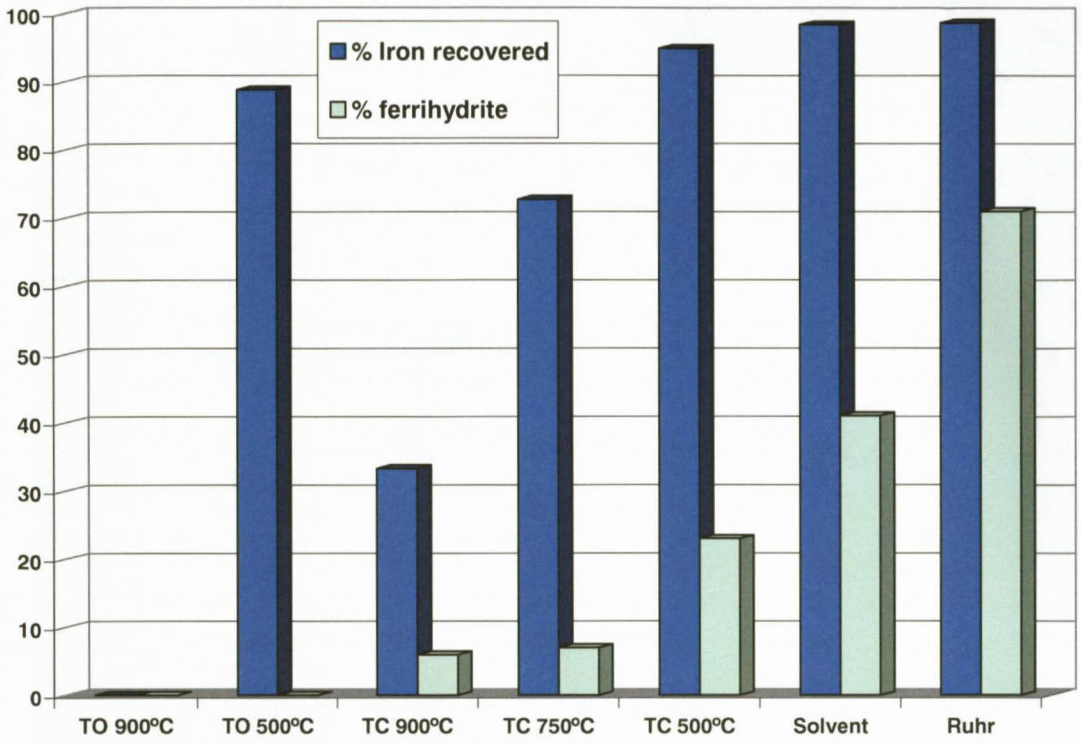

Figure 23. Iron recovered as a function of the amount of ferrihydrite. TO - Thermally oxidized, TC - Thermally cracked, Solvent - Solvent extracted, Ruhr - Ruhrchemie type iron-based catalyst precursor.

In light of the finding that hematite negatively affects the recovery of iron it was decided to purchase a sample of hematite from a commercial supplier and also test it in the same dissolution tests thus far employed for the other dissolution behaviour studies. These dissolution tests should allow correlation of iron recovery with the presence of hematite. The presence of hematite needed to be confirmed before any dissolution tests were done on the commercially purchased hematite sample. Mössbauer analyses were performed on the commercially purchased hematite sample and it was found that it consisted of 86 % hematite (α-Fe_2O_3) and 14 % goethite (α-FeOOH).

Although the sample contained some goethite it should be possible to conclude on the dissolution behaviour of the predominantly hematite phase. The amount of iron that was recovered from this sample was 87 %. This is in contradiction with results from the previous dissolution experiments where it was impossible to recover most of the iron in the hematite phase. It was then decided to calcine the commercially purchased hematite sample at various temperatures in order to try and lower the surface area and potentially link the dissolution behaviour to the surface area of the various samples instead of only iron phase.

Table 12 was constructed to verify the initial iron phase and the effect of the temperature treatments on the commercially purchased hematite sample as analysed by Mössbauer spectroscopy.

Table 12. Iron phase of various calcined samples.

Sample	% Contribution	
	Hematite	Goethite
Commercial Hematite	86	14
Commercial Hematite (calcined at 500 °C in air for 2 h)	100	0
Commercial Hematite (calcined at 900 °C in air for 2 h)	100	0

From **Table 12** it can be seen that as the temperature of calcination is increased the amount of hematite becomes 100%. In this case complete conversion to hematite is already attained at 500 °C.

Table 13 indicates the surface area of the various calcined commercial hematite samples. This data can be used to ascertain the affect that surface area has on the recovery of iron because the phase stays constant (hematite) and only the surface area differs.

Table 13. Surface area of various calcined commercial hematite samples.

Sample	Surface area (m^2/g)
Commercial hematite as received	34
Commercial hematite – calcined at 500 °C in air	18
Commercial hematite – calcined at 900 °C in air	3.6

Table 13 indicates that as the temperature of calcination increases the surface area decreases and from **Figure 24** it is evident that the amount of iron that was recovered also decreased as calcination temperature increased. It can thus be concluded that the surface area governs the amount of iron that can be recovered and not the iron phase *per se*, as previously indicated.

Figure 24 indicates that a large amount of the iron can be recovered from the commercial hematite (CH) sample (un-calcined) even though the iron is in the hematite phase. When the calcination temperature is increased it can be seen that the amount of iron that can be recovered decreases from 80.4% for the 500°C calcined sample to 58.2% for the 900 °C sample. It is thus obvious that a large amount of iron in the form of hematite can be recovered and it would not be correct to state

that the iron in the hematite fraction can not be recovered. The effectiveness of recovery of iron from hematite phases is linked to the surface area of the specific sample that is submitted to the dissolution process. By lowering the surface area, the amount of iron recovered will be less.

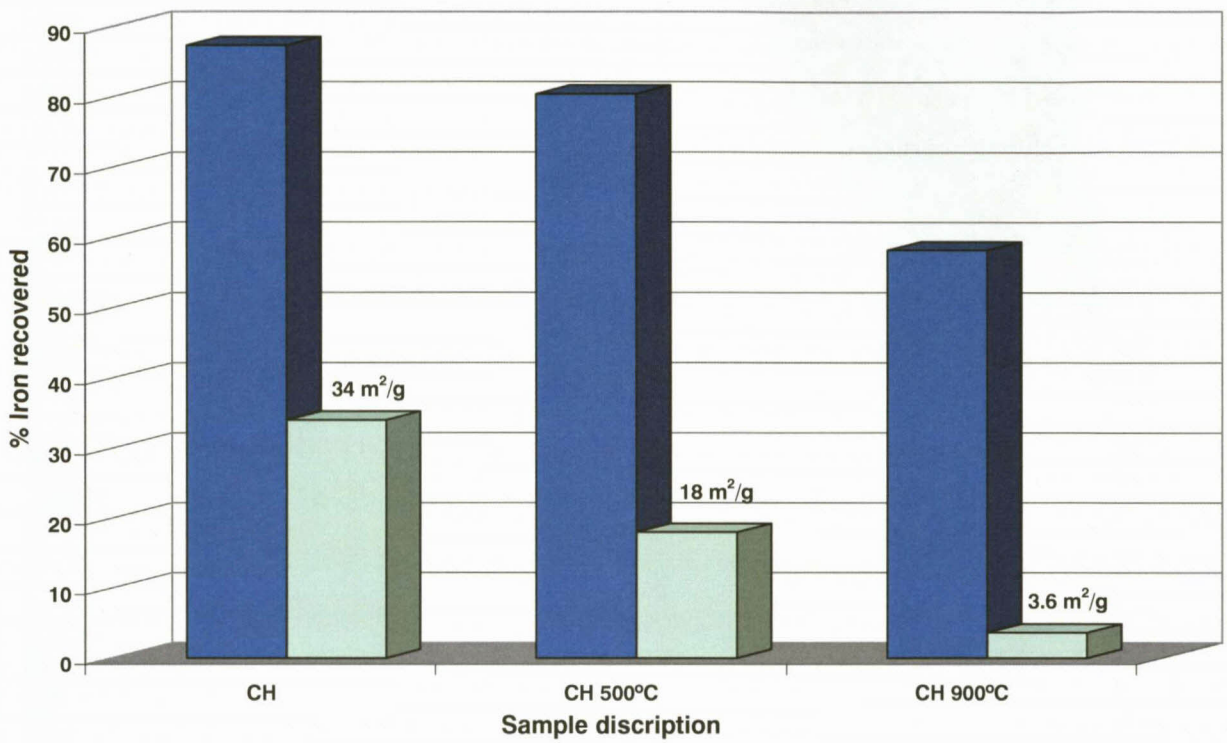

Figure 24. Iron recovered as function of calcination temperature of various hematite samples. CH - Commercial hematite as received, CH 500 °C - calcined at 500 °C in air, CH 900 °C - calcined at 900 °C in air.

When relating this information to the work that was done on the various wax removed samples it is apparent that the amount of iron that can be recovered can also be related to the surface area of the specific sample being investigated. **Table 14** contains the surface areas of the various wax removed samples.

Table 14. Surface area of various investigated samples.

Sample	Surface area (m^2/g)
Fresh Ruhrchemie type iron-based catalyst	220
Thermal oxidised (500°C)	55
Thermal oxidised (900°C)	1.1
Thermal cracked (500°C)	82
Thermal cracked (750°C)	15
Thermal cracked (900°C)	1.4
Solvent extracted	106

From **Table 14** it can be seen that the surface area decreases as the temperature at which wax is removed increases. The surface area is affected by the method of formation of the various phases, which is the dehydration or dehydroxylation of ferrihydrite to maghemite and hematite. A common feature of the dehydroxylation of all iron oxide hydroxides is the development of microporosity due to water expulsion. As the temperature increases the micropores coalesce to form mesopores and at temperatures above 600 °C the iron oxide sinters and the surface area drops considerably. This can be seen by studying **Table 14** where the amount of surface area decreases as the temperature increases.

The sample which was thermally oxidised at 500 °C has a surface area of 54.8 m^2/g and when the temperature is raised to 900 °C the surface area decreased to 1.1 m^2/g. Thus it can clearly be seen that the surface area decreases as the temperature increases. This is also observed when studying the thermally cracked samples. The surface area for the thermally cracked (500 °C) sample is 82 m^2/g and as the temperature increases the surface area decreases to 15 m^2/g for the thermally cracked (750 °C) sample and 1.4 m^2/g for the thermally cracked/decomposed (900 °C) as indicated in **Table 14.**

The effect of the surface area of the various samples on the dissolution behaviour of the various wax removed samples was also studied. **Figure 25** compares the amount of iron that can be recovered as a function of the surface area of the specific sample post wax removal prior to dissolution.

However when studying the dissolution behaviour of the commercial hematite, significant iron recovery is seen from samples containing only hematite. The reason probably relates to the formation of the various phases in wax removal treatments of the spent catalyst. What is important, however, are the parameters which govern the formation of hematite. It can be seen that the amount of hematite increases as the temperature which the spent catalyst is exposed to increases. When comparing the formation of hematite with the other formed phases it can be seen that the other phases form at relatively low temperatures and it has been shown in **Table 14** that the surface area decreases as the temperature which the catalyst is exposed to becomes higher. Thus the formation of hematite is associated with a high temperature when compared to the other phases and thus as the amount of hematite in the investigated samples increases, the surface area decreases and the recovery of iron decreases.

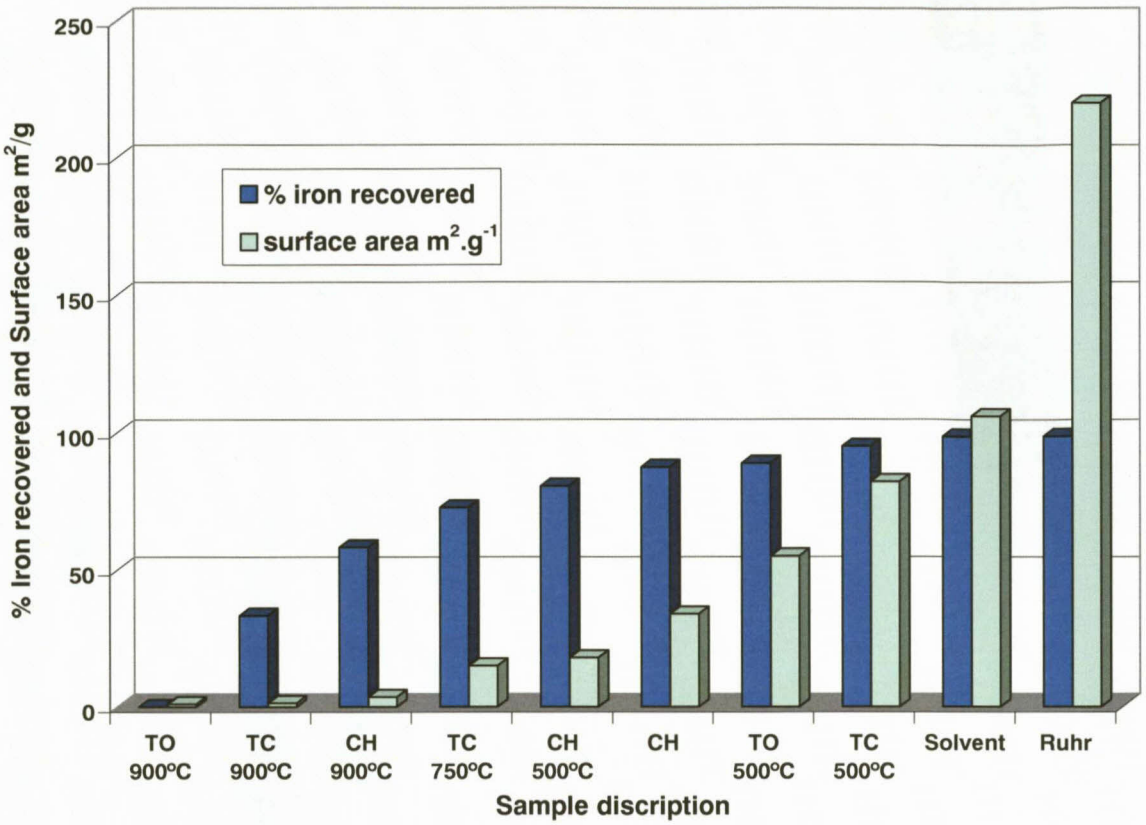

Figure 25. Iron recovered from various generated samples as iron nitrate in solution as function of surface area. TO - Thermally oxidized, TC - Thermally cracked, CH – Commercial hematite, Solvent - Solvent extracted, Ruhr - Ruhrchemie type iron- based catalyst precursor.

The fact that the catalyst contains silica and copper also increases the temperature where ferrihydrite and maghemite undergoes the phase changes to hematite. The hematite formed by thermally cracking the various samples is then by default formed in a region where high sintering can occur thus lowering the surface area even further. The presence of copper and silica in these samples may also retard the dissolution. In other words the hematite formed from the spent catalyst should be more difficult to dissolve.

As additional evidence for the statement that the iron recovery is linked to the surface area which is affected by the formation of hematite by the wax removal from the spent iron-based Ruhrchemie type catalyst treatments, a plot of the influence that the amount of hematite has on the surface area was constructed (**Figure 26).**

It can be observed from **Figure 26** that as the amount of hematite in the investigated samples increased the surface area decreased. Thus it is obvious that the formation of hematite from the

spent catalyst is associated with higher temperature which in turn lowers the surface area, which results in less iron recovered from the spent catalyst.

The spent catalyst also contains various other metals (copper, sodium, potassium and silica) of which the recovery is very important. The dissolution behaviour of these metals also has to be evaluated by comparing the various recoveries of the tested samples. Thus if the Iron recovery of two tested samples is similar but one method has a superior recovery for the other metals, it could be considered as the wax removal method of choice.

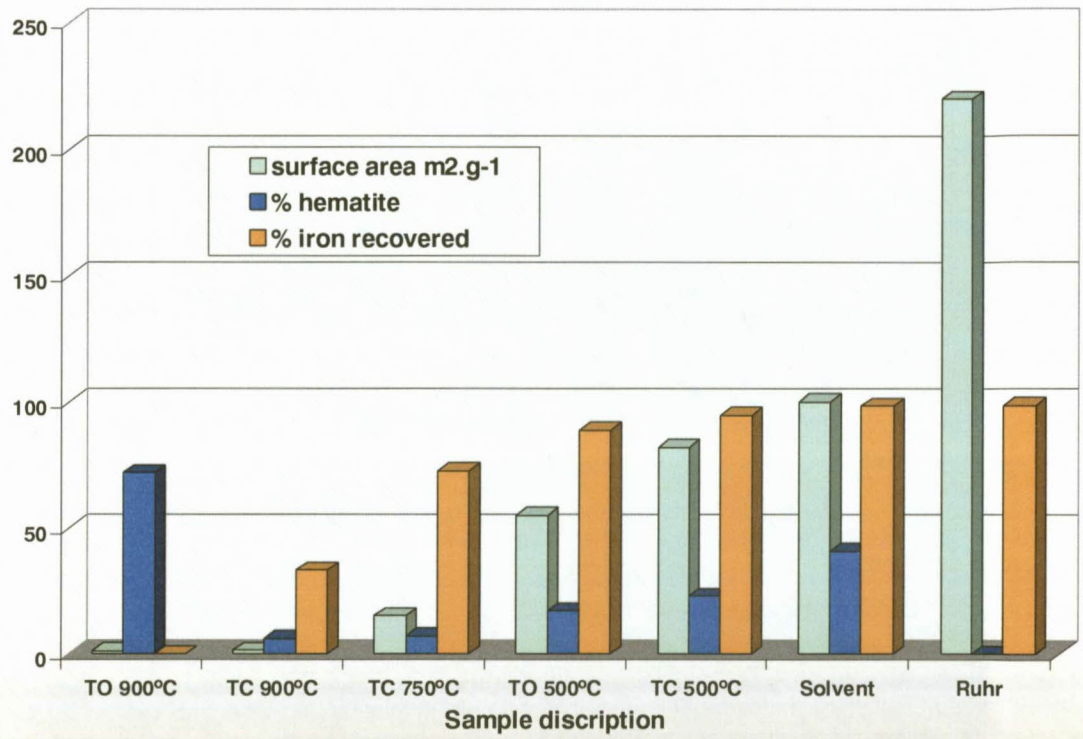

Figure 26. Percentage of hematite and percentage of iron recovered as a function of BET surface area. TO - Thermally oxidized, TC - Thermally cracked, Solvent - Solvent extracted, Ruhr - Ruhrchemie type iron- based catalyst precursor.

3.9 Recoveries of other catalyst constituents.

In order to evaluate the recovery of catalytic metals from spent iron-based Fischer-Tropsch catalyst further for possible industrial implementation, it is important to know where the other spent catalyst constituents end-up after dissolution in nitric acid. Should a residue (un-dissolved material) be generated during the recovery procedure, the composition of the residue will be important when disposal or alternative uses are evaluated.

The metal nitrate solution generated from recovery of spent iron-based catalyst will not only contain iron and copper nitrates as for the current commercial process. The metal nitrate solution from dissolving spent iron-based catalyst may also contain potassium, sodium, and other alkali metals, as well as silica, alumina, titania, or other suitable structural promoters. For incomplete dissolution the ratio of iron and copper in the metal nitrate solution may also be different and will require correction in order to prepare the same catalyst precursor. Therefore copper recovery was investigated for the different spent iron-based catalyst treatments. The results are summarized in **Figure 27**.

Figure 27 shows the copper recovery that was obtained after dissolution in nitric acid on the samples generated *via* the different spent catalyst treatments just as for iron recovery. When comparing the amount of copper that was recovered from the samples, it can be seen that most of the copper can be recovered by most the methods employed. For the thermally cracked sample at 900 °C higher % copper recoveries were found than for iron % recoveries. This could be ascribed to copper ejected to the surface and was more easily dissolved. For the thermally oxidized sample at 900 °C the recovery was also higher than the expected amount. The formation of an iron-copper spinel at the high temperatures which is resistant to acid attack or the loss in surface area may be the reason that prevents complete copper dissolution at 900 °C. The lower recoveries at higher temperatures could therefore be linked to surface area or possible sintering at elevated temperatures.

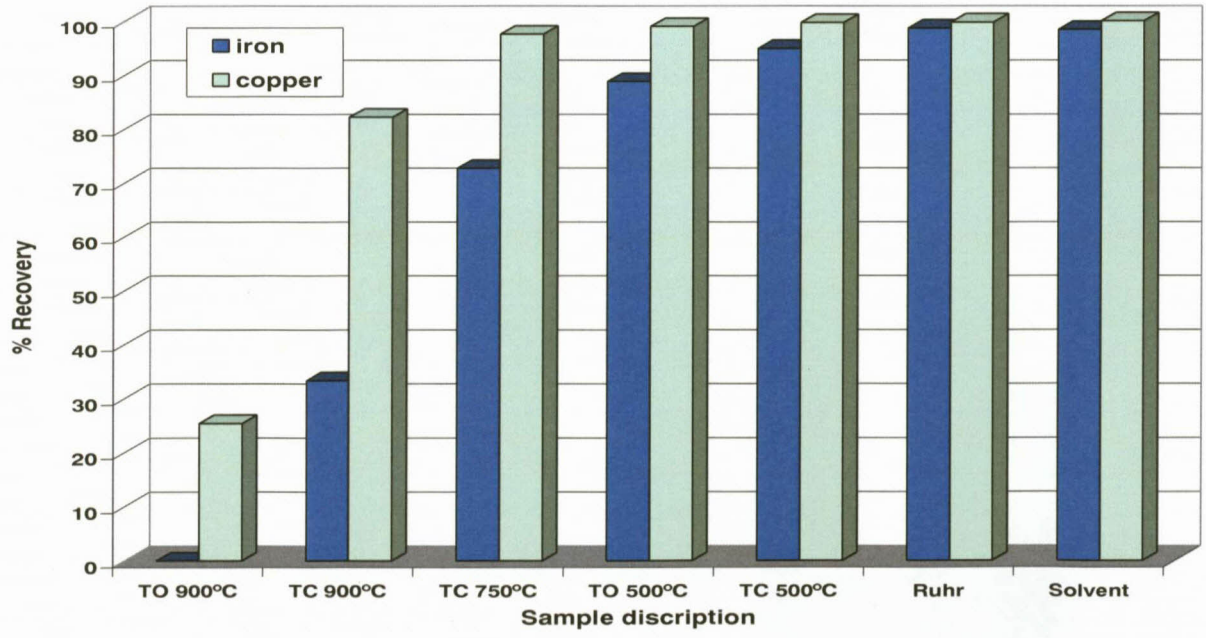

Figure 27. Copper recovered from various samples after nitric acid dissolution. TO - Thermally oxidized, TC - Thermally cracked, Solvent - Solvent extracted, Ruhr - Ruhrchemie type iron- based catalyst precursor.

The recovery of potassium from the seven recovery processes summarised in **Table 11** was also evaluated by inductive coupled plasma analysis of the generated solutions and is plotted in **Figure 28**. The recovery of potassium was expected to be high as potassium metal would easily react with nitric acid to form water soluble potassium nitrate, and potassium ions would simply dissolve in nitric acid media. The lower potassium recoveries observed for samples that were at 900 °C could be a result of K_2O decomposition at the high temperatures. It is therefore vaporized from the catalyst at the elevated temperatures and hence the seemingly low recoveries. More probably, however, is the trapping of potassium inside low surface area insoluble hematite that is generated at 900 °C. If potassium does not migrate to the surface of the hematite particle, as copper seems to do, potassium will be effectively shielded from the dissolution medium, here nitric acid, and hence will not dissolve. The same holds for the lower than expected sodium recoveries depicted in **Figure 29.**

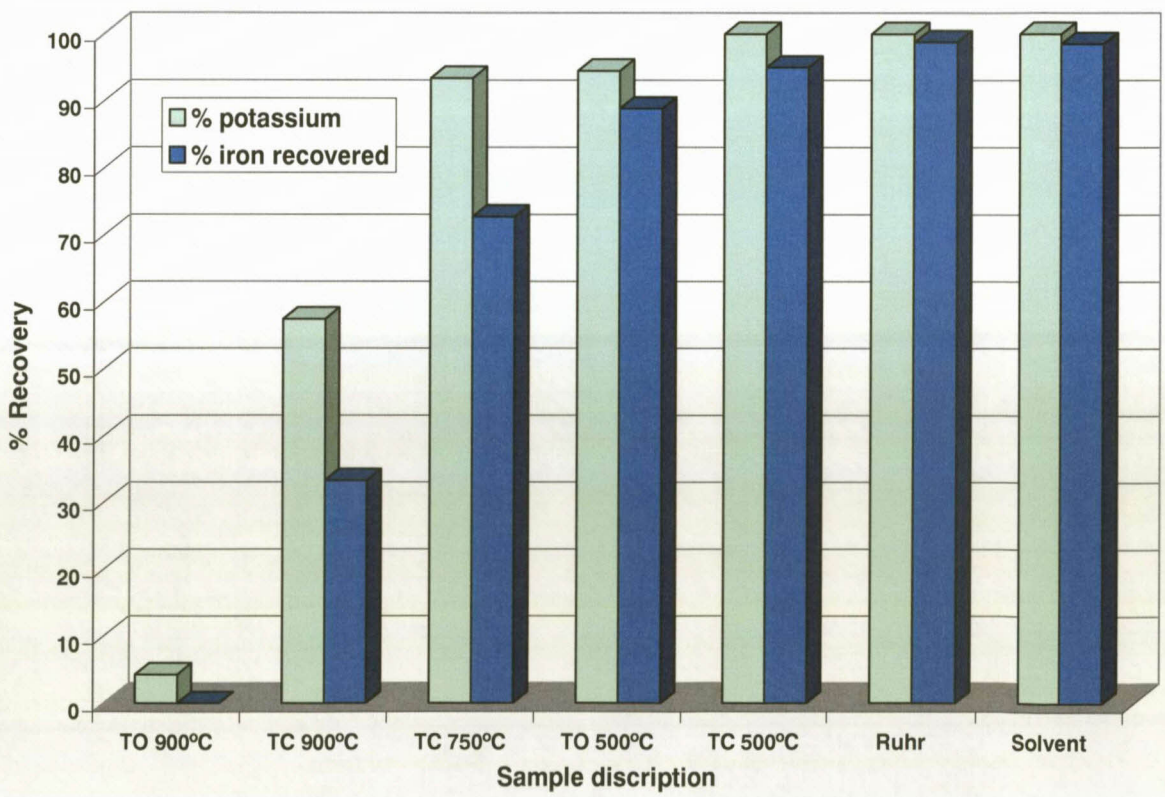

Figure 28. Potassium recovered from various samples. TO - Thermally oxidized, TC - Thermally cracked, Solvent - Solvent extracted, Ruhr - Ruhrchemie type iron- based catalyst precursor.

With exception of the thermally oxidised 500 °C sample, thermally oxidised 900 °C sample and fresh catalyst all the sodium was recovered from the investigated samples. It can be seen in **Figure 29** that all the sodium was recovered from the thermally cracked 500 °C sample.

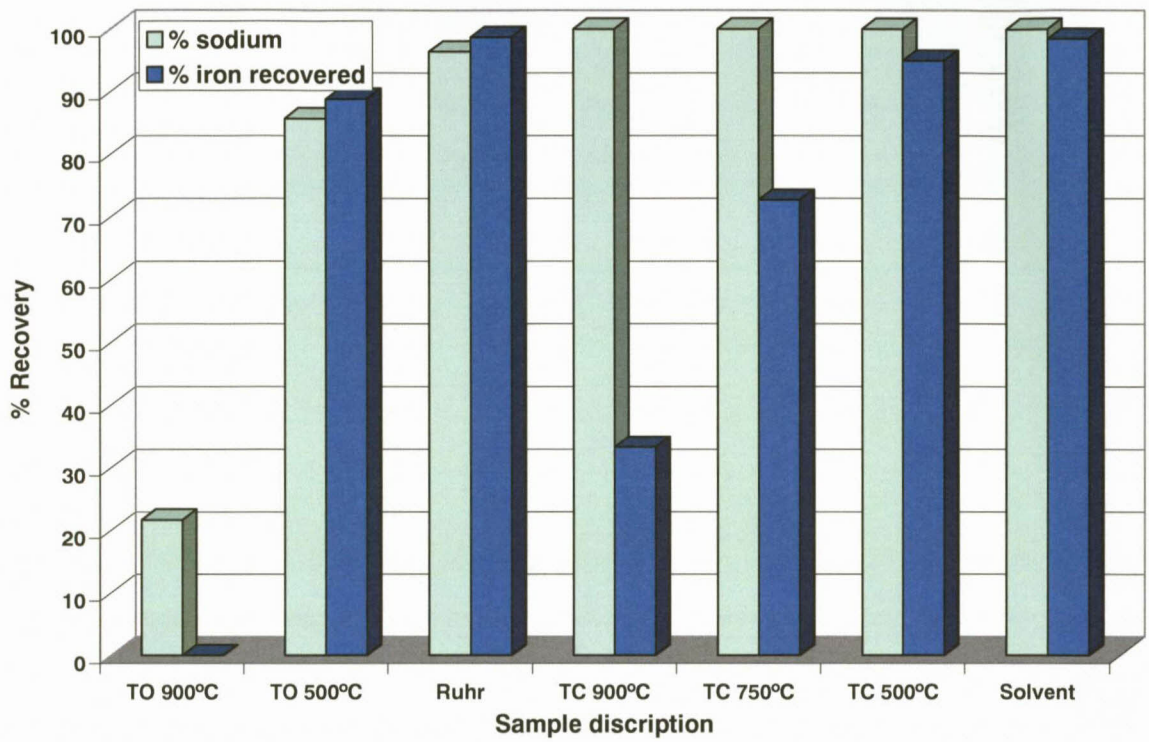

Figure 29. Sodium recovered from various samples. TO - Thermally oxidized, TC - Thermally cracked, Solvent - Solvent extracted, Ruhr - Ruhrchemie type iron- based catalyst precursor.

Figure 30 indicates the amount of silica that was recovered from the samples generated by the seven recovery procedures summarized in **Table 11**. Silica recoveries were determined by digesting the solid residue remaining after nitric acid dissolution in HCl under reflux. The resultant residue, containing the silica, was separated from the solution *via* filtration and then digested in sulphuric and hydrofluoric acid. Silica content was then calculated by mass difference between the residue before hydrofluoric and after hydrofluoric acid digestion. It can be seen that the recoveries of silica were generally low as is expected because silica dissolution is normally associated with high pH solutions. This contrasts the low pH recovery conditions required for iron recovery. There is obviously no significant advantage between any of the treatments when it comes to recovering silica. Lower temperatures than 900 °C led to higher recoveries. A possible explanation is that the silica is shielded from the acid media because it is encapsulated within the low surface area hematite matrix as for the copper, potassium and sodium species. The question, however, can be asked if silica recovery is beneficial and how the presence of silica in the resulting liquid would affect procedures when a new catalyst has to be prepared. The fate of silica needs to be further

evaluated because of the low recoveries under the investigated conditions. An option could be to remove the silica first and then recover the other metals. The silica could be removed by dissolving it in a strong base as mentioned before. However, this will convert the iron present to iron hydroxides which may have a completely different recovery profile than the iron from the samples summarized in **Table 11**.

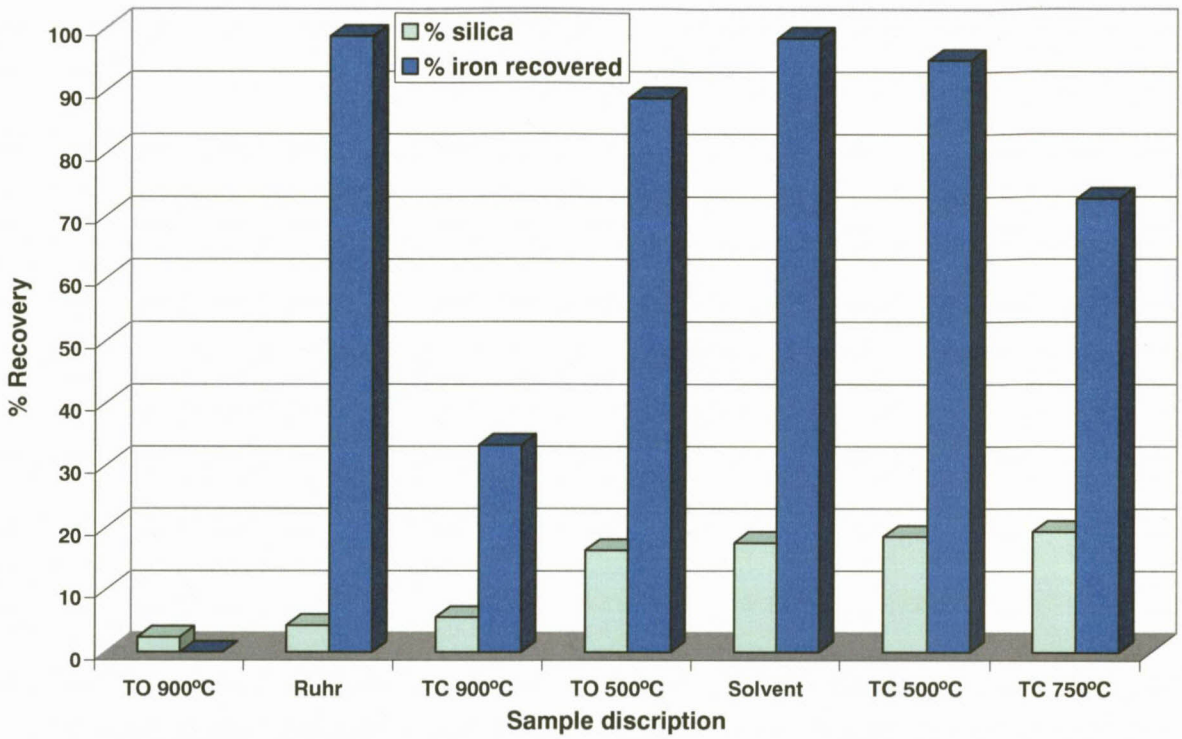

Figure 30. Silica recovered from various samples. TO - Thermally oxidized, TC - Thermally cracked, Solvent - Solvent extracted, Ruhr - Ruhrchemie type iron- based catalyst precursor.

When considering the recovery of all the metals from the spent iron-based catalyst it seems that the sample generated from the wax removed by thermal cracking of the wax covering the spent catalyst at 500 °C would probably be the wax removal method of choice. This method could be optimised by potentially lowering the temperature of wax removal thus yielding more of the wanted iron phases with higher surface areas. The addition of some form of carbon might facilitate the reduction of Fe(III) to magnetite which yields very positive dissolution behaviour.

It also seems that the copper, potassium, sodium and silica recovery is not as sensitive to the surface area when compared with the iron recovery. However at very high temperatures the recovery of these metals also lowers significantly. This could be because at these temperatures various spinels are formed which retard the dissolution process by potentially "shielding" the Fe(III) from the acid medium. This, however, needs to be confirmed.

3.10 Residence time effect.

Research described in section 3.7 of this study showed that the calcination temperature had a marked effect on the hematite content and surface area of the sample. Results indicated that the surface area was more important than the hematite composition but that the hematite composition can be used as an indication of the surface area as samples with high hematite composition normally had low surface areas. The effect of the residence time at different temperatures could influence the final iron oxide phased attained, as well as the final surface area attained. It was decided to investigate the effect of residence time, at specific temperatures, on the spent iron-based catalyst. From research discussed in section 3.3 of this study, wax removal from the spent wax coated catalyst prior to dissolution in nitric acid would be preferred. Therefore it was decided to use the solvent extraction method described in section 3.7 to remove the wax from the spent wax coated catalyst as this process involves the lowest temperature and would therefore have the least influence on results that investigate temperature and residence time. Various industrial thermal oxidation technologies exist and each has a particular set of preferred operating conditions and therefore knowing the effect of residence time on iron oxide phase and surface area is needed to choose the correct option. The lowest possible wax removal temperature and/or time will be needed in order to maximise surface area and thus increase the recovery of metals from the spent catalyst.

The wax-removed spent catalyst was then calcined at various temperatures and residence times as shown below:

1. 350 °C for 20, 120 and 600 minutes.
2. 500 °C for 20, 120 and 600 minutes.
3. 600 °C for 20, 120 and 600 minutes.
4. 750 °C for 20, 120 and 600 minutes.

To observe the effect of the various calcination experiments on the wax-extracted spent catalyst, the iron phases and surface area of the solid had to be determined before any temperature treatments. The effect of the temperature treatments can then be obtained when comparing the results before and after calcination. The samples were characterized by Mössbauer adsorption spectroscopy and X-ray diffraction to determine the phases present and the surface area was determined by gas adsorption analyses utilizing the BET method.

The effect of temperature on the surface area is illustrated in **Figure 31**. The surface area at each investigated temperature is plotted for the specific time interval thus indicating the effect of the temperature and residence time on the surface area. From **Figure 31** it is evident that the temperature of exposure has an effect on the surface area of the sample. The surface area remains almost constant when the temperature is increased from 350 °C to 500 °C irrespective of the residence time. The surface area decreases slightly when increasing the temperature from 500 °C to 600 °C. Upon increasing the temperature from 600 °C to 750 °C there is a large decrease in the surface area. It can also be observed that the effect of residence time at 750 °C is greater than at the lower temperatures. At 750 °C, upon changing the calcination residence time from 20 min to 600 min, the surface area decreased by 80%. At 600 °C the decrease was ca. 16%, while at 500 °C the decrease was less than 8%.

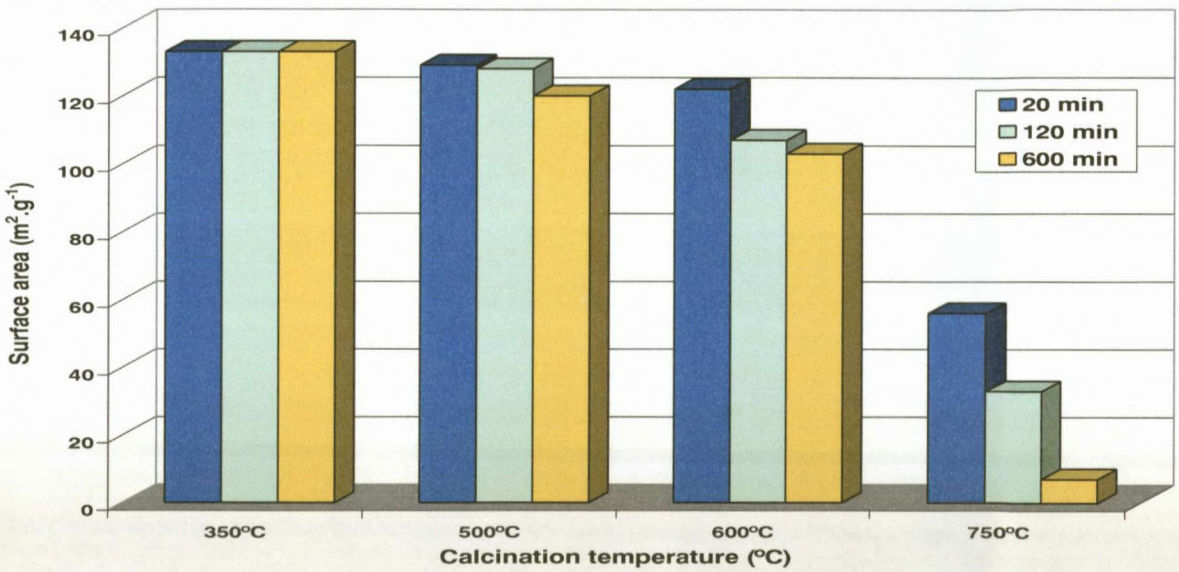

Figure 31. Effect of temperature and residence time on surface area.

The complete results from the BET analysis are tabulated in **Table 15**.

From the results depicted in **Table 15** it can be seen that the pore volume also decreases as the heat treatment becomes more severe. Pore diameter shows an increase but this is due to smaller pores collapsing at higher temperatures and creating larger pores but at the expense of surface area.

Table 15. Full results from BET surface area and pore volume analysis.

Sample name	Surface area ($m^2.g^{-1}$)	Pore volume ($cm^3 g^{-1}$)	Average pore diameter (nm)
350 °C – 20 min	133	0.31	9.3
350 °C – 120 min	133	0.34	10.3
350 °C – 600 min	130	0.35	10.5
500 °C – 20 min	129	0.34	9.9
500 °C – 120 min	128	0.35	10.6
500 °C – 600 min	120	0.36	10.7
600 °C – 20 min	122	0.34	10.2
600 °C – 120 min	107	0.28	9.7
600 °C – 600 min	103	0.29	10.1
750 °C – 20 min	56	0.26	14.3
750 °C – 120 min	33	0.18	18.3
750 °C – 600 min	7	0.02	- *

* Surface area to low to allow for reliable pore diameter evaluation.

As mentioned previously the amount of hematite in the sample is an indication of the temperature to which the sample was exposed. Thus a higher content of hematite in the spent iron-based slurry catalyst indicates exposure to higher temperatures resulting in a drop of the surface area and thus lower metal recoveries. **Figure 32** is a plot of the effect that the amount of hematite and maghemite (as determined by room temperature Mössbauer spectroscopy) has on the surface area after different calcination residence times and temperatures. It is noticeable that as the amount of hematite stays constant the surface area remains low and *vice versa*.

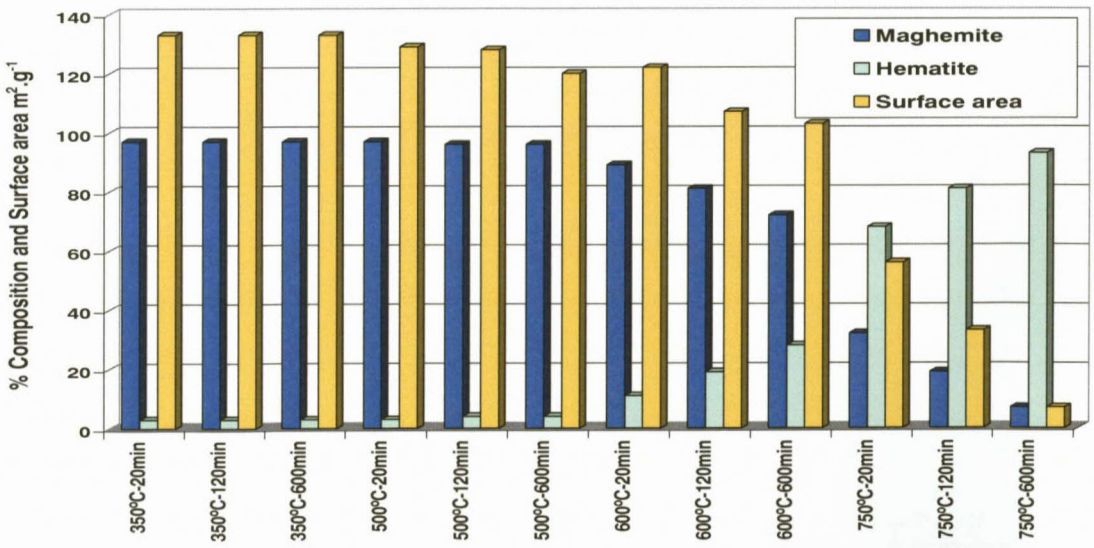

Figure 32. Correlation between surface area, hematite and maghemite content, as determined by Mössbauer spectroscopy, of spent de-waxed catalyst heat treated at various temperatures and residence times.

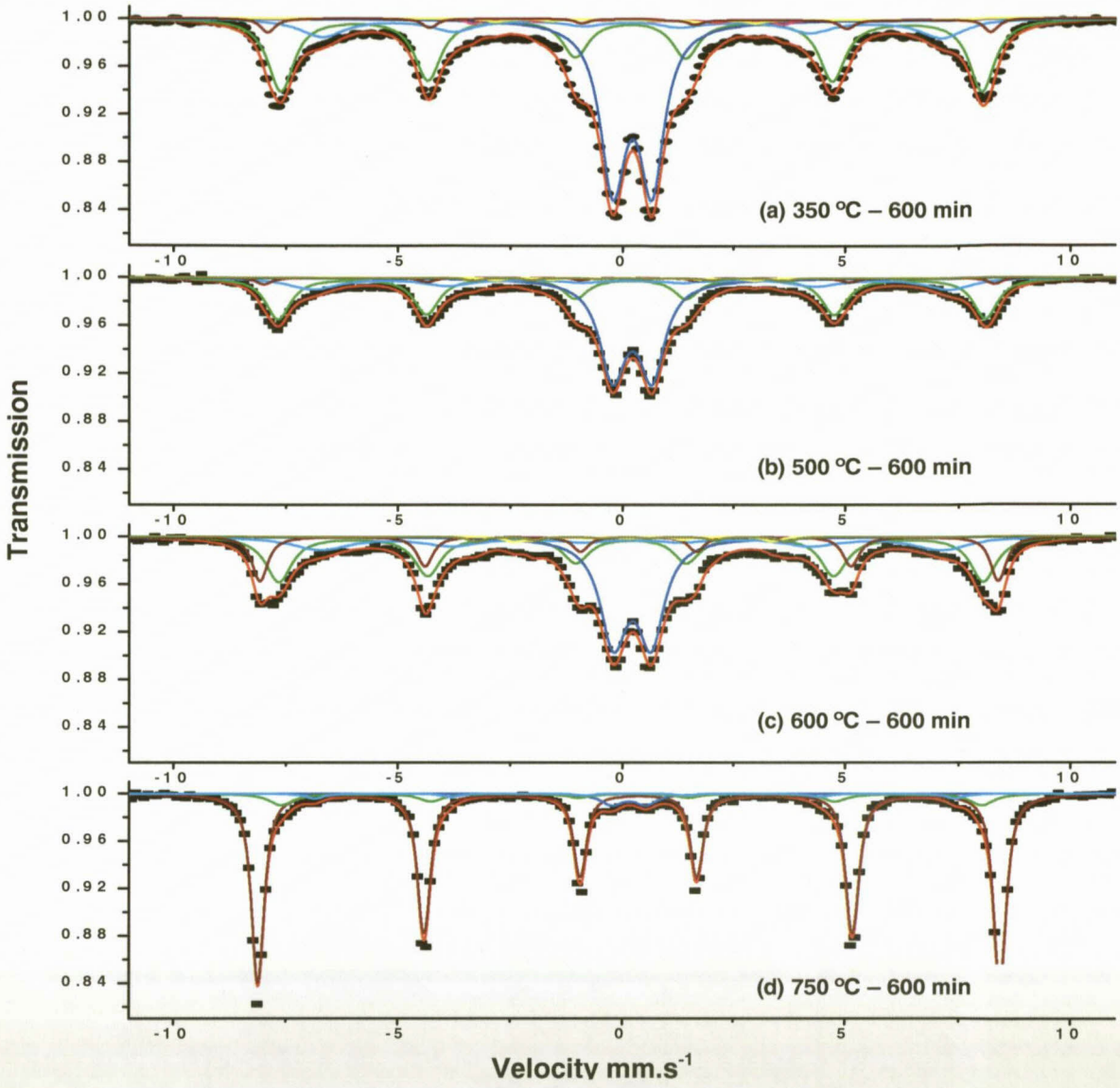

Figure 33. Selected Mössbauer patterns for the longest residence time for the various calcination temperatures tested. For (a) – (d) the red spectrum is the experimentally determined spectrum. Other coloured lines represent the theoretical relative contribution of different iron phases to generate the practically determined Mössbauer spectra.

Figure 33 shows selected Mössbauer patterns for the longest residence times for the various temperatures. From **Figure 33** it can clearly be seen that the doublet in the middle depicting Fe(III) species (blue) become smaller at elevated temperatures. The broad sextet representing maghemite also become smaller with elevated temperatures and the sharp sextet that represents hematite is the final phase reached at 750 °C for 600 min.

3.11 Conclusion

From the study described in the above paragraphs it is concluded that as the temperature and residence time to which the spent catalyst was exposed increases, the surface area decreases. When considering that the wax needs to be removed from the spent catalyst it becomes obvious that a technology should be chosen that either has low oxidation temperatures or low residence times, ideally both. It is therefore suggested that the temperature of wax removal should not exceed 500 °C and the residence can be up to 10 hours without affecting the surface area and metal recoveries. The use of a "flash calciner" where the temperatures are in the 800 °C+ range, but have residence times of a few seconds, may also yield positive results and should be investigated. From the three wax removal techniques studied, namely: solvent extraction, thermal oxidation and chemical cracking, the extraction method led to more efficient iron recoveries, thermal cracking allowed recovery of wax as short chain hydrocarbons and thermal oxidation led to complete loss of the high value wax component of spent FT catalysts. Which of these techniques are eventually chosen for industrial use will be determined by the economic driving forces of the time, the specific conditions of infrastructure at a specific plant, and from an environmental point of view, by the specific legislation of the time.

3.12 Reference

[1] Steynberg, A.P., Dry, M.E., in *Fischer Tropsch Technology, Studies in Surface Science and Catalysis*, 2004, Elsevier, 533.

[2] Cornell, R.M., Posner, A.M., Quirk, J.P., *Crystal morphology and the dissolution of goethite. J. Inorg. Nucl. Chem.,* **1974**, 36, 1937.

[3] Cornell, R.M., Giovanoli, R., *Acid dissolution of hematites of different morphologies.* Clays Clay Min., 28, **1993**, 223.

[4] Van der Marel, H.W., *γ-ferric oxide in sediments.*, J. Sed. Petrol., **1951**, 21,12.

[5] Schwertmann, U., Heinemann, B., *The presence of Maghemite in northwestern German soils.*, Neues Jahrb. Miner., **1959**, 174.

[6] Schwertmann, U., Cornell, R.M., in *The Iron Oxides – Structure, Properties, Reactions, Occurrences and Uses*, **1998**, Second Edition, Wiley – Vch, Table 14.2, 394.

[7] Sidhu, P.S., *Transformation of trace element-substituted maghemite to hematite.*, Clays Clay Min., 36, **1988**, 31.

Chapter 4 - Experimental

This chapter describes the experimental details of the research performed by the author.

4.1 Elemental Analysis.

Elemental analysis was performed to determine the concentrations of constituents in solutions and solid material generated during dissolution experiments as well as to evaluate the composition of the freshly prepared catalyst in terms of elemental specification.

4.1.1 Iron Analysis.

For catalyst precursor samples, due to high concentration of iron in the catalyst precursor as well as in the metal nitrate solutions generated during dissolution experiments, a titration method was employed rather than inductive coupled plasma (ICP). ICP analysis requires a large dilution ratio for high concentration elements and therefore decreases the accuracy of this method. For catalyst precursor samples the solid material was digested in hydrochloric acid under reflux and the un-dissolved solids were filtered out. Stannous chloride was used to reduce the iron(III) present in solution to ferrous-iron. Excess stannous chloride was then oxidized by adding mercury dichloride. The ferrous iron solution was diluted with distilled water and titrated with a 0.5N $K_2Cr_2O_7$ solution. Di-phenyl amine sulphonate was used as an indicator giving a colour change from green to violet. The volume and molarity of the $K_2Cr_2O_7$ titrated was used to determine the mass percentage of the iron.[1]

4.1.2 Copper, Potassium and Sodium Analysis.

Catalyst precursors, metal nitrate solutions generated from dissolution experiments and residue material after dissolution were digested in HCl under reflux. In some cases un-dissolved residues were treated with mixtures of acids containing H_2SO_4, HNO_3 and HF. After the residue was filtered off the solution was analyzed on a Varian Vista AX CCD, Simultaneous Inductively Coupled Plasma – Atomic Emission Spectroscopy (ICP-AES). The absorption of the sample, a standard and a blank sample was used to determine the concentrations by ICP AES.

4.1.3 Silica Analysis.

Samples were digested in HCl under reflux. The residue, containing the silica, was separated from the solution *via* filtration and then digested in sulphuric and hydrofluoric acid. Silica content was then calculated by mass difference between the residue before hydrofluoric and after hydrofluoric acid digestion.

4.2 BET Surface Area.

A Micromeritics Tristar® analyzer was used for BET surface area analysis for all samples. 250-350 mg of sample was weighed into a sample tube and degassed overnight at 200 °C under a 50 ml/min N_2 flow in a Micromeritics FlowPrep 060 instrument. Degassing was done to remove any moisture or volatiles from the pores of the catalyst samples. After degassing the sample was reweighed and loaded into the sample port of the instrument. Prior to the analyses, all the sample tubes were evacuated (to ensure a clean surface for analysis). N_2 was then dosed into the sample tubes at various pressures and the volume of the monolayer at liquid nitrogen temperatures (76.15 K) was determined for each absolute pressure. Nitrogen adsorption experiments were then performed using a Micromeritics Tristar instrument at liquid nitrogen temperatures. Micromeritics software was used to determine the pore volume and surface area *via* the *Brunauer-Emmet-Teller* (BET) equation. The total pore volume of the sample is determined at P/P_0 of 0.995.[1]

4.3 Mössbauer Atomic Absorption Spectroscopy.

Mössbauer adsorption spectroscopy (MAS) measurements were performed by using a constant acceleration spectrometer equipped with a Co/Rh source. Initial activity of the cobalt source is 20 mCi. The spectrometer was operated in a symmetric constant acceleration mode with 100 μs dwell time per channel. Spectra were collected over 1024 channels, in mirror image mode, to obtain at least 500 000 counts per channel. Spectra were then analyzed by means of a least squares program "Normos" that models data as a combination of quadruple doublets and sextets based on a Lorentzian line-shaped profile. Individual adsorption features were identified on the basis of their isomer shift, quadruple splitting (Δ) and magnetic hyperfine field (B_{hf}) values. The relative amount of each phase was determined from the area of the absorption peaks. The isomeric shift values are reported relative to *alpha* iron.[1]

4.4 X-Ray Diffraction.

X-Ray diffraction samples were ground to a fine powder using a pestle and a mortar. Each sample was then placed onto a smooth, flat, stainless steel sample holder. Approximately 0.5 g of sample was loaded into the diffractometer. X-ray powder diffraction experiments were performed using a Philips X'pert Pro diffractometer with Fe filtered Co Kα radiation as a primary X-ray beam. Analysis parameters are tabulated in **Table 1**.

Table 1. Operating parameters for X-Ray diffractrogram analysis as used for analysis of samples for this study.

Parameter	Setting
Voltage	40kV
Amperage	40 mA
Divergence slit	1.0 °
Anti-scatter slit	2.0 °
Scan from	5 ° (2θ)
Scan to	120 ° (2θ)
Soller slits	0.04 °
K α	1.79031 Å
Scanning	Continuous
Duration of scan	3 – 14 hours

4.5 Thermo Gravimetric Analysis (TGA).

Spent iron-based, wax coated, Fisher Tropsch catalysts were obtained from both fixed bed and slurry bed operation and had varying wax content. Wax content was determined with thermo gravimetric analysis (TGA) using a Thermal Analysis Instruments SD7260 Simultaneous DSC – TGA. Data interpretation and presentation were performed with Universal Analysis 2000 software. Analysis conditions were set for a ramp rate of 5.00 °C/min from ambient conditions to 900 °C in the presence of a constant flow of 150 $ml.min^{-1}$ synthetic air.[2]

4.6 pH Determination.

All pH measurements were performed with a Yokogawa model PH82 pH meter equipped with model PH72SN style S1.0 probe. The pH meter was calibrated using Mettler Toledo pH 4.01, pH

7.00 and pH 9.21 buffer solutions. When not in use the pH probe was stored in a Mettler Toledo 3 mol/l KCl solution.

4.7 Solid Content Determination of Iron-bearing Slurry.

Solid content of the iron-bearing slurry before spray drying was performed in a Sartorius MA30 moisture analyzer. Analysis was performed isothermally at 130 °C until no mass loss was measured for more than 10 min. The moisture content was then noted and subtracted from the total sample mass to determine the solid content of the iron-bearing slurry.

4.8 Reagents for Dissolution Experiments.

4.8.1 Nitric Acid.

Nitric acid was obtained from the commercial plant. Nitric acid is commercially prepared by dissolving/absorbing gaseous NOx through water absorption towers. Water used in the adsorption towers are "A grade" steam condensate with specifications listed in **Appendix Table 1**. Nitric acid concentration is controlled by using the specific gravity of the liquid produced in the absorption towers. The plant specification for the absorption towers is for a specific gravity (SG) of 1.20. The absorption tower nitric acid is then mixed with concentrated nitric acid supplied by Sasol Nitro® to give a final density specification of 1.25 -1.26 SG. A SG value of 1.24 – 1.30 can be used for dissolution, but 1.26 is preferred. Nitric acid specifications are listed in **Appendix Table 2**. Different nitric acid concentrations prepared for experimental work was achieved by dilution of the commercially obtained solution with de-ionized water.

4.8.2 Spent Iron-based Fischer-Tropsch wax-coated catalyst.

Spent iron-based Fischer-Tropsch catalyst from both fixed bed and slurry bed reactors were used during the study. Spent iron-based catalyst samples collected for this study contained varying wax mass fractions. Individual samples were therefore submitted for Thermo Gravimetric Analysis (TGA) to determine the wax mass fraction present and the analysis method used as described in section 4.5.

4.8.3 De-ionized Water.

All the water used during experimentation for dilution, dissolution and adjusting reactor liquid levels to compensate for evaporation was supplied through a Millipore Elix® 5 with Progard 1 pre-treatment pack and conductivity specification of < 0.2 µS/cm compensated to 25 °C.

4.9 Wax Coated Catalyst Dissolution Experiment (heated - mild agitation).

All experiments were performed inside a fume cupboard. Stirring was performed using an overhead Heindolph type RZR1 stirrer with digital rpm display. The impeller used was a stainless steel propeller type impeller with 3 blades and a total diameter of ca. 40 mm. Typically, 1000 g of 55% nitric acid solution was diluted with 250 g de-ionized water in a 2000 ml Duran® beaker of dimensions Ø = 132 mm, h = 185 mm. The solution was then heated with a stirrer hotplate of model FMH electronics STR-MIT. The hotplate temperature was controller by connecting the supply current of the hot plate to a control box utilizing a REX C100 PID controller module. Temperature was measured in the solution with a *type J*, $^1/_8$" stainless steel thermocouple held in place by a retort and clamp. Stirring was activated at 120 rpm and the solution was then heated to and controlled at 80 °C. Due to evaporation and resultant moisture loss at 80 °C, the liquid level was noted with a permanent marker before and after spent wax coated catalyst addition and maintained by adding distilled water for the duration of the run. At 80 °C the spent wax coated catalyst was added. These conditions were chosen as they closely resemble operating conditions on the commercial plant where iron metal is added to nitric acid at 80 °C. The hotplate and beaker assembly was placed inside a stainless steel drip tray in case of nitric acid spillage or beaker failure.

Deviations from standard procedure.

1. The escaping gasses caused foaming that reached 2,5 times the height of the original liquid level. Foaming caused the experiments to be abandoned due to overflowing. Later experiments were performed in a Duran®, high form beaker of dimensions Ø = 135 mm, h = 280 mm.
2. High shear mixing experiments were performed with a Silverson Machines L5M laboratory stirrer fitted with a general purpose disintegrator head of model L4RT. Impeller diameter was ca. 40 mm with four blades. Clearance between the blades and static circular head was ca. 1 mm. Stirring was set to 800 rpm.

4.10 Thermal Oxidation of Spent Iron-based Wax Coated Catalysts.

Thermal oxidative removal of wax was done by placing an amount (ca. 500g) of spent-wax coated iron-based catalyst onto a stainless steel (grade SS 310) tray with dimensions: 300 mm wide, 400 mm long and 25 mm high. The catalyst bed height was maintained at 10 mm for all experiments. Oven dimensions were 500 mm wide, 500 mm in length and 500 mm deep. The oven was then heated to the desired experimental temperature in static air and then kept at the desired temperature for 2 hours. Thereafter the oven was cooled to room temperature, the sample was removed from the oven, and analyzed.

4.11 Thermal Oxidation of Spent Iron-based Wax Coated Catalysts with Varying Sample Volume and Bed Height.

For all experiments the same oven of dimensions: 500 mm wide, 500 mm in length and 500 mm deep were used. Sample sizes varied depending of the container used. The oven was heated from ambient temperature to 600 °C within 150 min and then maintained at 600 °C for 1 hr and allowed to cool to ambient temperature in 2 hours. Experiments were performed in the presence of static air. Temperature control for the oven was measured by a *type K* thermocouple and controlled with a TOHO model TTM-309 programmable controller. Oven temperature control was done with a thermocouple protruding from the rear vertical wall of the furnace by 100 mm with the entry point 300 mm from the base of the oven and 250 mm from the side.

Three cubic sample containers were manufactured of dimensions 50 mm, 100 mm and 200 mm. On each of the cubic containers, fittings for a $^1/_8$" thermocouple was attached that could be blanked when not in use. This configuration allowed for the thermocouple to be placed such that it could measure the surface temperature of the samples with different bed height. The temperatures for the oven and catalyst bed surface were logged with a Eurotherm® model 4101C, 100 mm continuous strip chart recorder.

4.12 Wax Removal from Spent Iron-based Catalysts *via* Solvent Extraction.

A solvent extraction method was used to remove the wax from the spent catalyst before the different temperatures and residence times could be evaluated. 500 g of wax-coated catalyst was added to a pressurized filter system and the filter was heated to 90 °C. The filter rig consisted of a 25 l stainless steel vessel with filter material of type Watmann 542 at the base of the vessel on a

porous stainless steel metal disc and a removable lid which is closed when pressure filtration is performed. Heating was facilitated by electrical tracing wound around the vessel. Temperature control was done by measuring and controlling the temperature *via a type J* thermocouple between the electrical tracing and the outer surface of the vessel and insulation. The thermocouple and electrical tracing were connected to a control unit utilizing a REX C100 PID controller module. A C_9-C_{11} paraffin cut was added to the filter and stirred for 30 minutes. The dissolved wax and paraffin solution was then filtered by pressurizing the filter to 5 bar with nitrogen. This procedure was repeated three times thereby removing most of the wax. Resultant catalyst cake was then pacified with dry ice as the catalyst is still reduced and rapid oxidation will lead to an exotherm that could influence the results.

After the dry ice had sublimed the solid was taken from the pressure filter and heated under nitrogen to 250 °C and kept there for 2 hours to render a free flowing solid. A small amount of solvent extracted catalyst was then heated in a muffle furnace to 500 °C in a static air environment and kept there for 2 hours. The mass of catalyst left after this treatment was subtracted from the mass of loaded catalyst to obtain the amount of wax that was removed by the solvent extraction and temperature treatment methods employed.

4.13 Calcination of Wax Removed Spent Iron-based Catalysts at Varying Residence Times and Temperatures.

The calcinations were performed in a laboratory scale glass fluidized calciner with solvent extracted and passivated spent catalyst by loading 20 g of the wax removed spent catalyst into the calciner and then flowing 1.2 $l.min^{-1}$ of air through the catalyst bed, which also facilitates fluidization of the catalyst. Temperature was elevated from room temperature to the desired end temperature with a heating rate of 3 $°C.min^{-1}$. Once the calciner reached the desired temperature the temperature was kept there for the proposed time intervals after which the temperature was lowered to room temperature. Samples were then removed from the calciner and submitted for various characterization analyses. Air flow rate was maintained throughout the calcination experiment.

Fluidized sample temperature was monitored by a *type K* thermocouple placed in the catalyst bed and recorded by a temperature logger. Temperatures were logged throughout the experiment to ensure that there were no temperature excursions during the calcination experiments.

4.14 Catalyst Precursor Synthesis.

In this study an iron-based catalyst precursor, with chemical and structural (strength) promoters (additives), similar to the original Ruhrchemie catalyst precursor was prepared from metal nitrate solutions generated by the dissolution of spent iron based catalysts in nitric acid. The catalyst preparation procedure employed was also based on the Ruhrchemie process with the exception that the metal nitrate solution came from dissolved and treated spent catalyst and not from the dissolution of iron and copper metal in nitric acid as the Ruhrchemie process describes. Metal nitrate solutions generated were diluted with deionized water to the required concentrations of 40 g/l of iron and 2 g/l of copper after the initial solution concentrations were determined. The precipitating agent, sodium carbonate (Na_2CO_3), was supplied as high density soda ash by CHC Global, South Africa.

Na_2CO_3 was dissolved in de-ionized water to a concentration of 100 $g.l^{-1}$. 10 litres of both of the precipitation reagents were prepared. The solutions were then heated to 60 °C by indirect steam heating. The temperature of the solutions was monitored with *type J* thermocouples connected to digital temperature displays. Both solutions were agitated during heating for increased heat transfer across the ¼" stainless steel tube containing the 2.4 bar steam used as indirect heating medium. The temperature was adjusted by regulating the steam flow through the tubing by means of a needle valve. The carbonate solution was transferred at 60 °C to the precipitation vessel with a volume of 30 litres. Here the carbonate solution was maintained at 60 °C with a similar steam heating system. Agitation was performed with an overhead stirrer/motor configuration with variable speed control. A propeller type impeller with 3 blades and a total diameter of 100 mm was used operated at 250 rpm. The metal nitrate solution was added into an agitated sodium carbonate solution over a time period of ca. 20 minutes with a calibrated peristaltic pump of model Watson Marlow 505S. The metal nitrate solution was added until the resulting slurry containing solution reached a pH of ca. 7. Iron-bearing slurry was then transferred to a small plate and frame filter of dimensions 150 mm X 150 mm X 20 mm with 10 plates. The iron-based precipitate was then washed with de-ionized water heated to 40 °C. Conductivity of the filtrate was monitored and when a value of 100 $\mu S.cm^{-1}$ was reached the washing process was terminated. Washed precipitate was then re-slurried with de-ionized water using the same precipitation vessel. A solid content of ca. 12 mass% was aimed for. Approximately 500 g Potassium silicate "waterglass" was now added to the re-slurried mixture and agitated.

The resulting slurry was pH corrected to pH 7 by addition of 45 mass% nitric acid. The slurry was then filtered to remove additional potassium as the potassium/silica ratio in the added potassium

silicate mixture is higher than the required ratio in the final catalyst precursor. After filtration the filter cake was re-slurried with de-ionized water to a solids content of ca. 20 mass%.

Slurry was then spray dried in a pilot scale counter current Niro® spraydrier using a 0.9 mm hollow cone spray nozzle with a slurry supply pressure of ca. 1 bar. Spray chamber inlet air temperature was maintained at 450 °C and the outlet temperature to 120 °C. The catalyst precursor was then calcined at 450 °C for 2 h in a shallow bed inside a muffle furnace in the presence of an air atmosphere, after which it is ready for use.

4.15 Micro slurry Fisher Tropsch Laboratory Reactor Configuration.

A continuous stirred tank reactor (CSTR) was used for reduction of the iron based catalyst as well as Fischer-Tropsch synthesis performance evaluations.

4.15.1 Gas Supply, Mixing and Sampling.

High purity feed gases were supplied by AFROX with the following specifications

Argon (N5.0)[3]	:	> 99.999 vol %
Hydrogen (N5.0)[4]	:	> 99.999 vol %
CO (N2.3)[5]	:	> 99.3 vol %

Feed gases were situated in a gas cage outside the laboratory with in-line pressure regulating in order to supply constant feed gas pressure to the laboratory. Gas flows were regulated using Brooks mass flow controllers of model 5850S Smart Mass Flow and are shown in **Figure 1**. Brooks mass flow controllers were calibrated for 20 bar pressure drop between the 40 bar supply pressure and 20 bar micro reactor pressure. Individual flow controllers were also separately calibrated for the specific gas utilized. Brooks controllers use the specific heat capacity of gases to control accurately and any errors were negated by calibrating with the gas to be used. All flows were normalized to standard temperature and pressure (STP) conditions. Calibrations were verified by detailed gas composition analysis.

Brooks mass flow controllers were protected by 8 μm gas filter elements installed on the gas feed line to prevent any particulate matter from entering the flow controller. Individual gas lines were also fitted with non-return valves to prevent cross contamination of gasses when combined in the reactor feed stream. The total feed gas stream was also fitted with a non-return valve before

entering the micro slurry bed reactor in order to limit molten wax from flowing into the feed line causing blockages. A sample line connects to the combined gas feed and was routed to an online gas chromatograph (GC) for feed gas analysis. A pressure transmitter was fitted on the feed gas line to measure reactor pressure conditions. The measured pressure was also connected to an alarm in case of over pressure conditions.

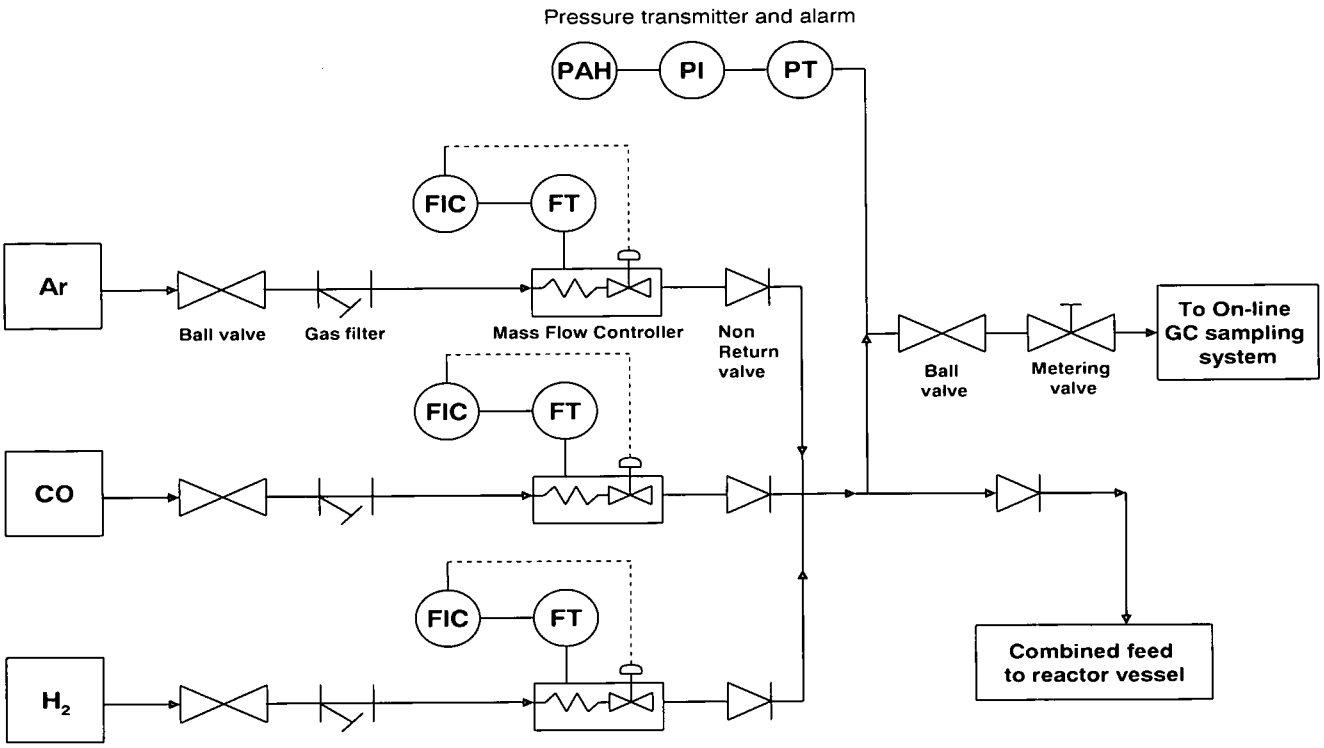

Figure 1. Reagent gas supply through Brooks mass flow controllers to laboratory scale continuously mixed reactor used for evaluating the Fischer-Tropsch synthesis performance of catalytic material.

4.15.2 Reactor Vessel.

The reactor was manufactured from stainless steel (grade 116) and had a volume of 1000 ml. During experimentation the liquid component (wax) amounted to ca. 750 ml. Maximum operating pressure and temperature for the vessels was designed for 300 °C and 100 bar. The vessel was flanged with the top flange connected to the reactor skid and to the vessel with 8 bolts. When the vessel was unloaded the bolts are loosened and the reactor removed by lowering the vessel with a pneumatically actuated lift. During operation the reactor was heated by an external heating element that clamps tightly around the vessel to ensure high heat transfer efficiencies. Due to the large vessel wall thickness temperature control has to be done by a dual temperature control system. A master and slave controller configuration is employed. Master controller (RX-900)

receives a temperature signal from a thermocouple submerged in the wax reactor medium. The output signal of the master controller was used to control the slave controller (RX-400) which heats the heating element and uses a thermocouple between the heating element to control the element temperature. This control configuration allows for very accurate temperature control (± 0.2 °C from setpoint). The system is depicted in **Figure 2**.

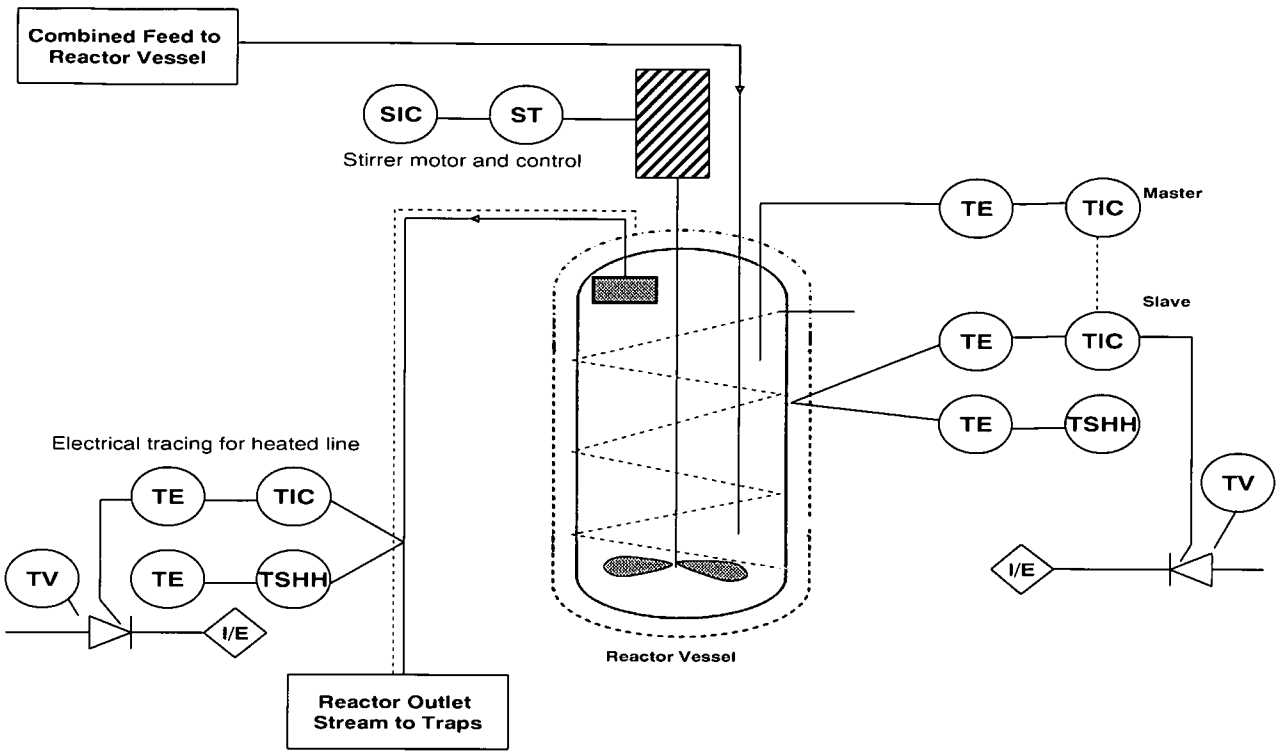

Figure 2. Micro slurry reactor with temperature control system and stirrer motor with control.

4.15.3 Reactor Vessel Internals.

The internal of the reactor can be dived into three sections namely:

1. Temperature control elements
2. Mixing related internal and
3. Reagent and product addition and removal

The reactor and internals are shown in **Figure 3**.

1. *Temperature* was measured by a $^{1}/_{8}$" *type J* thermocouple connected through the top flange with the measurement taken 5 cm above the reactor base. This ensured that temperature within the wax medium was directly measured.

2. *Mixing* was achieved *via* an impeller configuration connected to a variable speed motor. The motor and impeller shafts were connected *via* a permanent magnetic coupling that negates the use of high temperature and pressure seals to isolate the internal high pressure under which reactions are investigated. Magnetic shaft coupling has the additional advantage that should the impeller become stuck the motor would not be damaged as the magnetic coupling would slip when the torque applied by the motor exceeds the magnetic force. The vessel was also fitted with three, symmetrically placed, baffle plates with an offset from the vessel wall. Having an offset ensures that catalyst does not build-up in front of the baffle plate but is "washed" out through the space between the baffle and the reactor wall. Baffle plates are introduced to facilitate radial and axial mixing and counter vortex formation. Vortex formation impact negatively on mixing efficiency. Individual baffle plates are connected together *via* a ring at the bottom of the baffles to improve the structural integrity of the baffle configuration and are situated close to the bottom of the vessel. The impeller configuration consists of two impellers connected to the singular shaft. The first impeller consists of 4 blades at an angle of between 30 - 45 ^{o} from horizontal and is roughly halfway down the impeller shaft. Impeller blades cause downward mixing thereby reducing surface turbulence and are employed to facilitate solids suspension of the catalyst particles in the wax medium. The second impeller was attached to the bottom of the impeller shaft and was situated just below the baffle ring. The impeller consists of 4 symmetrically placed, flat, vertical blades, 15 mm high. Clearance between reactor vessel internal base and the impeller is ca. 5 - 15 mm. This impeller functions as an additional mixing element but also for gas liquid distribution. Feed gas is introduced just above the mixer and is evenly distributed at the bottom of the reactor.

3. *Reagent and product removal and addition* is done continuously. Feed gas enters though $^{1}/_{8}$" stainless steel tubing connected through the reactor flange. Gas exits the tube just above the bottom impeller to ensure maximum gas dispersion throughout the reactor. Gaseous and liquid products are removed *via* a sintered disc situated at the top of the reactor vessel and connected through the flange by $^{1}/_{8}$" stainless steel tubing. Placement of the filter element determine the liquid level inside the reactor as the liquid is forced through the filter when completely covered with wax. Products, gaseous and liquid leave the reactor *via* heated (200 ^{o}C) ¼" stainless steel tubing once outside the reactor to the liquid recovery section.

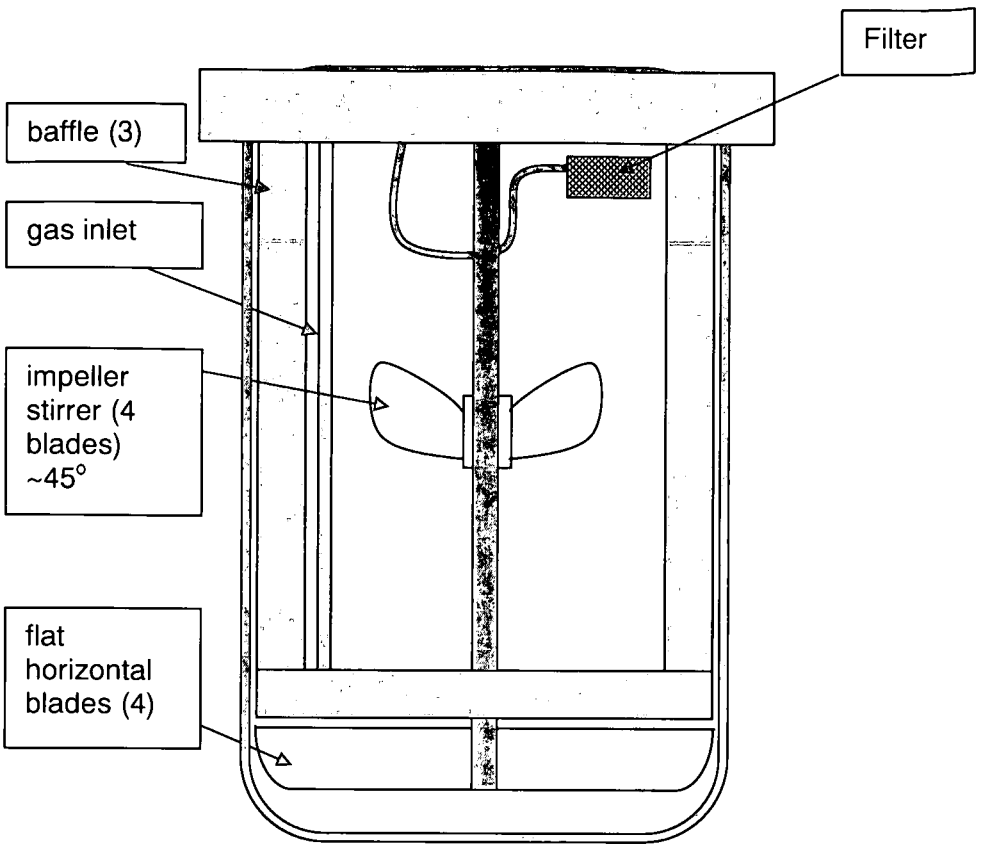

Figure 3. Micro slurry reactor and internals used for catalyst activation and Fischer-Tropsch synthesis performance evaluations.

4.15.4 Liquid Recovery System.

Liquid and gaseous products and un-reacted reagents exit the reactor and flows along heated stainless steel tubing into a 1000 ml stainless steel vessel of type Swagelok® 304L-HDF-1000. ¼" line as well as the vessel is heated *via* electrical tracing wound around the tubing and vessel and further insulated with a suitable insulation material. Temperature control of the electrical tracing is achieved with RKC REX-D400 temperature controller. The ¼" stainless tubing enters the top of the vessel and continues down to ca. 80 mm from the bottom of the vessel forming a "dip tube". Liquids that liquefy at the control temperature collect in the vessel and the rest of the stream exits at the top of the vessel and continues to the next vessel through ¼" stainless steel tubing. The dip tube configuration allows for maximum residence time in the vessel to ensure optimum separation. The vessel is fitted with a block valve and needle valve through which the product collected is

periodically manually drained, weighed and submitted to more detailed product analysis if required. The system is shown in **Figure 4**.

Gasses leaving the first heated sample vessel continues to an addition 2250 ml vessel at ambient temperature with similar dip tube configuration as the first vessel. Lighter hydrocarbons and water collect in this vessel and is also periodically manually drained though a similar valve configuration.

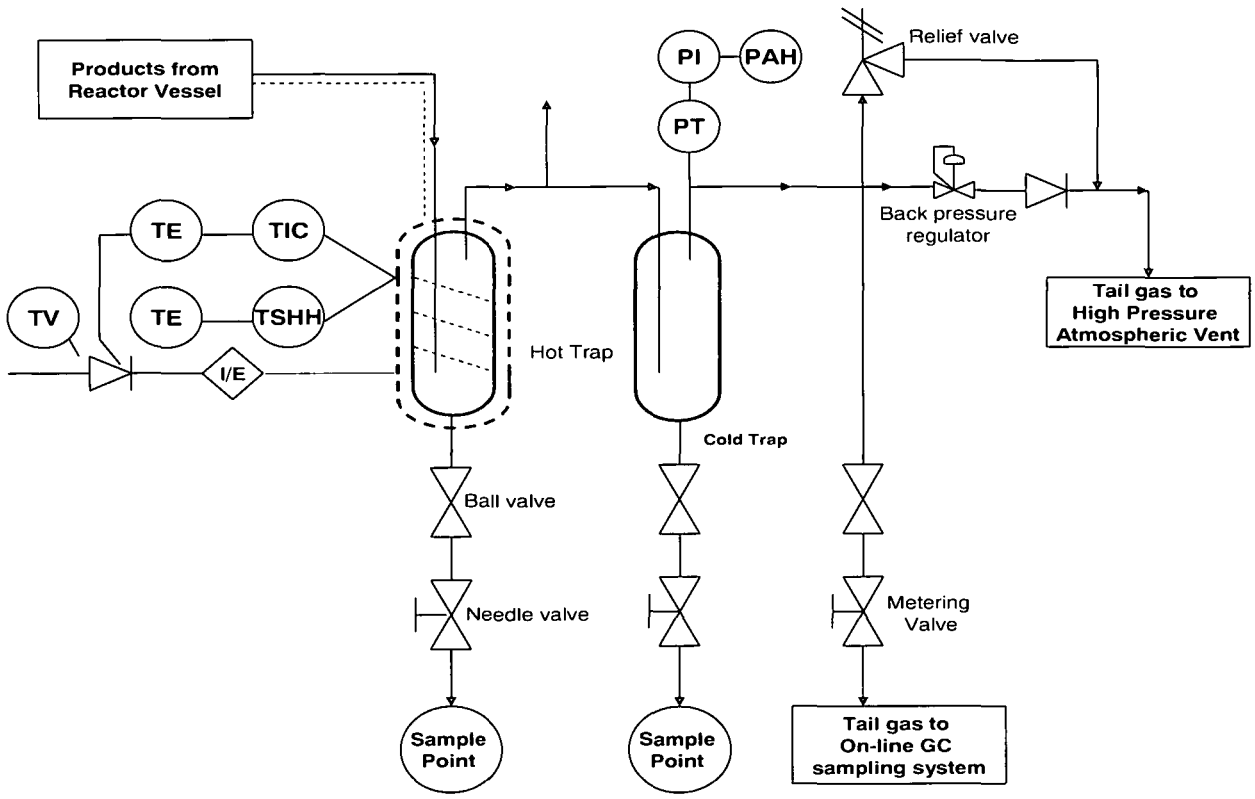

Figure 4. Hot and cold liquid sampling system as well as tail gas sample system on micro slurry reactor.

4.15.5 Gas Sampling Configuration.

After liquid product removal the gas stream consisting of products and un-reacted feed gasses flows through ¼" stainless tubing to a back pressure regulator. The regulator controls the process pressure. Before the back pressure regulator a sample line is connected that can remove the exit gasses though a block valve and metering valve configuration and flow the gasses to an online GC system. A pressure transmitter also connects to the ¼" line before the back pressure regulator for pressure indication as well as safety interlocks connected to overpressure alarms. A relieve valve to protect the equipment against overpressure is also added before the regulator. After the valve configuration the stainless steel tubing is reduced to $^{1}/_{8}$" thereby reducing the volume on gas in the

line that needs to be flushed before a representative sample can be injected into the gas chromatograph.

4.15.6 Micro Slurry Continuously Stirred Tank Reactor Operation.

The iron based catalyst precursor was dried in an oven set at 120 °C in order to remove all moisture so that varying moisture content would not influence the amount of catalyst loaded. 10 g of dried catalyst precursor is accurately weighed on a ± 5 mg accuracy scale. The reactor, unconnected to the flange system and therefore open, is loaded with 350 g of H1® (hydrogenated hard wax – Sasol Wax). The wax was melted at 150 °C and then the weighed catalyst is slowly added to the molten wax in the reaction vessel. The vessel fitted to the flange and sealed by tightening the bolts. Stirring is now activated and set to 450 rpm. Reactor pressure is now slowly increased by addition of argon through the argon mass flow controller and adjusting of the back pressure to higher pressure values. When the desired reduction pressure was reached the argon flow was turned off and the system pressure checked for 1 hr to ensure that system has no gas leaks. Argon flow was reintroduced and product vessels are completely drained. Activation gas of required composition was now introduced while the argon flow is reduced to 10% of the gas flow and used as internal standard. For the purpose of this study identical activation and Fischer-Tropsch synthesis conditions were chosen to compare a standard catalysts with the catalyst produced from reclaimed metal nitrate solutions. After reduction the flows of the reagent gasses were adjusted to Fischer-Tropsch synthesis conditions and catalyst performance evaluated. On completion of the run the argon flow was increased followed by closing the reagent gasses. The temperature was reduced to 150 °C, the stirrer switched off and pressure was slowly reduced to atmospheric. Once atmospheric pressure conditions were reached the argon flow was closed and the reactor opened. The wax and catalyst mixture was left to congeal and cool before being removed from the reactor.

14.5.7 Sampling Procedure.

For this study synthesis gas conversion, as well as methane and carbon dioxide selectivities were reported. To determine these parameters the online GC was used. Analysis of H_2, CO, CH_4, CO_2, Ar and N_2 were done on a GOWMAC GC. The GC is quipped with two split/splitless injectors and two thermal conductivity detectors (TCD). A valve configuration and two packed columns consisting of a 2 meter, $^1/_8$" molecular sieve (5A) and a 2 meter $^1/_8$" Restek Shincarbon column per channel were used. On one channel helium was used as the carrier gas in order to determine the

CO, CO_2, CH_4, Ar and N_2 concentrations, while the carrier gas for the other channel was argon in order to determine the H_2 concentration. The GC oven temperature was constantly controlled at 110 °C. Typical feed gas and tail gas analysis are shown in **Figure 5 and 6**.

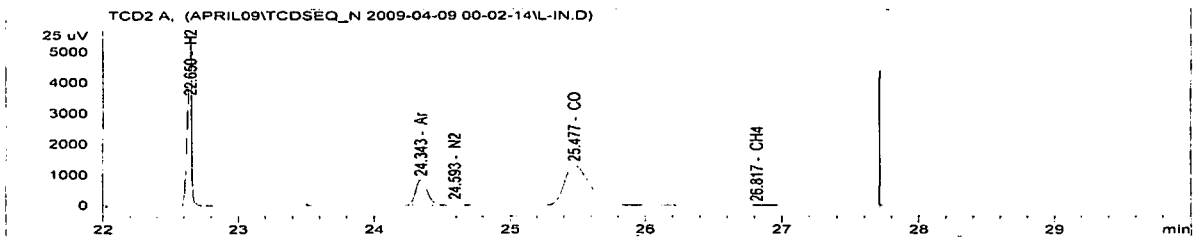

External Standard Report

Sorted By : Signal
Calib. Data Modified : 16 February 2009 12:11:51 PM
Multiplier : 1.0000
Dilution : 1.0000
Use Multiplier & Dilution Factor with ISTDs

Signal 1: TCD2 A,

RetTime [min]	Type	Area [25 uV*s]	Amt/Area	Amount [AREA]	Grp	Name
22.650	VB	1.14113e4	4.65814e-3	53.15532		H2
24.343	BV	4940.45459	1.96554e-3	9.71065		Ar
24.593	VB	564.80908	2.04033e-3	1.15240		N2
25.477	BB	1.69940e4	2.10989e-3	35.85556		CO
26.817	BB	62.10693	2.79511e-3	1.73596e-1		CH4
28.291		-	-	-		CO2

Totals : 100.04753

Figure 5. Typical feed gas analysis to micro slurry reactor during Fischer-Tropsch synthesis conditions.

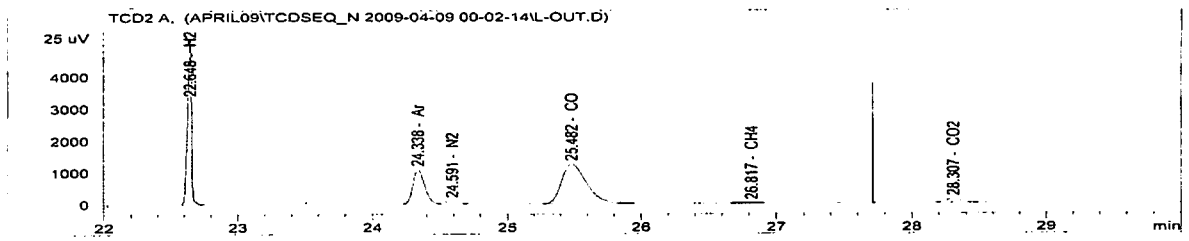

External Standard Report

Sorted By : Signal
Calib. Data Modified : 16 February 2009 12:11:51 PM
Multiplier : 1.0000
Dilution : 1.0000
Use Multiplier & Dilution Factor with ISTDs

Signal 1: TCD2 A,

RetTime [min]	Type	Area [25 uV*s]	Amt/Area	Amount [AREA]	Grp	Name
22.648	VB	1.06125e4	4.65814e-3	49.43473		H2
24.338	BV	6352.08984	1.96554e-3	12.48528		Ar
24.591	VB	715.81860	2.04033e-3	1.46051		N2
25.482	BB	1.60445e4	2.10989e-3	33.85211		CO
26.817	BB	168.92003	2.79511e-3	4.72150e-1		CH4
28.307	BB	1063.82080	1.90029e-3	2.02157		CO2

Totals : 99.72634

Figure 6. Typical tail gas analysis to micro slurry reactor during Fischer-Tropsch synthesis conditions.

14.6 References.

---

[1] Calculations and procedures are in-house developed by Sasol. Similar procedures are to be found in instrumental handbooks.

[2] Gas: Compressed air, purity nitrogen 78 pct, 21 pct, argon 0.9 pct, carbon dioxide 0.03 pct, container 8.5 kg, Mnfr: African Oxygen Ltd.

[3] Gas: Argon: Grade N5.0, Cas. registration number 7440-37-1, molecular formule Ar, container capacity 17.4 KG, purity: 99.999 PCT; Mnfr: African Oxygen Ltd.

[4] Gas: Hydrogen, purity 99.999 PCT, container capacity 0.74 KG, Instrument grade N5.0; Mnfr: African Oxygen Ltd.

[5] Gas: Cometh-cal, purity Carbon monoxide 120-140 vpm, methane 1.4-1.6 pct, oxygen 19-22 pct, balance nitrogen; Mnfr: African Oxygen Ltd.

Chapter 5 – Summary and Conclusions

5.1 Introduction.

Spent iron-based, low and high temperature Fischer-Tropsch (FT) catalysts are generated in excess of 10 000 tons per annum as a result of the commercial production of synthetic chemicals, fuels and waxes. Current disposal methods for spent iron-based catalysts include oxidation followed by dilution and disposal in ash generated from coal gasification or steam generation activities. Raw feed materials for catalyst manufacture have been available at relatively low cost but recently steel and iron prices have risen by more that 200% and hence recovery of spent catalyst metals is becoming increasingly important. Regardless of whether raw materials are expensive, the aim to develop environmentally benign processes has a strong focus towards recycling and reuse of large quantities of spent FT catalysts.

5.2 Summary of Results.

It was first attempted to recover iron from spent iron-based, wax-coated, FT catalyst by nitric acid leaching and to separate the wax and un-dissolved spent catalyst particles from the resultant metal nitrate solution. This process, if successful, could be implemented commercially with minimal capital expenditure.

However, wax-coated spent iron-based FT catalyst reacted vigorously when contacted with a 45 mass% nitric acid solution at 80 °C and mild agitation similar to commercial reference conditions. Large volumes of noxious gasses were generated and the process caused liquid foaming and boiling acidic solutions due to the exothermic dissolution process. Foaming and NOx production led to a more than 150% volume increase in the dissolution vessel. The observed foaming and volume increase would necessitate larger than anticipated vessels to recover spent catalyst in this way. Alternatively some means of controlling the foam level has to be implemented. The rapid NOx release implied substantial NOx off-gas handling capacity will be required if this method is employed industrially. Recoveries of iron, from spent catalyst dissolution, were however, far from efficient during the nitric acid leaching process since only 75% of the iron was recovered.

In order to utilize the heat of dissolution to heat the solution, and to decrease the initial reaction rate of NOx formation and foaming from wax oxidation, the catalyst was added to an ambient temperature nitric acid solution of similar concentration. Experiments proved successful in that similar iron recoveries of 75 % were achieved and the milder process conditions led to less rapid

evolution of NOx and less foaming. It was also shown that the exothermic reaction could be used to heat the acid solution for higher dissolution rate without external heating. The molten waxy product generated was, however, contaminated with un-dissolved spent catalyst particles and silica upon cooling. Filtration to remove un-dissolved spent catalyst particles and the metal nitrate solution posed serious challenges. It was thought that more vigorous agitation would ensure better mixing and acid contact, and that this would yield a cleaner wax fraction. It was found that vigorous agitation, however, increased the dissolution reaction rate which resulted in faster NOx evolution that caused excessive foaming as before. Emulsion-like waxy solutions were formed and wax nitration probably also occurred. As a result wax polarity increased substantially which aids in emulsion formation. Waxy emulsions posed severe phase separation and filtration challenges.

Experiments were also done with fixed bed, spent, iron-based catalyst extrudates. The chemical composition of the spent, fixed bed, iron-based catalyst is similar to the iron-based slurry catalyst. Fixed bed extrudates, however, improves experimental accuracy due to the more constant wax to catalyst ratio and ease of handling. Reaction rates of these extrudates were found to be more controllable as the smaller external surface areas of the larger particles caused slower reaction rates. Despite the smaller surface area, addition of the spent fixed bed catalyst to a 45 mass% nitric acid solution at 80 °C, and vigorous stirring, had similar results as with the finely divided slurry bed spent catalyst in terms of NOx production, foaming, boiling solutions and inevitably filtration difficulties. Upon cooling, the waxy product was also still contaminated with catalyst and overall metal recoveries were similar. When extrudates were added to ambient temperature nitric acid, with vigorous agitation, a similar overall metal recovery of 75% was achieved and a solution temperature of 78 °C was reached. Foaming and NOx generation for extrudate addition to ambient nitric acid was less intense. The waxy product generated was, however, still contaminated with un-dissolved particles.

Experiments were performed where the vigorous agitation was terminated after dissolution. By aging the obtained solution temperature without stirring un-dissolved particles settled and the wax floated to the top of the aqueous acid metal nitrate solution due to density differences. This method led to a much cleaner wax fraction that could be removed by hand sorting upon cooling. Manually removing the solidified wax fraction would however be difficult to do on large industrial scale. Mild agitation was therefore introduced to the cooled solution to see if the wax layer would break-up into more manageable pieces. Unfortunately even very mild agitation caused an emulsion type waxy solution that did not separate again. Filtration at 5 bar followed by centrifugation separated all wax and particles but the process took 24 h to render a filtrate. It is concluded that commercially, this process is not viable due to filtration difficulties and spent catalyst contamination of the wax by-product.

Due to the filtration and separation difficulties of the wax coated spent catalyst after dissolution it was realized that more problematic effluent streams were generated by using wax coated spent catalyst as opposed to removing the wax first. Hence, initial removal of the wax by thermal oxidation, thermal cracking and solvent extraction was evaluated as wax removal technologies prior to the catalyst recovery step. Thermal oxidation has the advantage of process simplicity, but is the most difficult to control accurately within a certain temperature range due to the highly exothermic nature of wax combustion. It was found that excessive temperatures eventually lowered catalyst surface area and lead to the formation of stable irrecoverable iron oxide phases. Thermo-gravimetric analysis showed that the wax auto ignites at 280 °C and therefore low temperature removal of wax by oxidation is a viable option. When the wax was removed by thermal oxidation on slightly larger scale it was realized, from varying final product iron phase compositions, that the targeted wax burn–off temperatures were exceeded due to the rapid combustion of the wax inside the oven. This meant the combustion chamber had to be redesigned to allow more accurate temperature control. A study where the spent wax-coated iron-based catalyst sample bed height and volume were varied, during thermal oxidation, using different sample holders and monitoring catalyst bed temperatures as well as oven temperatures was then conducted. It was shown that a catalyst bed height of 1 cm had a small temperature difference between the oven and sample temperatures whereas a 2 cm bed showed a marked increase ($\Delta T >$ 80 °C) in the spent catalyst bed. Larger depths and volumes did, under the tested conditions, only prolong the temperature effect but did not exaggerate it. Further elevations in temperatures are probably limited by the availability, and mass transfer limitations, of oxygen in the oven and through the catalyst bed. Care will therefore have to be taken when a commercial process is chosen as the actual catalyst surface temperature cannot be measured and may be significantly higher specifically if better oxygen transfer is achieved. Higher than expected temperatures will lead to unwanted sample surface area loss or iron oxide phase transformations. In this study thermal oxidation tests were performed with samples with a 10 mm bed height.

Having optimized the best layout in the thermal oxidation chamber, wax removal by thermal oxidation was investigated as a function of temperature. Oxidation temperatures of 500 °C and 900 °C were chosen. Paraffin (C_9–C_{11}) solvent extraction of wax as well as thermal cracking, in the presence of a nitrogen atmosphere, was also tested under similar conditions.

Thermal oxidation of the wax in air at 500 °C converted the iron of the remaining spent catalyst to a mixture of 72% maghemite and 19% hematite and some analytically unresolved Fe(III) species as evaluated by Mössbauer spectroscopy. After acid leaching the remaining residue was again analyzed and it was found that the residual solid consisted almost entirely (96%) of highly

crystalline hematite. This indicated that the hematite iron oxide phase, specifically if very crystalline, would be difficult to recover and hence the presence of hematite was carefully monitored during all the wax removal technologies.

Thermally oxidized samples at 500 °C and 900 °C differed mainly in the relative amounts of hematite and maghemite. As the temperatures increased the amount of hematite also increased from 0% in the spent catalyst before heat treatment to 17% after thermal oxidation at 500 °C and 72% after thermal oxidation at 900 °C respectively. These hematite phases could not be recovered implying that thermal oxidation of wax in air at the higher temperatures is not viable for ultimate spent iron catalyst recovery.

Anoxic thermal cracking (i.e. in the absence of oxygen) of wax at 500 °C, 750 °C and 900 °C had a less pronounced effect on the phase transformations under the prevailing non oxidizing conditions. A noticeable difference between oxidation and cracking procedures was the generation of magnetite and ferrihydrite phases which were not formed during thermal oxidation. Ferrihydrite is present in the spent catalyst at 71% but was rapidly transformed during thermal oxidation. For thermal cracking the ferrihydrite phase was maintained to a much larger degree - 23% remained after cracking at 500 °C, 7% remained after cracking at 750 °C and 6% remained after cracking at 900°C. A maghemite content of 66% was noted at 500°C which showed that a large percentage of ferrihydrite converted to maghemite. In contrast during thermal oxidation at 500 °C, 78% maghemite remained. During thermal oxidation, 17% hematite was also formed which is significantly less than the quantity formed during thermal cracking, 4%. As the temperature of thermal cracking was increased, product iron oxide phases shifted from ferrihydrite to magnetite and hematite. The shift to hematite was also noted for thermal oxidation but also a shift to maghemite as opposed to magnetite as for the thermally cracked samples. Shifts to Fe(III) during oxidation in air is expected. The shift to Fe(II) species during thermal cracking can be explained by the inert atmosphere, as well as the reducing environment that exists in the presence of carbonaceous (here the wax) material. The presence of ferrihydrite, even at the elevated thermal cracking conditions, is also indicative of the less severe phase transformation conditions that exist. In summary, hematite increased from 4% after cracking at 500 °C to 49% after cracking at 750 °C and 65% after cracking at 900 °C. Magnetite content changed from 0% to 39% and finally 24% during the different cracking temperatures. Lower magnetite abundance when going from 750 °C to 900 °C cracking temperatures showed that higher temperatures outweigh the reducing environment, or, that all the carbonaceous material was completely decomposed at the higher temperatures and hence the transformation could not be influenced by the reducing environment any longer. Anoxic thermal cracking of wax at 500 °C thus proved the best way of wax removal which still allowed recovery of the iron of the remaining spent FT catalyst.

Finally wax removal by extraction was investigated. Wax extraction by a C_9-C_{11} paraffin fraction led to residues containing 57% maghemite and a very small amount of 2% hematite. The remainder of the spent catalyst after wax removed by extraction was ferrihydrite. This means that after the wax is removed by extraction a still reduced iron-bearing material is produced. Subsequent exposure to air will lead to oxidation and temperature increases. Contact with nitric acid will therefore also lead to NOx generation.

In all the wax removal methodologies used, it was noted that none of the iron carbide phases, present in the spent catalyst, were retained after the various treatment processes. It is also important to note that NOx generation, and hence the recovery processes dealing with the NOx, is greatly reduced by using an oxidized iron oxide for nitric acid dissolution. This implies thermal cracking of wax at 500 °C is also more environmentally (and industrially) friendly than wax removal by extraction.

A study to establish dissolution characteristics of products from the various wax removal processes gave interesting results. Samples were contacted with nitric acid (45 mass%) at 80 °C under vigorous stirring. The starting material and residue was analyzed and quantified in order to determine recoveries. Iron recoveries were highest for the wax removal by solvent extraction and worst for the 900 °C thermally oxidized sample. Copper recoveries were generally more efficient than iron recovery and could be due to copper being ejected to the particle surface during the various treatments, or during Fisher Tropsch synthesis. Copper recoveries were less than desirable at the higher treatment temperatures and could be due to spinel formation, or the copper is captured inside the irrecoverable hematite iron matrix and not accessible for acid leaching. The copper recovery from the thermally cracked samples at 900 °C (82.2%) and thermally oxidized 900 °C (25.4%) samples were, however, still significantly higher than the iron recoveries of 33.3% and 0% respectively. Iron recoveries declined as the treatment temperature increased, which also correlates with the amount of hematite present in the samples.

Recoveries for sodium and potassium were high for the lower temperature treatments but at increased temperatures the recovery declined. It is thought that some potassium and sodium may be captured inside the iron residue due to collapsing pores at the elevated treatment temperatures. At 500 °C, K^+ recovery was 99.9% for the thermally cracked sample and 94.4% for the thermally oxidized sample, whereas at 900 °C the recovery was 57% for the thermally cracked sample and only 4.3% for the thermally oxidized sample. Na^+ recovery was 100% for the thermally cracked sample at 500 °C and 85.7% for the thermally oxidized, sample whereas at 900 °C the recovery was 100% for the thermally cracked sample and only 21.7% for the thermally oxidized sample.

Silica balances obtained for the study was insufficient. Silica in the original catalyst is well dispersed between the iron bearing crystallites and consists of very small particles. When the metal framework is dissolved the silica is liberated into the solution as small particles. Silica does not dissolve appreciably at low pH but the particles are probably very small and therefore passed through the filter used for recovery. Additional silica was not reported after the preparation of the fresh catalyst precursor from recovered spent FT catalysts. Therefore the silica was not "captured" in the iron matrix during the precipitation of the iron bearing slurry with addition of the iron bearing nitrate solution to the sodium carbonate solution. The silica may therefore be present in the wash water stream used to remove the sodium nitrate from the iron bearing slurry.

It was next investigated how shorter and longer residence times at elevated temperatures will influence the product generated as the highest surface area product should be targeted for the wax removal process. The wax was first removed from the spent catalyst *via* solvent extraction so that the actual temperature of the process could be accurately monitored without the wax combustion effecting temperatures.

The following sets of conditions, where heat treatments at different temperatures were maintained for different time durations, were evaluated:

1. 350 °C for 20, 120 and 600 minutes.
2. 500 °C for 20, 120 and 600 minutes.
3. 600 °C for 20, 120 and 600 minutes.
4. 750 °C for 20, 120 and 600 minutes.

After the various heat and time treatments the surface areas of the generated samples were evaluated. Samples were also submitted for phase analysis by means of Mössbauer spectroscopy. It can be concluded that up to 600 °C heat treatment the residence time had little effect on the surface area generated. At 750 °C the effect of residence time on surface area loss was already pronounced after 20 min. However the commercial hematite sample with a surface area of only 34 $m^2.g^{-1}$ that was used for this study had an iron recovery of 88%. Pore volume also decreases as the heat treatment becomes more severe. Pore diameter shows an increase but this is due to smaller pores collapsing at higher temperatures and creating larger pores, but at the expense of surface area. Results clearly indicate the amount of hematite in the sample is an indication of the temperature to which the sample was exposed. Thus a higher content of hematite in the de-waxed spent catalyst indicates exposure to higher temperatures resulting in a drop of the surface area and thus lower metal recoveries. The overriding conclusion of this study is that the hematite phase

is to be avoided for iron recovery from spent FT catalysts unless it can be coupled with a high surface area.

After initial wax coated spent iron-based catalyst dissolution experiments, where a metal nitrate solution was prepared, a catalyst precursor was prepared (aim 4 of study Chapter 1, Introduction, paragraph 1.2). Failure to produce a suitable iron-based catalyst precursor from the recovered spent catalyst material would defy the ultimate purpose of the study. A fresh, iron-based, catalyst precursor was prepared by using the resultant metal nitrate solution obtained from metal recovery of the spent FT catalyst and met specification with regards to chemical composition and physical properties. Standard catalyst precursor activation, and Fischer-Tropsch synthesis, conditions were used to test catalyst performance in a micro slurry reactor. Fischer-Tropsch synthesis performance, as well as basic selectivities, were on par with the standard commercial iron-based catalyst under similar conditions (aim of study 5, Introduction, paragraph 1.2).

In conclusion, this study developed a chemically viable method of recovering spent iron-based FT catalyst and using the recovered material to prepare fresh, active FT catalysts. If applied commercially the developed technology will benefit protection of the environment and may allow more economic use of large quantities of spent FT catalysts.

5.3 Future Perspectives.

As a starting point for this study, nitric acid concentration and process conditions such as temperatures and product concentrations were used a basis for the investigation. Should an entirely new iron-based catalyst precursor preparation plant be build, many of these constraints must be further evaluated. Therefore different acids (mineral and organic) could be investigated for further process optimization or for environmental and safety reasons. From this study it was shown that various iron oxide phases and mixtures of iron oxides can be readily recovered and converted to new, active FT catalysts. However, not only spent FT catalysts have to be used as a source of iron recovery for new FT catalysts. Basically any waste source of iron metal can be utilized for this purpose, including old car engines, or any other scrap metal source. These other "waste" or less expensive iron sources could be evaluated as raw material for the manufacture of new catalyst precursor. Within the Sasol group, the high temperature iron based Fischer-Tropsch catalyst is also discarded in significant amounts. The dissolution of this iron based spent catalyst should be investigated in detail as this could serve as a further iron source for the low temperature iron based catalyst.

Dissolution of the spent iron based catalyst and subsequent preparation of a new catalyst precursor was only evaluated for one dissolution cycle. Continuous recycling could cause the build-up of unwanted metals in the raw material previously ignored because the spent catalyst was simply discarded after use. Therefore a study should be initiated to evaluate the effects of continuous recycling on catalyst composition and Fischer-Tropsch Synthesis performance. In addition the silica balance for the current study was not closed and should be investigated thoroughly. Silica removal, by base dissolution, at various process steps must be one of the actions that require further investigation.

One alternative wax removal process that was not investigated within the boundaries of this study was the hydrogenation of the wax in a hydrogen or synthesis gas atmosphere at elevated temperatures. This process has the benefit of recovering hydrocarbon rich gases from the wax that could easily be integrated into the current product refinery process. Surface area and phase changes under these conditions should be carefully investigated. An advantage of this methodology would be that the iron phase could be maintained in an easier dissolvable oxidation state during the wax removal (hydrogenation) process.

This study only addressed iron recovery for new FT catalyst precursors for the low-temperature iron-based FT process. However, cobalt is the active primary metal for low-temperature cobalt-based FT and is also generated in large volumes of cobalt containing waste material. A study to recover cobalt effectively for economic as well as environmental reasons is thus of primary importance. Such a study will include optimization of all parameters that will influence such a recovery process including temperature, time and the influence of any other material present in the spent catalyst mix, including zirconia, titania, alumina, ruthenium, platinum, gold and silver. The recovered cobalt should then also be converted to a new active cobalt-containing FT catalyst precursor with subsequent Fischer-Tropsch synthesis performance evaluations compared to the current commercially available catalyst precursor.

Appendix

Table 1. Specification for A Grade steam condensate as used to absorb NOx gasses to produce nitric acid.

Component	Maximum		Maximum
	ppb		ppm
Sodium (Na)	10	Ammonia (NH_3)	0.5
Silicon (Si)	20		
Iron (Fe)	10		
Copper (Cu)	3		
Oxygen (O_2)	5		

Table 2. Nitric acid specification for commercial dissolution process as well as concentrated nitric acid added to obtain suitable nitric acid concentrations.

Nitric acid used for dissolution			Concentrated nitric		
Component	Minimum	Maximum	Component	Minimum	Maximum
	mass%	mass%		mass%	mass%
Nitric acid	55	60	Nitric acid	56	60
Water (H_2O)	45	40		g/cm^3	g/cm^3
	ppm	ppm	Density	1.34	1.40
Ammonia (NH_3)	-	100			